Design of future ultra-high by-pass ratio turbofans

A synergy of low-NO_x combustion technologies

Ieke de Boer

Technische Universiteit Delft

TU Delft

Design of future ultra-high bypass ratio turbofans

A synergy of low-NO_x combustion technologies

by

Ieke de Boer

in partial fulfilment of the requirements to obtain the degree of

Master of Science
in Aerospace engineering

at the Delft University of Technology
to be defended publicly on Friday December 1, 2023 at 14:00.

Student number:	4499034	
Project duration:	November 2022 - November 2023	
Thesis committee:	Prof. Dr. ir. A. Gangoli Rao,	TU Delft, Chair
	Dr. F. Yin,	TU Delft, Supervisor
	Dr. ir. M.F.M. Hoogreef,	TU Delft, Examiner
	Dr. ir. A. Heidebrecht,	TU Delft, Examiner

TU Delft

Preface

This thesis is a culmination of my seven years at the faculty of aerospace engineering at Delft University of Technology. This long period of studying was both intentional and unintentional, as I have immensely enjoyed the first few years of my student life before ending it on a more serious note. I chose this thesis subject because I felt like it would keep me interested and motivated throughout the entire duration of the project, which it did. Hopefully, this can in some way be my tiny contribution the global warming problem that my generation and younger generations are expected to solve.

Firstly, I want to thank my daily supervisor Feijia and chair Arvind for their guidance during this year long period of writing my thesis. Their understanding of how I approached a long and difficult period of at the beginning of this calendar year is deeply appreciated. At the start of my literature study, I felt like I hardly understood what I was doing and that my knowledge somewhat lacked. During the thesis, I felt myself becoming more confident in my growing expertise on this subject, which I see as a result of our collaboration. So, thank you both for this.

I also want to thank the friends that I tried very hard to convince to join me in studying at the faculty, especially during the summer when it was difficult to motivate myself. But most importantly, I want to thank my family for their undying support during the past eight years. My mom, who sends me (too many) messages asking me how I am doing and if I need any help with anything, thank you. My dad, who asks me aerospace related questions to make me feel smart and has devoted himself to reading this entire technical report even though he has limited knowledge on the subject, thank you.

Ieke de Boer

Executive Summary

The aviation industry is continuously growing, resulting in an increase of 3-4% CO_2 emissions by aviation per year. Despite continuous efforts to limit the growing climate impact of the aviation industry, it appears a stagnation point in terms of fuel efficiency might be reached in the near future. Additionally, the effects of non-CO_2 emissions also have non-negligible contribution to global warming. Several international aviation organisations have set guidelines for emissions and fuel efficiency that are to be achieved in certain time-frames to minimise the overall climate impact of aviation. Additionally, multiple technology development scenarios have been evaluated against the maximum achievable CO_2 reduction. It appears that with the current technology improvement outlook, the climate goals cannot be achieved in the desired time-frames. The need for unconventional aircraft technologies becomes urgent, but it also requires many resources and time to get these unconventional technologies certified, by which it might already be too late to achieve the climate impact reduction goals.

The literature review that was conducted prior to starting this thesis explores various technologies, including low-NO_x combustion techniques, different thermodynamic cycles and several engine architectures. Preliminary studies and experimental set-ups have demonstrated the performance enhancement and emissions reduction potential of these technologies compared to existing engines. Alternative engine architectures show significant improvement potential, but also present drawbacks related to integration challenges, weight penalties and noise. A comparison against a baseline engine model was made to show a meaningful overview of the emissions reduction potential of conventional and alternative architectures. It was shown that, based on recently performed studies, the alternative architectures show a slightly better performance than the conventional architectures. However, research combining multiple future technologies into one engine and their impact on engine performance is lacking. Combining a conventional turbofan with an ultra-high bypass ratio and low-NO_x combustion techniques may rival the benefits of alternative architectures. The need for a detailed study assessing these combinations arose, addressing the question whether conventional turbofans remain suitable as standard in the future for short-to-medium range aircraft, if the ambitious emission reduction goals are to be achieved. This aim of this thesis is to answer this question.

It was chosen to evaluate the performance of four different engine models: a direct-driven and geared driven engine option, for both 2035 and 2050. These engine models were optimised as ultra-high bypass ratio engines (BF-models), after which three low-NO_x combustion techniques (water injection (WI), inter turbine burning (ITB) and lean burning combustion (MPLDI)) were implemented to make the upgraded future engine models (UF-models). The improvement of the BF-models in terms of thrust specific fuel consumption (TSFC) was around 9% for the 2035 engines and 15% for the 2050 engines compared to state-of-the-art engines. The addition of the low-NO_x combustion techniques were evaluated within a large design space for a range of overall pressure ratios (OPR), combustor outlet temperatures (T_4) and water-to-air ratio (WAR)/ITB energy percentage contribution (E%). The design space showed that with the addition of WI or ITB, there was still a trade-off that could be made between a larger TSFC improvement or a larger EI_{NO_x} improvement. By combining WI and ITB with MPLDI, this trade-off was made easier. Choosing the point of lowest TSFC for the WI and ITB options and correcting the NO_x emissions index (EI_{NO_x}) for a MPLDI combustor ensured both a great TSFC performance and a great EI_{NO_x} reduction. The EI_{NO_x} performance for the UF-models at the point of lowest TSFC improved greatly from -55 to -90% in design condition when MPLDI was added to WI and ITB. For off-design, the range was approximately -45 to -95%.

The performance trade-off showed a more favourable scenario for water injection than for ITB for TSFC in all cases. ITB did perform exceptionally well in off-design conditions (-75 to -96% NO_x emissions), but the validity of these results is questionable due a lack of a proper EI_{NO_x} correlation for ITB-MPLDI engines. The combined improvement of TSFC and EI_{NO_x} of the WI-MPLDI made that this option was chosen as final design option. For the 2035 case, this combination proved better for the geared turbofan engine than the direct drive engine, but due to the large weight increase of the GTF-2050 engine model compared to a modern engine, this was not the case for 2050. The direct-driven 2050 engine model showed a better trade-off between TSFC, EI_{NO_x} and weight.

Comparing the WI-MPLDI engine models to the alternative engine architectures explored in the literature study showed that both the TSFC improvement and EI_{NO_x} improvement is now able to rival those of the alternative engine architectures. Additionally, with the 2035 WI-MPLDI engine it is likely that the fuel burn and emission goals for the 2035 time-frame can be met. For 2050 this remains not likely, even not when the 2050 WI-MPLDI is combined with an advanced airframe.

List of Figures

List of Tables

Contents

Nomenclature

List of Abbreviations

BPR	Bypass ratio
CO	Carbon monoxide
CO_2	Carbon dioxide
DD	Direct drive
DDTF	Direct-drive turbofan
DP	Design point
FAR	Fuel-to-air ratio
FPR	Fan pressure ratio
GTF	Geared turbofan
HPC	High pressure compressor
HPR	High pressure compressor pressure ratio
HPT	High pressure turbine
IFPR	Inner fan pressure ratio
IPC	Intermediate pressure compressor
IPR	Intermediate pressure compressor pressure ratio
ITB	Inter-turbine burning
LBCC	Lean burning combustion chamber
LPT	Low pressure turbine
MPLDI	Multipoint lean direct injection
NO_x	Nitrogen oxides
OD	Off-design
OFPR	Outer fan pressure ratio
OPR	Overall pressure ratio
SOT	Stator outlet temperature
TIT	Turbine inlet temperature
T/O	Take-off
TSFC	Thrust specific fuel consumption
UHC	Unburned hydrocarbons
UHBPR	Ultra-high bypass ratio
WAR	Water-to-air ratio
WI	Water injection
Suffixes	
-B	State-of-the-art baseline engine model
-BF	Baseline future engine model
-ITB	Inter-turbine burning upgraded future engine model
-MPLDI	Multipoint lean direct injection upgraded future engine model
-UF	Upgraded future engine model
-WI	Water injection upgraded future engine model

List of Symbols

Symbol		unit
η_c	Core efficiency	-
η_{is}	Isentropic efficiency	-
η_p	Polytropic efficiency	-
η_{th}	Thermal efficiency	-
$E\%$	Energy contribution of the second combustor	-
EI_{NO_x}	NO_x emission index	g/kg
F_s	Specific thrust	Ns/kg
$HC10$	Last HPC rotor blade heigth	cm
$\dot{m}_{f1}$	First combustor fuel mass flow	kg/s
$\dot{m}_{f2}$	Second combustor fuel mass flow	kg/s
P_{t3}	Combustor inlet total pressure	kPa
S_{NO_x}	NO_x severity index	g/kg
T_{t3}	Combustor inlet total temperature	K
T_{t4}	Combustor exit total temperature	K
T_{t44}	Second combustor inlet total temperature	K
W_1	Inlet mass flow	kg/s

1
Introduction

It is well known that global warming is currently one of the biggest threats to livability on Earth. The aviation industry contributes to this problem, being responsible for 2-3% of the total CO_2 emissions in the world and accounts for even more of the total climate impact [1]. In the past couple of decades many studies have been conducted to decrease fuel consumption by developing more efficient aircraft, as this reduces CO_2 emissions and is economically desirable. One way to do this is by changing the airframe. Subtle changes like blended winglets caused an increase in payload-range and decreased the mission block fuel by 4% [2]. Radically different designs like the Flying-V claim to reduce fuel consumption by 20% compared to the Airbus 350 for the same flight [3]. Next to airframe changes, continuous development of gas turbines has led to more fuel-efficient engines by, for example, increasing the overall pressure ratio (OPR) and introducing composite materials.

Despite continuous aircraft improvements, an increase of around 3-4% CO_2 emissions per year is still expected as the aviation industry keeps growing [1]. Additionally, an increased efficiency and subsequent decrease in fuel consumption does not necessarily imply a decrease of non-CO_2 emissions e.g., NO_x emissions. Although CO_2 is a major contributor, other aircraft emissions like nitrogen oxides (NO_x), carbon monoxide (CO), water vapour (H_2O) and unburned hydrocarbons (UHCs) also impact the rate of global warming. A higher OPR actually stimulates thermal NO_x formation due to higher operating temperatures, diminishing the effect of the fuel efficiency on the total emissions reduction and the overall climate impact. Since NO_x and contrail cirrus are responsible for two thirds of aviation's climate impact (in 2018), the focus of aircraft design has shifted from solely decreasing the fuel consumption to a combination of fuel consumption and non-CO_2 emissions decrease [4].

1.1. Historic emissions reduction

There are several studies that aim to predict the greenhouse gas emissions reduction for aircraft on short- and long-term, but past research often hints at a linear decrease or even stagnation point in the future. Singh and Sharma analysed 277 articles on fuel consumption optimisation from 1973 to 2014 and found that while there was a 15% fuel burn improvement in the 15 years before 2000, there was only 11% improvement in the 15 years afterwards [5]. They also showed there was an average fuel efficiency improvement of 1.5% per annum between 1960 and 2008, but the annual fuel efficiency improvement in recent years was smaller than that of the earlier years. The fuel burn per passenger is shown in Figure 1.1.

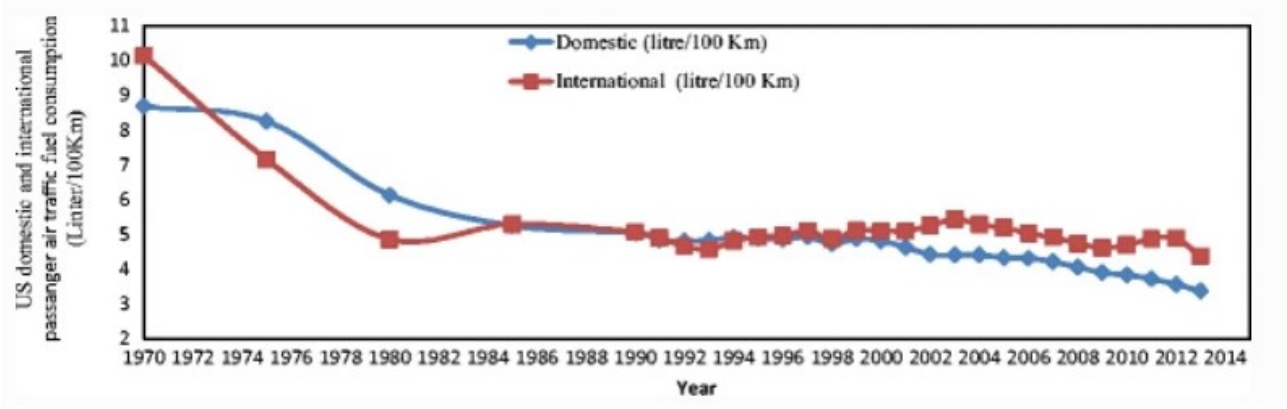

Figure 1.1: US domestic and international fuel efficiency trend from 1970 to 2014[5]

[6] supports this, noting a 1.3% average fuel efficiency improvement per annum between 1968 and 2014. The recent fuel efficiency improvement is back to 1.1% per annum (in fuel/passenger-km, as seen in Figure 1.2) after a stagnation around 2000.

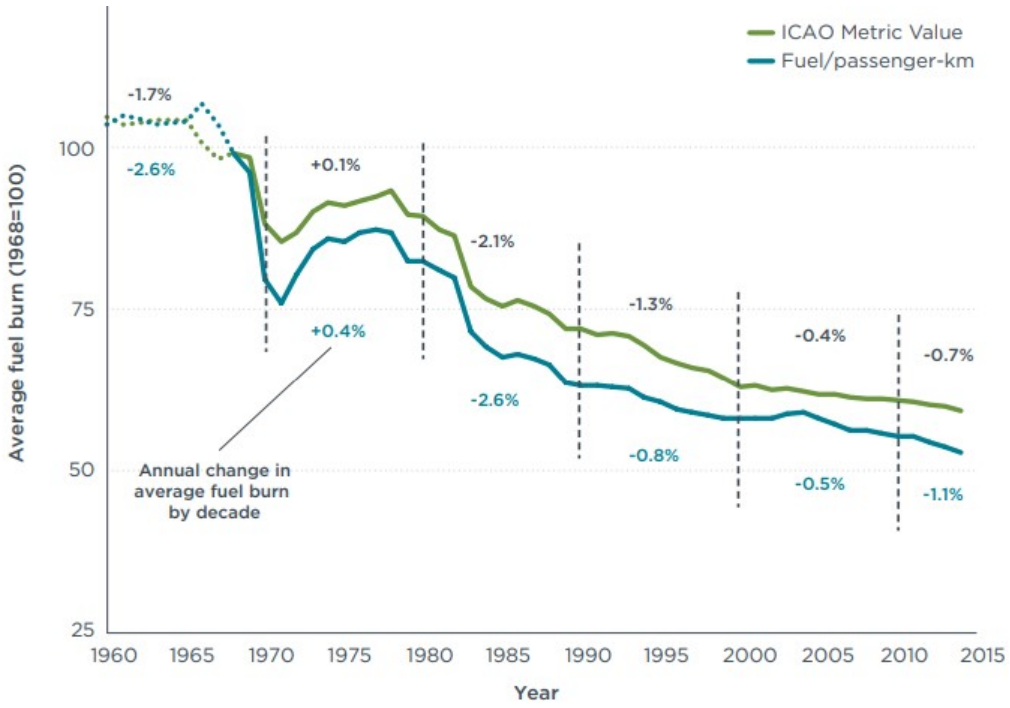

Figure 1.2: Annual change in average fuel burn per decade for jet aircraft [5]

The trend that can be seen is not due to lack of innovation. Only recently the geared turbofan (GTF) was introduced. Allowing for an optimised fan spool speed by means of a gearbox increased the fuel efficiency of the aircraft by up to 20% compared to the previous generation [7]. However, there is a limit to increasing the efficiency. Gas turbines operate according to the thermodynamic Brayton cycle. The ideal Brayton cycle efficiency is solely based on the OPR, but the real Brayton cycle has a theoretical maximum based on several loss mechanisms within the engine. Its thermal efficiency η_{th} can be described by Equation (1.1), where γ is the specific heat ratio of air, η_{comp} & η_{turb} are the compressor and turbine efficiencies, and T_{t4} & T_0 are the combustor exit temperature and compressor inlet temperature.

$$\eta_{th} = \frac{\left[1 - \frac{1}{OPR}^{\frac{\gamma-1}{\gamma}}\right]\left[\eta_{comp}\eta_{turb}\frac{T_{t4}}{T_0} - OPR^{\frac{\gamma-1}{\gamma}}\right]}{1 + \eta_{comp}\left[\frac{T_{t4}}{T_0} - 1\right] - OPR^{\frac{\gamma-1}{\gamma}}} \tag{1.1}$$

This equation shows that the thermal efficiency of the cycle does not necessarily increase by simply increasing the pressure ratio. With a limit on T_{t4} due to material properties and a limit on the component efficiencies due to irreversible losses, η_{th} also has a limit. Most modern high bypass turbofans have a thermal efficiency of around 45% [8]. The maximum achievable realistic thermal efficiency lies around 60% [9]. The total efficiency of a jet engine is defined by $\eta = \eta_{th} \cdot \eta_p$. η_p is the propulsive efficiency, which is dependent on the ratio between the intake velocity and the jet velocity. The propulsive efficiency of modern turbofans can reach more than 80% and is influenced by, amongst other parameters, the bypass ratio and the turbine inlet temperature [8]. The difficulty in increasing the total efficiency lies in the contradicting actions one should take regarding the engine design parameters. For example: increasing the TIT increases η_{th}, but decreases η_p. This, together with the opposite reactions of changing certain design parameters on the CO_2 and non-CO_2 emissions, makes engine improvement difficult.

1.2. Climate goals

To minimise the impact of the aviation industry on the environment, European and international aviation organisations set out guidelines that specify the necessary reduction of certain greenhouse gasses. The Advisory Council for Aviation Research and Innovation in Europe (ACARE) aims for the following goals regarding CO_2 and NO_x emissions [10]:

- "By 2030, net CO_2 emissions from all intra-EU flights and those departing the EU are reduced by 55% compared to the 1990 baseline."
- "By 2035 new technologies, fuels and operational procedures in service result in a 30% reduction in non-CO_2 climate effects of all intra-EU flights and those departing the EU relative to the 1990 baseline"
- By 2050:

- "net-zero CO_2 emissions has been achieved for all intra-EU flights and those departing the EU"
- "new technologies and operational procedures in service result in a 90% reduction in NO_x emissions from all intra-EU flights and those departing the EU relative to the year 2000"

The International Civil Aviation Organization (ICAO) specifies the following goals:

- From 2020 - 2050: carbon neutral growth and a 2% fuel efficiency improvement per annum for international aviation [11]
- By 2030: a 60% reduction in NO_x emissions compared to their 2008 reference [12]
- By 2050: net-zero CO_2 emissions for international aviation [13]

While one addresses Europe and the other international aviation, the end goal is the same: net-zero CO_2 emissions in 2050. The intermediate goals are put into place to ensure proper advancement towards this long term aspirational goal. These goals are intended to be met through a combination of technological advancements in aero-engines, airframe technology and operational measures, such as improvements in air traffic management and aircraft routing.

1.3. Improvement outlook

The ICAO has performed an extensive study with different development scenarios to assess the potential CO_2 reduction in the nearby and distant future [13]. The different development scenarios are classified as follows:

1. "**Low / nominal** — Current (c. 2021) expectation of future available technology, operations efficiencies, fuel availability, costs. Includes expected policy enablers for technology, operations and fuels. Low systemic change – no substantial infrastructure changes."
2. "**Increased / further** — Approx. mid-point. Faster rollout of future technology, increased operations efficiencies and higher fuel availability. Assumes increased policy enablers, therefore decreased costs for technology, operations and fuels. Increased systemic change – limited infrastructure changes."
3. "**Aggressive / speculative** — Maximum possible effort: technology rollout, operations efficiencies, fuel availability, costs. Assumes max policy enablers for technology, operations and fuels. High, internationally aligned systemic change e.g. significant and broad change to airport and energy infrastructure.

Single-aisle airliners make up the largest part of the current worldwide civil transportation fleet, as they are suited to fly short to medium range distances. It is expected that from 2040 onward around 75% of the worldwide civil transportation fleet will comprise of single-aisle [14]. Therefore, it is valuable to look at the reduction potential of this category. With an estimated earliest entry-into-service (EIS) of 2035, the CO_2 reduction potential of an advanced single-aisle airliner is relative to a 2018 reference aircraft is shown in Table 1.1. It also shows the reduction potential in 2050.

Table 1.1: CO_2 reduction potential of different development scenarios for a single aisle aircraft with EIS 2035 and 2050 relative to a 2018 reference aircraft[13]

Scenario		ΔCO_2 [%] 2035	ΔCO_2 [%] 2050
1	Lower progress	-8.7	-18.7
	Medium progress	-14.9	-24.2
	Higher progress	-20.8	-28.0
2	Lower progress	-13.2	-22.7
	Medium progress	-23.4	-31.8
	Higher progress	-32.7	-42.4
3	Lower progress	+9.6	-2.4
	Medium progress	-2.2	-12.8
	Higher progress	-24.8	-31.6

Comparing the lower and medium progress of scenario 1 and 3, and the lower progress of scenario 2 to the trends from Section 1.1, this is line with the observation that the fuel burn optimization is declining compared to previous decades. Scenario 2, described as implementing "significant architectural/configuration changes at the airframe, propulsion, or combination level" shows the most promise.

The annual increase of 1.1% fuel efficiency mentioned in Section 1.1 is not sufficient to meet the aforementioned climate goals, predicting a 12 year lag in meeting the ICAO 2030 goal [6]. Additionally, none of the discussed scenarios is able to achieve the desired 2% fuel efficiency increase per annum. These projections show that the margin for improvement of the conventional gas turbine is decreasing. Single-aisle airliners are currently powered by already very

efficient turbofans that are operating close their theoretical maximum efficiency. Based on these observations, it is evident that revolutionary technologies are required to achieve the climate goals and decrease the climate impact of the aviation industry.

1.4. Problem description and research question

Looking at the evolution of the conventional gas turbine, it is evident that the margin to increase efficiency becomes smaller and alternative architectures or thermodynamic cycles are essential to progress enough to reach future climate goals. Several aero-engine suppliers and aircraft manufacturers are working together with research groups to develop these revolutionary designs. However, this means that the focus is shifting towards other options than the conventional turbofan, The conventional turbofan has been the main engine option for single aisle airliners operating on short to medium distances. The solid performance of these aircraft types on longer distances result in an increase in use of these airliners in the future. Several future conventional and alternative engine options for single-aisle airliners were explored in a literature review (included in Chapter 2) that was conducted before this thesis and compared to each other and a baseline engine. The results of this study, compared with the the outlook on fuel efficiency and emissions reduction gave rise to the following research question:
Are conventional turbofans still suitable as standard for short-to-medium-range aircraft in the future?

The answer to this question would determine the required design direction for future aero-engines that are to be used with single-aisle airliners, or other unconventional short-to-medium range airframes. To answer this research question, the answers to the following sub- and sub-sub-questions first have to be answered:

1. What are the main drivers for engine design trends in the future?
   a What are the required fuel burn and emissions reductions of the propulsion unit based on its contribution to the total aircraft fuel efficiency in 2035 and 2050?
   b What is the effect of adjusting engine component characteristics on engine performance and emissions?
2. How can a future conventional gas turbine achieve the required fuel burn and emissions reduction specified in sub-question 1?
   a What future engine technologies can be combined into the same engine?
   b What combination of future engine technologies provides the biggest improvement potential in TSFC and NO_x emissions?
   c How does a future conventional turbofan with a combination of future engine technologies perform on different mission types and segments?
3. How does a future conventional gas turbine compare to different engine architectures and thermodynamic cycles in terms of fuel efficiency and NO_x?
4. What is the combined improvement potential of a future conventional gas turbine with advanced airframe technology in terms of fuel efficiency and NO_x?

In search for an answer for these questions it would be valuable to look at future aircraft technologies and their potential for efficiency and environmental improvement compared to a state-of-the-art aircraft. The literature review that was conducted prior to this thesis investigated such future engine technologies and determined some of the more promising technologies that could be able to achieve the climate goals stated in Section 1.2. The aim of this thesis is to analyse these promising technologies with an appropriate gas turbine simulation software and compare them to other revolutionary, alternative engine architectures. For a full evaluation, the performance of these promising engine technologies should also be combined with future airframe technology.

1.5. Structural overview

This thesis is structured as follows: First, the findings of the literature review are shown in Chapter 2, where a comparison is made between several future engine technologies. Next, Chapter 3 explains the methodology that will be used for modelling of the future engine technologies, the reference engines that are used as baseline, the engine design drivers for current and future engines and the future engine technologies that will be explored. Chapter 4 covers the set-up of the baseline future engines that will be used for reference for the 2035 and 2050 timeframes and how the other engine technologies will be implemented into these baseline future engine models to create the upgraded future engine models. The results of the simulations of the upgraded future engine models are discussed in Chapter 5, including a trade-off to determine the best engine design and a comparison with alternative engine technologies. Lastly, the conclusions will be presented in Chapter 6, where recommendations for future work are also discussed.

2
Literature review

This chapter contains the literature review that was conducted before starting the thesis. It discusses current and future engine technologies in Section 2.1 and an architecture comparison of different conventional and alternative engine architectures in Section 2.2.

2.1. Current and future technologies

Aircraft are under constant development to increase their performance and decrease their emissions. An aircraft's ability to be retrofitted with the newest technology results in simultaneous but parallel development of airframe and propulsion technology, and therefore no one state-of-the-art passenger aircraft exists. A combination of different existing technologies can roughly provide the same overall flight performance, thus this section shows an overview of several current state-of-the-art technologies in Section 2.1.1. In an effort to achieve the emission goals stated in Section 1.2, new technologies are in development that could be used on future aircraft, which are summarised in Section 2.1.2. Section 2.1.3 elaborates on the engine cycles used in current aero-engines and several future engine architectures. The improvement potential of these engine architectures is discussed in Section 2.1.4.

2.1.1. Current aircraft technologies

Table 2.1 shows some of the most prominent state-of-the-art aircraft technologies. Current aircraft technologies were often introduced to increase the aircraft's (fuel) efficiency and therefore its performance, as this is a good measure of decreasing the CO_2 related emissions while becoming increasingly more cost effective. However, some existing technologies were developed to specifically reduce the non-CO_2 emissions of the aircraft. Therefore, the technologies are grouped together in their respective category. It should be noted that some technologies both enhance performance and decrease emissions, but they are grouped in their dominant category.

Table 2.1: List of current aircraft technologies

CURRENT TECHNOLOGY	
Performance	**Emissions**
Composite blades	Rich-burn, Quick-quench, Lean-burn (RQL)
Composite Matrix Ceramics (CMCs)[1]	Lean combustion
Advanced, thinner, shorter nacelles	Biofuels (life cycle emissions)
Higher TIT and HPC exit temperatures	Axially staged combustor
Reduction of fan hub-to-tip ratio	Double annular combustor
Geared turbofan (GTF)	Twin annular premixing swirler (TAPS)
Fan pitch control	
Intercooling	
Increased BPR and OPR	
Blended winglets	

These state-of-the-art aircraft technologies are not all necessarily introduced in the last couple of years, but some have been dominating high performance or low emissions technologies since their introduction. For example, increasing the turbine inlet temperature (TIT), high pressure compressor (HPC) exit temperature, bypass ratio (BPR) or overall pressure ratio (OPR) have continuously been applied to the past generations of aero-engines but continue to enhance the engine performance when increased even higher. Others, like the GTF, have only recently been introduced.

2.1.2. Future aircraft technologies

Current aircraft technologies are focused on performance enhancement more than on overall environmental impact reduction. Now that it is apparent non-CO_2 emissions also have a severe environmental impact, future aircraft technology development tends to focus more on the total emissions reduction. Table 2.2 shows an overview of these technologies, along with some technology readiness levels (TRLs). A TRL of 4-6 should be applicable to aircraft with an EIS in 2030 and TRL 3-4 is said to require another 10-15 year of development [12]. Technologies with a TRL of 2-3 are expected to be introduced as a means to reach the climate goals of 2050. Some TRLs are deduced based on the estimated EIS.

[1] Only for combustion chamber and nozzle liner

Table 2.2: List of future aircraft technologies including TRL

FUTURE TECHNOLOGY		
Performance	**Emissions**	**TRL**
Ultra-high BPR engine	Hybrid-/fully electric propulsion	
All composite structure	CMCs with improved cooling technology	4 [15]
Distributed propulsion	Multipoint lean direct injection (MPLDI)	3 [15]
Reduced cruise speed	Intercooled-recuperative aero-engine	4
Unconventional airframe configurations	Improved swirler and front end combustor	4 [15]
Advanced manufacturing	Axially controlled stoichiometry combustor (ACS)	4 [15]
Intentional mistuning	Increased air fraction	4 [15]
Compressor booster	Sustainable aviation fuels	4-8 [16]
	Pulse detonation combustion	2-3 [17]
	Flameless combustion	2-3
	Lean pre-mixed pre-vaporized combustor (LPP)	4-5 [18]
	Water/steam injection	3 [19]
	Next generation TAPS	4 [15]
	Composite cycle engine	2 [20]
	Liquid hydrogen (LH_2)	$\leq$ 7 [21]
	Lean direct injection (LDI)	6 [15]
	Open rotor propulsion	5 [22]
	Inter-stage turbine burner	

As was already mentioned in Section 1.2, there is a need for revolutionary technologies to achieve the climate goals. One way to eliminate almost all emissions is by flying (hybrid-)electric or on LH_2. The difficulty with these concepts is the energy density of the fuel. While the mass energy density of LH_2 is more than three times as much as jet fuel, its volumetric energy density is about three times as low. For batteries, the mass and volumetric energy are both considerably lower (15-50x) than jet fuel. The size of the fuel tanks or fuel cells required to power the aircraft would have to exponentially increase for a linear increase in range, even in combination with lifting airframes like a blended wing-body. This makes these types of propulsion not yet suitable for short-medium ranges and beyond. Another challenge for LH_2 is the drastic change in infrastructure needed to supply hydrogen to the airports.

Another radically different future technology compared state-of-the-art aircraft are the unconventional airframe configurations. The Flying-V mentioned in Chapter 1 is expected to enter service around 2040. According to NASA, other unconventional/advanced airframes like the box-wing or double-bubble configuration are expected to enter service as soon as 2030-2035. Some advanced airframes are designed to rely on different (electric) propulsive concepts compared to the current state-of-the-art, managing promising results in terms of fuel-efficiency. One of these propulsive concepts is the ultra-high bypass ratio engine (UHBPR). The UHBPR (EIS ~2035) is an advanced version of the state-of-the-art turbofans in use today, with a fan diameter much larger to achieve a lower specific thrust and higher propulsive efficiency. The difference in layout compared to an engine with a BPR of 5 can be seen in Figure 2.1. With the addition of a gearbox the low pressure spool can run at a higher rotational speed, decreasing the number of required IPC and LPT stages. This shortens and lightens the engine, although part of the weight savings are offset by the addition of the gearbox and the increased weight of the fan.

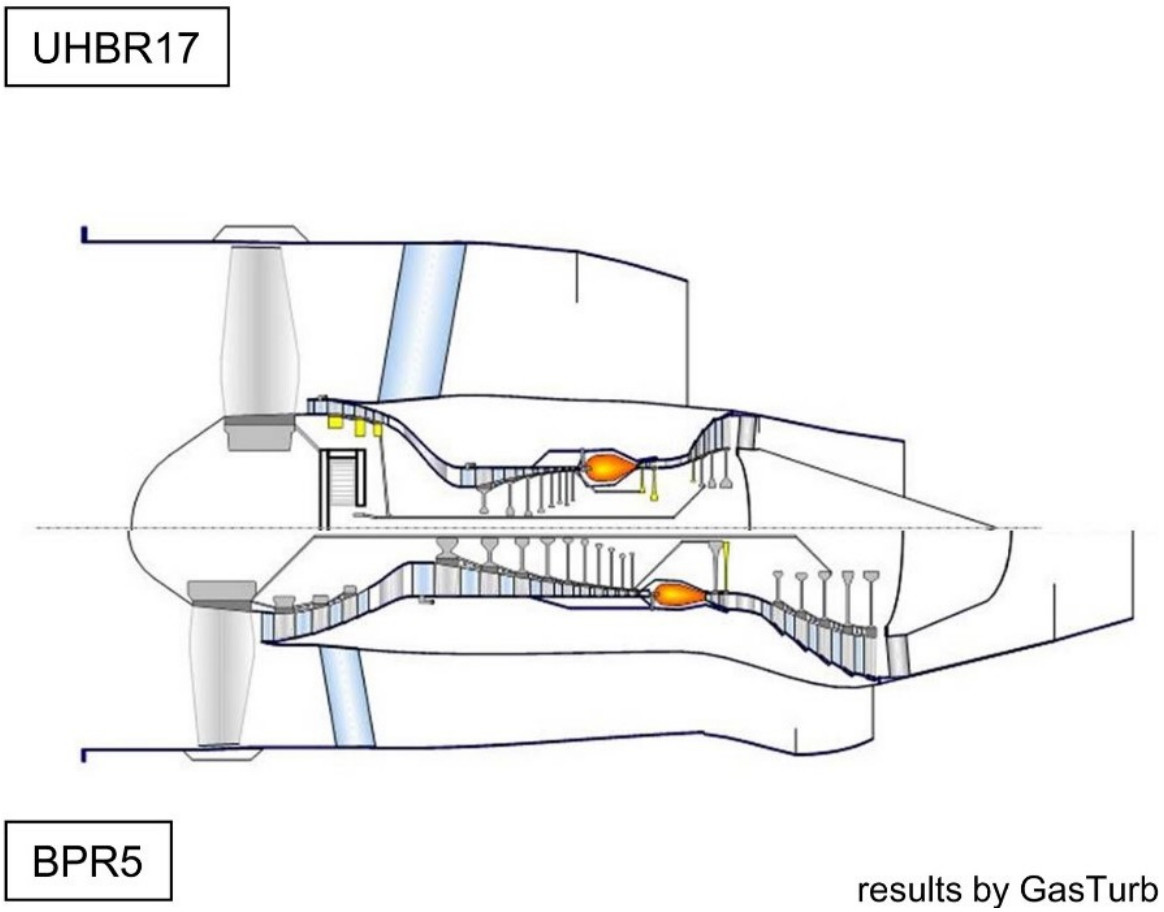

Figure 2.1: Geometry of a UHBPR engine with a BPR of 17 (top) compared to an engine with a BPR of 5 (bottom) [23]

While the use of a very high BPR is mainly beneficial for the thrust specific fuel consumption (TSFC), its conventional architecture allows it to be combined with several future emissions reduction technologies. For example, (MP)LDI, ACS, LPP and the next-generation TAPS are improved low-NO_x combustion techniques that are designed to be integrated into future conventional gas turbines. Next to this, there are also future aircraft technologies that propose new engine architectures. Some architectures, like the intercooled-recuperative aero-engine (IRA) and inter-stage turbine burning (ITB), require less change to the internal engine architecture than more revolutionary concepts like the water injected (water-enhanced turbofan, WET) engine or the composite cycle engine (CCE). The open rotor (OR) also has a similar internal architecture to a conventional turbofan, but with a different fan and nacelle design, as can be seen in Figure 2.2. It has a longer nacelle and total length compared to a conventional turbofan. Next to this, its fan rotors have a much larger diameter than the turbofan. The rotors can also be designed to be contra-rotating. The increased weight due to these changes are compensated by a great decrease in TSFC and in the landing and take-off cycle (LTO) NO_x emissions.

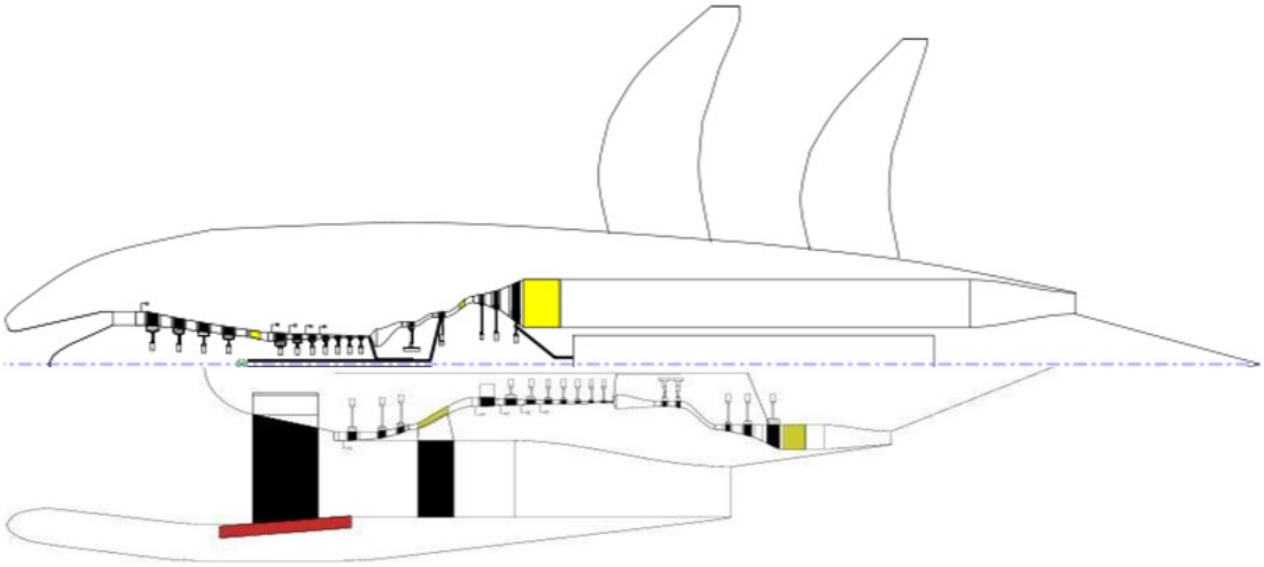

Figure 2.2: Open rotor architecture (top) compared to a conventional turbofan (bottom) (modified from [24])

These alternative architectures promise not only performance enhancement but most importantly a great reduction in emissions. Most emission reduction techniques, including these architectures, are designed such that they will also be compatible with sustainable aviation fuels, reducing the climate impact even further. It would therefore be interesting to look deeper into these alternative architectures and associated thermodynamic cycles further and see how they compare to each other.

2.1.3. Engine architectures and thermodynamic cycles

Aero-engines have been through many redesigns after the first powered aircraft took flight. With the introduction of the gas turbine, the thermodynamic cycle that describes the operation of the engine also changed. This subsection describes the thermodynamic cycles of the conventional gas turbine and OR (Brayton cycle), IRA and ITB (alternative Brayton cycle), the WET engine (Cheng cycle) and the CCE (composite cycle).

Brayton cycle – Conventional gas turbine

Modern gas turbines, the OR engine and the UHBPR engine follow the Brayton cycle (also called Joule-Brayton cycle), as illustrated in Figure 2.3 on the left. The basic (actual) Brayton cycle consists of four processes, from inlet (1) to exhaust (4):

- 1 → 2: adiabatic compression
- 2 → 3: isobaric internal heat addition (combustion)
- 3 → 4: adiabatic expansion
- 4 → 1: isobaric heat rejection (into atmosphere)

The latest generation high BPR gas turbines, operating according to this cycle, reach a thermal efficiency of around 45%. Increasing the OPR, TIT and component efficiencies could drive the thermal efficiency towards 60%, but NO_x emission restrictions set a practical limit of around 55% [8].

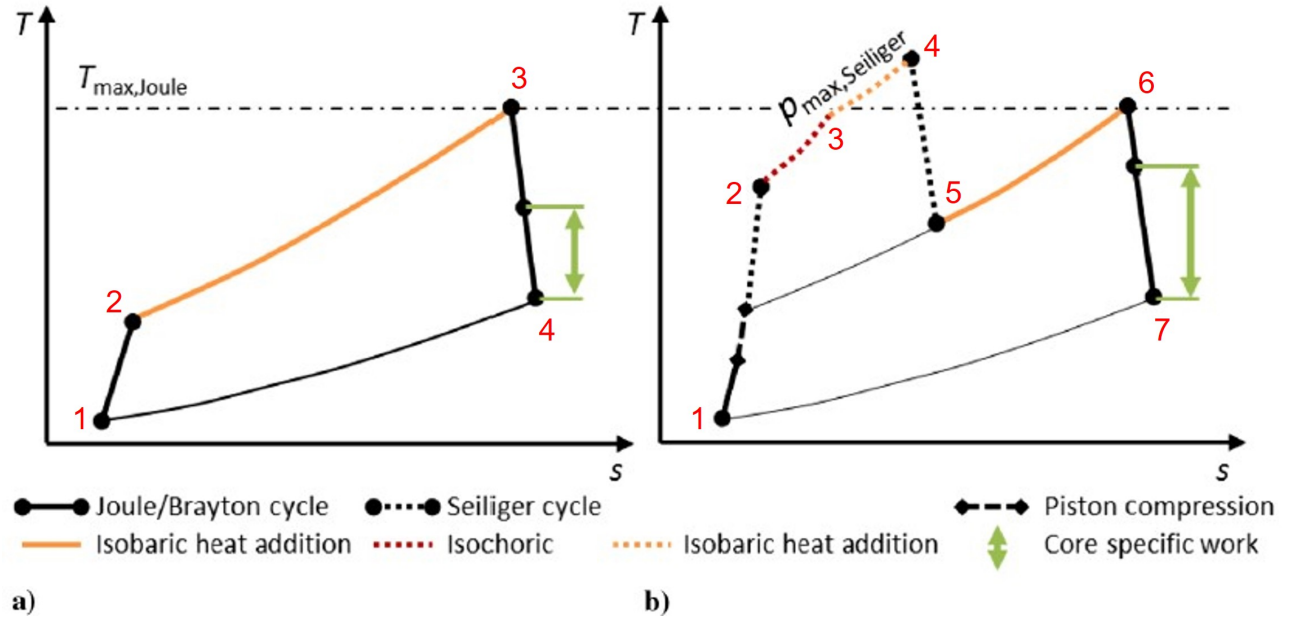

Figure 2.3: T-S Diagram of the basic Brayton cycle (a) and the composite cycle (b)[25]

The previously mentioned concepts of the IRA and ITB both follow an alternative Brayton cycle. The IRA is characterised by a cooling process ($Q_{intercooling}$) between 1 → 2' and exhaust heat addition ($Q_{recuperation}$) at 2' → 3, as seen on the left side of Figure 2.4. An engine with ITB adds another isobaric heat addition process (Q_{ITB})in 3 → 4', shown on the right side of Figure 2.4.

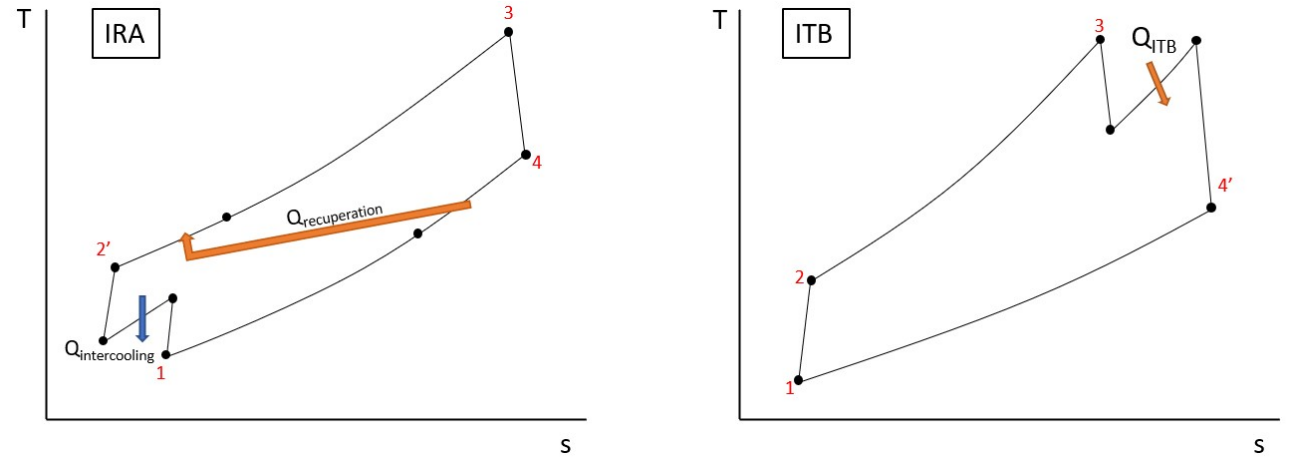

Figure 2.4: Thermodynamic cycles of the IRA (left) and ITB engine (right)

Heat recuperation already improves the thermal efficiency of the engine, but combining it with inter cooling can substantially increase the amount of recuperated heat, adding to the thermal efficiency increase. Although IRA works best at low OPRs (with thermal efficiencies up to 60%), it could provide a higher thermal efficiency than a conventional turbofan up to an OPR around 45-50 [26]. The thermal efficiency is greatly influenced by the heat exchanger effectiveness, decreasing substantially when the heat exchanger effectiveness decreases. The downsides of heat recuperation are the increased combustion inlet temperature, which negatively influences the NO_x emissions, increased weight due to the heat exchangers and the relatively low optimal OPR. A sufficient decrease in fuel burn could however compensate for this.

An engine with ITB can be implemented with a lower HPT and TIT to decrease the NO_x emissions while maintaining the same specific power. Even though lower combustion temperatures decrease the thermal efficiency of the system, the HPT component efficiency is increased substantially due to a reduced need for cooling flow. Next to this, the thrust requirement during take-off can be provided by the ITB, allowing the engine cycle to be optimized for maximum cruise efficiency. This will cause the overall mission fuel burn to decrease compared to a conventional turbofan[8]. ITB can also be combined with intercooling and recuperation, which is investigated in [27]. The downside of an ITB engine is the increased weight and higher CO and UHCs emissions due to a low residence time.

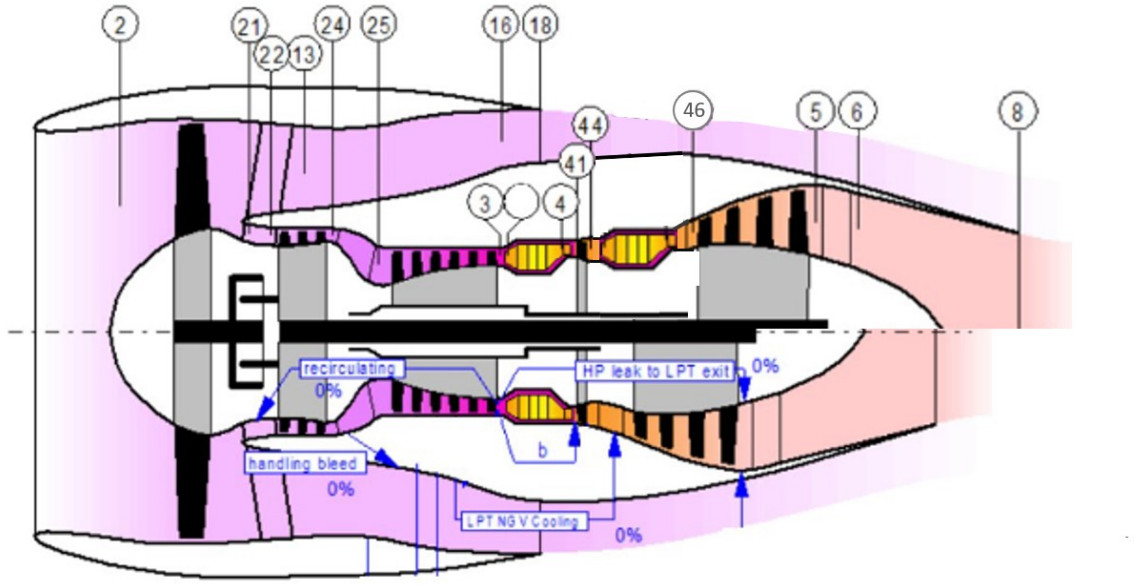

Figure 2.5: Inter turbine burning engine (top) compared to a conventional turbofan (bottom) (modified from [28])

Rankine cycle

The (non-ideal) Rankine cycle describes the thermodynamic process of a steam turbine or reciprocating steam engine, by means of the following four processes:

- 1 → 2: adiabatic compression
- 2 → 3: isobaric external heat addition for vaporisation
- 3 → 4: adiabatic expansion
- 4 → 1: isobaric condensation

A real Rankine cycle is often characterised by superheating the steam in process 2 → 3' to produce a drier steam, hereby preventing water droplet formation and subsequent decrease in turbine efficiency and life-cycle. The Rankine and superheated Rankine cycle can be seen in Figure 2.6.

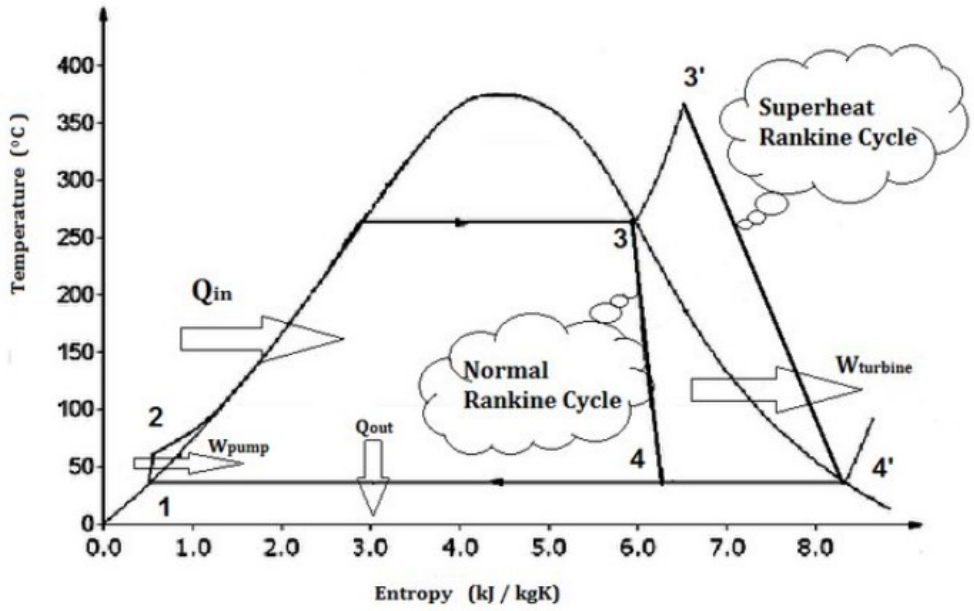

Figure 2.6: T-s diagram of the Rankine and superheated Rankine cycle [29]

Cheng cycle – WET engine

The principle of water injection into a gas turbine is not a new technology. Back in the 1970s, gas-to-gas heat recovery was used for improved cycle efficiency. However, the potential for maximum heat recovery was limited. Using a liquid for the bottoming cycle showed a better heat recovery potential. The Cheng cycle is a parallel dual fluid cycle where gas and steam are used, and is thus a combination of the (open) Brayton and (closed-loop) Rankine cycle. Increasing the Rankine cycle operating temperature to the same as the Brayton cycle turned out to raise the thermodynamic potential of the Ranking working fluid immensely. This cycle describes the operation of the WET engine. A schematic of the wet engine can be seen in Figure 2.7. The exhaust heat from the Brayton cycle is used as the external heat source to vaporise water (5 → 65 in Figure 2.7), which is then expanded by a steam turbine. This is injected as superheated steam into the combustion chamber of the aero-engine (3 → 4), increasing the heat capacity and mass flow rate of the core mass flow. This allows for a higher specific work extraction by the gas turbine (4 → 5). The steam is condensed (65 → 7) and recovered (7 → 8) after the gas turbine in the nozzle and fed back into the vaporiser through a feed pump [19]. The Rankine cycle operating temperature is increased to the same temperature as that of the Brayton cycle, thereby greatly elevating the thermodynamic potential of the working fluid in the Rankine cycle [30]. This combined cycle can reach a thermal efficiency of around 60%, much higher than modern turbofans [31]. The addition of the water condensation and recovery system increases the weight of the engine significantly, offsetting some of the benefits.

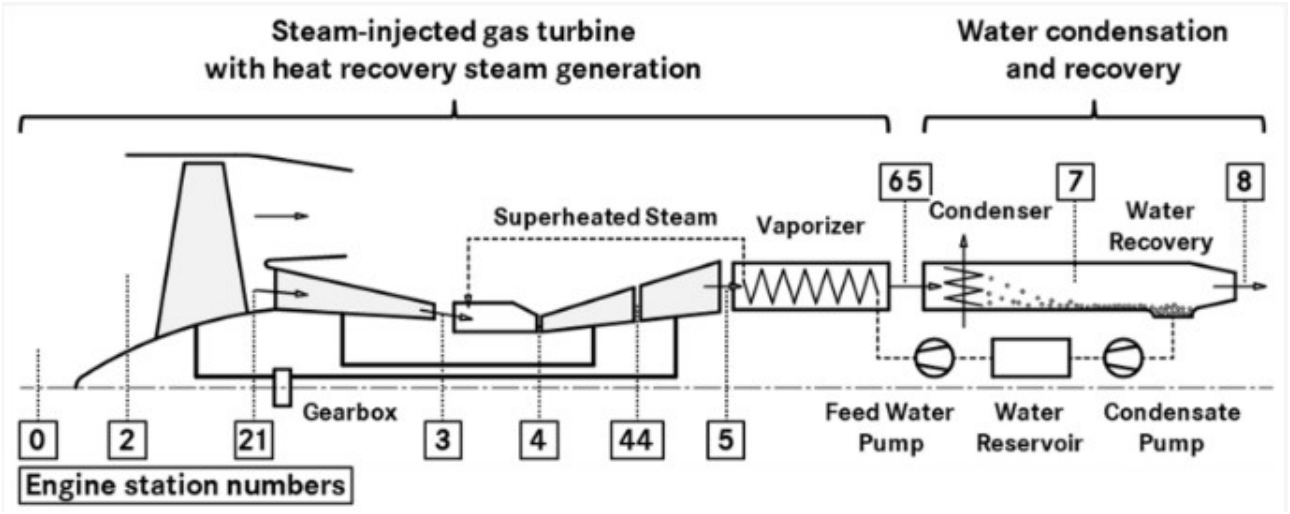

Figure 2.7: Basic schematic of the WET concept with international station nomenclature [19]

Composite cycle – CCE

The composite cycle is used to describe the operating cycle of the CCE. It is a combination of the Seiliger cycle and Brayton cycle. The Seiliger cycle is a combination of the Otto and Diesel cycle. Pre-WWII engines mostly relied on reciprocating piston engines operating according to the Otto cycle. This is a spark-ignited cycle for an internal combustion engine. The Diesel cycle is also an internal combustion engine cycle, but without spark-ignition. Instead, the ignition occurs from heat generated by compression. This dual combustion cycle adds heat partly at constant volume and partly at constant pressure, and can be described by the following processes, illustrated in Figure 2.8:

- 1 → 2: adiabatic compression
- 2 → 3: isochoric heat addition
- 3 → 4: isobaric heat addition
- 4 → 5: adiabatic expansion
- 5 → 1: isochoric heat release

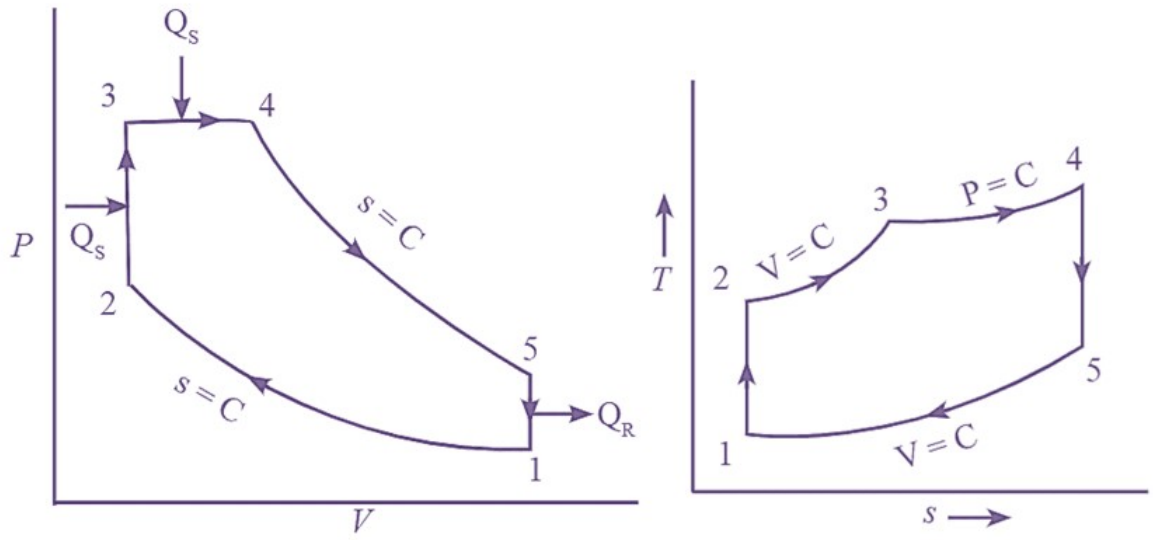

Figure 2.8: T-s and P-v diagram of the Seiliger cycle [32]

The composite cycle can then be described by the following processes, which is illustrated in (b) of Figure 2.3:

- 1 → 2: adiabatic compression (first axial compressor, then piston)
- 2 → 3: isochoric heat addition in piston
- 3 → 4: isobaric heat addition in piston
- 4 → 5: partial adiabatic expansion in piston
- 5 → 6: isobaric heat addition in conventional combustion chamber
- 6 → 7: adiabatic expansion
- 7 → 1: isobaric heat rejection (into atmosphere)

The augmentation of the Seiliger cycle on top of the Brayton cycle increases the specific work that can be extracted from the engine. Next to this, the extremely high pressure due to piston compression increases the thermal efficiency of the CCE compared to a conventional turbofan. A lay-out of the CCE can be seen in Figure 2.9. The piston systems replace the axial HPC and are circumferentially placed around the core of the engine. There are three working principles for a CCE: the piston engine is used to deliver gas work potential, all excess power is used to deliver shaft power, or both.

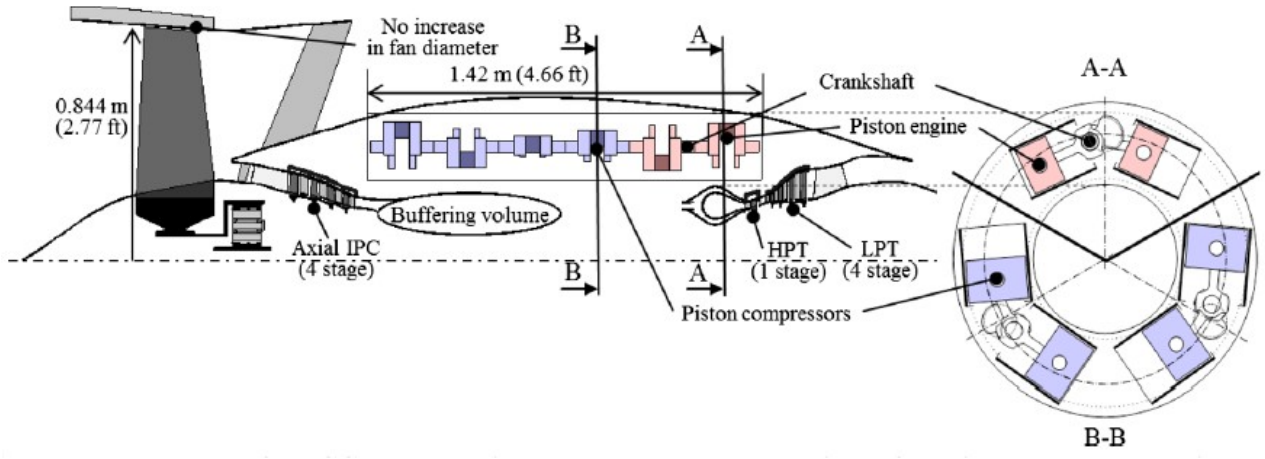

Figure 2.9: Lay-out of the CCE [25]

The overall workings and thermodynamic cycles as described above have shown the potential of the alternative engine architectures compared to the conventional architecture. The increased thermal efficiencies of the alternative thermodynamic cycles should have a positive influence on the total engine efficiency. However, the thermal efficiency is not the only important parameter. To see which architecture shows the most promise should be investigated by

looking at the total improvement potential of the entire engine, which will be done in the next section.

2.1.4. Total improvement potential of future engine architectures

Research into UHBPR engines (depicted in Figure 2.1) has shown a potential TSFC improvement of 23.9% compared to a 2000 engine standard [23], or around 15% compared to 2015 technology standards. The WET concept with an estimated EIS in 2035 shows a 13% increase in fuel efficiency and a possible 90% reduction in NO_x emissions [19]. The CCE, with an EIS of around 2035 as well, is said to provide a 16% fuel burn reduction and a 10% NO_x emissions reduction. However, innovative designs operating according to the Brayton cycle also still show promise for efficiency improvement. The IRA concept, also with an expected EIS around 2035, predicts a TSFC reduction of up to 8% and a NO_x reduction of 10%, with higher reduction potential if used in combination with low-NO_x combustion technology [27]. The OR, ground- and flight-tested in several configurations, is predicted to decrease the fuel consumption by 12-18% while decreasing the LTO NO_x emissions as much as 35% [24]. A more elaborate overview of how these engines compare to their own reference engine can be seen in Table 2.3 and Table 2.4. Dark green indicates an outstanding feature compared to the other concepts, green indicates a good feature, orange a questionable feature and dark orange indicates a bad feature.

Table 2.3: Different conventional architecture concepts and their improvement potential

Architecture	**"Conventional" architecture**		
Concept	**UHBPR**	**IRA**	**Open rotor**
Reference	Year 2000 turbofan	Year 2050 GTF	Year 2015 GTF
Thrust(-SFC)	-23.9% TSFC	Dependent on configuration and heat exchanger type. Range -7% with ITB and SFC to +25% TSFC.	-13% TSFC at TOC -39% TSFC at SLS
Fuel burn	-32.2% block fuel compared to year 2000 engine.	Fuel burn possibly not compensated by TSFC reduction due to increased weight.	-18% and -12% fuel consumption for 500 nm and 3250 nm mission respectively.
NO_x	Slightly lower than GTF	Up to -10% with ITB. Increase due to higher combustion inlet temperature possibly not compensated by TSFC reduction.	-35% in LTO. Higher total NO_x emissions during cruise.
Noise	Increased fan size increases fan noise.	Same noise level as modern turbofans.	Higher noise level than GTF, especially tonal noise. Noise level is low enough for future restrictions.
Weight/volume	Too large nacelle increases weight that offsets efficiency improvement.	Fuel burn possibly not compensated by TSFC reduction due to increased weight.	Additional airframe weight due to integration, 28% lower thrust-to-weight ratio than GTF.
Integration	Ground clearance should be kept in mind, but over-the-wing configuration is also possible.	Innovative core design is required to accommodate the heat exchangers and compensate for weight increase.	Wing or fuselage mounted possible. Noise requires sonic fatigue, structural and additional acoustic treatment of the fuselage.
Complexity & Reliability	Entire engine architecture is similar to modern turbofans, except for a larger fan and nacelle.	Heat exchanger effectiveness is very dominant for overall performance.	Counter rotating fan stages decrease reliability due to additional moving parts, but that can be overcome by having one rotating stage and one row of non-rotating guide vanes.
Adjustments	SAF, (MP)LDI, LPP, ACS, NextGen TAPS, water/steam injection, boundary layer ingestion, ITB.	SAF, LPP, water/steam injection, ITB.	SAF, low NO_x combustion technology, geared.
		IRA with OR, but weight penalty might be too severe.	

Table 2.4: Different alternative architecture concepts and their improvement potential

Architecture	**Alternative architecture**	
Concept	**WET**	**CCE**
Reference	Year 2030 GTF	Year 2025 GTF
Thrust(-SFC)	-13% TSFC for semi-closed cycle -12% specific thrust	-18.2% TSFC at TOC -11.8% TSFC for LTO
Fuel burn	-10% fuel burn, accounted for additional nacelle drag.	-15.2 to -16% fuel burn
NO_x	Up to -90%	-10%
Noise	Increased fan size will likely increases fan noise.	To be investigated.
Weight/volume	Longer nacelle required, weight addition due to water injection and recovery system. Approx. +40%.	High pressure system completely replaced by piston system, but the size remains relatively equal. Overall weight increased by 31%. Compensated by TSFC reduction.
Integration	Ground clearance should be kept in mind. Additional structural and mounting weight are accounted for in the climate impact and fuel burn.	Due to same size engine, integration can be the same as modern turbofans. Internal integration is dependent on function of the piston system.
Complexity & Reliability	New nacelle design required for the core flow. Water recovery dependent on vaporizer and condenser effectiveness. Additional parts due to water injection system.	Reliability is expected to be the same as modern turbofans. Complexity and reliability are both dependent on function of the piston system.
Adjustments	Lean burn combustor could be used, but this could push the flame temperature towards stability limit.	Intercooling could reduce NO_x and thermal problems, but bears another weight penalty.
	SAF, NextGen Taps, ACS	Four-stroke or Wankel type piston to be investigated

It should be noted that these five concepts are all compared to a different technology standard GTF and should thus not be seen as a comparison against the same baseline model. They can also therefore not be directly compared to Table 1.1 in terms of CO_2 reduction potential. To see the actual potential of these different architectures with respect to each other and the current state-of-the-art, a comparison should be made against the same baseline model.

2.2. Architecture comparison

While evaluating the engine improvement potential of five different engine architectures (UHBPR, IRA, OR, WET & CCE), it was apparent that the results of their preliminary studies couldn't be compared to each other directly. Due to limited research on the WET and CCE concepts, there is little literature available on engine advancements in comparison to established engine technologies. The CCE is compared to a "regional GTF from 2025 with a max OPR of 50" [25], while the WET is compared to a "technologically similar GTF from 2030+" [19]. For the IRA concept, the paper that provided the most information on several recuperating architectures and recuperative capabilities (including inter turbine burning and secondary fluid recuperation) compares these concepts to a GTF with a 2050 technology standard [27]. The UHBPR engine was compared to a year 2000 technology level turbofan while the UHBPR itself was modelled according to a 2030 technology standard [23]. Lastly, a NASA study on the performance assessment of the OR compares it to its own 1990s baseline model and a GTF from 2015 [24]. Next to the varying technology levels, the engines and their comparison models all have different design specifications in terms of OPR, BPR, T_{t4}, etc. Thus, there are five different engine architectures, compared to five different turbofans with five different technology levels.

To compare these different engine architectures to each other, all of them need to be compared to the same baseline model. The baseline model will be based on the GTF from 2015 from [24] and the P&W 1100G series. This baseline model is then compared against future GTF models from 2025, 2030 and 2050, which will be designed according to given design specifications in the associated literature. Since the comparison of the architectures with these future models is given in literature, this will then give a comparison between the architectures and the 2015 baseline model. As the UHBPR is based on a year 2030 technology standard, the year 2030 GTF can be adjusted to represent the UHBPR as the internal architecture is very similar. This section describes the set-up of the 2015 baseline model in Section 2.2.1. The future engine models are described in Section 2.2.2. A meaningful comparison is then made in Section 2.2.3, along with the encountered limitations. Section 2.2.4 provides a conclusion on the comparison of the architectures.

2.2.1. Baseline model

An attempt at providing a meaningful comparison between all engines resulted in the formation of a GTF 2015 baseline model, named GTF-2015B, in gas turbine modelling software GasTurb [28]. This model is based on state-of-the art existing GTF, the P&W 1100G series, that entered service in January 2016 and can therefore be deemed technologically equal. The design specifications and performance characteristics of the P&W 1100G series that are publicly available are relatively close to those mentioned in [24]: ≤ 2.7% for thrust (sea level standard conditions), fan diameter, fuel flow and TSFC. The bypass ratio is lower, while the overall pressure ratio is higher. However, this series has sufficient publicly available information to fill in the design specifications that are omitted there, ensuring a technologically equal baseline model.

The OR in [24] is compared to a GTF at the top of climb (TOC). Combining the design specifications of that GTF, as taken from [33], with those of the P&W 1100G series gives the following set values:

- Outer Fan Pressure Ratio (OFPR) = 1.5
- HPC PR = 10.0
- Design BPR = 12.7
- OPR = 28.8
- Thrust = 21.04 kN
- T_{t4} = 1316 K
- Fan diameter = 205.74 cm

GasTurb requires many inputs, such as component efficiencies, altitude, inner fan pressure ratio (IFPR) and many more. The fuel heating value and T_{t4} were taken from the Type Certificate Data Sheet of the P&W 1000G [34], component efficiencies were taken from a performance and optimization GasTurb study on the P&W 1100G series [35]. Realistic guess values for the IPC and IFPR were entered and iterated until the desired OPR was reached, minimising for TSFC.

Running the model showed that the ideal jet velocity ratio V_{18}/V_8 took on an unrealistic value (< 0). After adjusting the engine parameters, it was found that no valid engine model could be produced based on the given inputs. To achieve a valid model the T_{t4} had to be increased to 1540 K, which is a reasonable value for a state-of-the-art aero-engine. After this adjustment, the baseline model provided a reasonable output that can be found in Table 2.5.

Table 2.5: Difference between some output values of the baseline engine GTF-2015B and the given values of the 2015 GTF from [24]

	Value	Difference
Net thrust [kN]	21.04	0.0%
TSFC [g/kNs]	15.10	-
OPR [-]	28.8	0.0%
Fan diameter [cm]	201.30	-2.2%

Since the GTF-2015B model was designed for the same net thrust and OPR as the 2015 GTF, the difference is 0 %. Fan diameter is close to the design value. As there is no available value for the TSFC of the P&W 1100G at TOC, the value cannot be compared to this directly. However, it is about 3.3% lower than the one in [35]. This can be attributed to the use of different component pressure ratios and a different T_{t4}. A TSFC of 13.99 g/kNs is given for the GTF in [24]. This value seems to be very low compared to the TSFCs of the future GTF models from [25], [19] and [27], hence this is not used for comparison. The value of 15.10 g/kNs is instead deemed reasonable for an engine with this technology level.

2.2.2. Future engine models

The engine models for 2025, 2030, and 2050 were developed based on multiple papers that evaluate geared turbofans anticipated to enter service in those respective years. As with the baseline engine, given engine parameters such as pressure ratios, T_{t4} and component efficiencies are used as input values. Input parameters of the GTFs that were not given in the text of the papers were either interpolated/extrapolated or taken from literature on GTFs with the same technology level and similar engine characteristics.

The OPR is expected to increase considerably towards 2050 as this has a large positive influence on the engine performance. As mentioned before, the CCE architecture is compared to a 2025 GTF with an OPR of 50 (labelled GTF-2025). The WET engine is compared to a 2030 GTF, which has an expected OPR in the range 50-65 (labelled GTF-2030). Lastly, the IRA architectures are compared to a 2050 GTF, where OPRs are expected to be closer to 75 (labelled GTF-2050). The IRA concept in [27] is likely based on the MTU Aero Engines intercooled-recuperated concept, which has a OPR of 30 [26]. This value is much lower than the expectation of 75. It was chosen to model GTF-2050 with a much higher OPR (75.4) than 30 to more accurately represent the expected 2050 technology standard. In GasTurb the differences in OPR have a significant effect on the output parameters and most noticeably on the NO_x severity index S_{NO_x}. This would

lead to an unfair comparison, as S_{NO_x} is a function of only the HPC outlet pressure P_{t3} and temperature T_3. Table 2.6 provides a selection of output parameters of the future engine models to show the difference with GTF-2015B, which has a S_{NO_x} of only 0.721 at an OPR of 42.

Table 2.6: Selection of output values of the future engine models

	GTF-2025	GTF-2030	GTF-2050
TSFC [g/kNs]	15.37	13.94	12.81
S_{NO_x} [-]	1.07	1.00	1.82
OPR [-]	50.00	53.00	75.40

The dependence between S_{NO_x} and the OPR is obvious, with the exception of GTF-2030. Although it has a slightly higher OPR than GTF-2025, it has a slightly lower S_{NO_x}, but this can be attributed to a difference other design parameters. The correlation between the TSFC and OPR also shows dependency, but in a less strong manner than S_{NO_x}. To provide a good comparison, the future engines are therefore first modelled according to the available engine characteristics, after which they are scaled. How the output parameters of the future engine models compare to a selection of original design specifications can be seen in Table 2.7.

Table 2.7: Selected output parameters of the future engine models with the difference between their original design specifications

	GTF-2025	**% diff.**	GTF-2030	**% diff.**	GTF-2050	**% diff.**
Net trust [kN]	18.40	**0.0**	21.00	**0.0**	49.97	**0.00**
TSFC [g/kNs]	15.37	**-0.5**	13.94	**-1.8**	12.81	**-8.30**
fuel flow [kg/s]	0.283	**-0.5**	0.293	**-1.8**	0.640	**-8.30**
OPR [-]	50.00	**0.0**	53.00	**0.0**	75.40	**0.00**
Fan diameter [cm]	167.0	**-1.1**	217.2	**-1.3**	284.0	**-0.01**

All models show good correlation with the given output parameters of the respective GTFs (≤1.8 %). The only noticeable differences are the TSFC and fuel flow of the GTF-2050 engine. Since there is limited research on 2050 engines, the design parameters were taken from different papers with similar engine characteristics. As mentioned before, the OPR was increased significantly, lowering the fuel flow and hence also the TSFC compared to the 2050 GTF from [27]. Since the future engine models will be scaled down towards an OPR of 42 corresponding to GTF-2015B, this discrepancy will not have a significant effect on the engine architecture comparison. The scaling was done by varying the engine characteristics that were not specifically mentioned in the paper, most often being the IFPR, intermediate pressure compressor (IPC) PR or the HPC PR.

2.2.3. Comparison against baseline model

With all engine models now established, a proper comparison can be made between the engine architectures. The results of the comparison can be found in Table 2.8, where the architectures are compared to GTF-2015B in terms of TSFC and NO_x decrease. GasTurb outputs a value for S_{NO_x} as a function of P_{t3} and T_3, which can be linearly scaled to EI_{NO_x} by multiplying with 23 (dual annular combustor) or 32 (conventional combustor) [36]. This does not take T_{t4} into account, which has a significant influence on the production of thermal NO_x. Since it would be interesting to compare this as well, a correction is applied to the value for EI_{NO_x} by means of Equation (2.1) [27]:

$$EI_{NO_x} = 0.007549 \cdot T_{t4} \cdot \left(\frac{P_{t3}}{30.267985}\right)^{0.37} \cdot exp\left(\frac{1.8T_3 - 1471}{345}\right) \tag{2.1}$$

Table 2.8: Comparison between GTF-2015B and the four different engine architectures

	ΔTSFC [%]		ΔS_{NO_x} [%]		ΔEI_{NO_x}
	Associated GTF	GTF-2015B	Associated GTF	GTF-2015B	GTF-2015B
OR	-13.4	**-19.7**	-35.4	-35.3	-26.6
CCE	-18.2	-16.3	-10.0	-0.3	+17.4
WET	-13.0	-16.8	-90.0	**-90.3**	**-90.2**
IRA	-7.3	-10.0	-10.0	-12.0	+7.8
UHBPR	-23.9	-16.1	N/A	-12.9	-1.12

The left side of the $\Delta TSFC$ and ΔS_{NO_x} columns correspond to the difference of the architectures with their respective GTF engine models from the associated literature papers. The right columns correspond to the difference with GTF-2015B based on the same OPR and thrust output as the baseline. For ΔEI_{NO_x} the column corresponds to the value of EI_{NO_x} based on Equation (2.1), with the pressure and temperatures taken from GasTurb.

With the largest decreases indicated in bold, in can be seen that the OR has the largest TSFC improvement compared to the baseline engine even though the UHBPR promised the biggest improvement. This is not surprising, since the UHBPR was compared to a 2000 reference engine and its improvement potential is therefore overestimated compared to a 2015 GTF. The actual value for TSFC is the lowest for the OR, making this the most fuel efficient concept. The CCE, WET and UHBPR also show a significant improvement compared to GTF-2015B. Since the IRA was already modelled with a technology level of 2050, its improvement potential of 10% is very low compared to the other concepts. Looking at the NO_x emissions, the decrease is largest for the WET engine. The reduction of 90% stated in [19] was a much larger reduction than any of the other architectures, so this is not a surprising result. The high T_{t4} of the OR, CCE, IRA and UHBPR compared to GTF-2015B make these concepts perform worse in terms of EI_{NO_x} compared to S_{NO_x}. Again, as the IRA is modelled with 2050 technology, an increase of 7.8% is exceptionally large. It should also be mentioned that for the OR, a value of -35% was chosen for the calculations for NO_x. However, this is only the decrease during LTO operations. As mentioned in [24], the total NO_x emissions for the entire mission are actually higher than that of the reference engine. Additionally, the design point for GTF-2015B is TOC, thus the NO_x reduction of OR is severely overestimated.

Limitations and accuracy

There are several limitations with GasTurb and this analysis:

- Not all design specifications that are required as input for GasTurb are mentioned in the papers where the architectures are compared to their different technology GTFs. These values were taken from other papers or interpolated, possibly decreasing the accuracy of the results.
- S_{NO_x} and subsequent EI_{NO_x} are only based on P_{t3}, T_3 and T_{t4}. While there is an adjustment for S_NO_x to represent a conventional or dual annular combustor, this might not be very accurate and does not take into account all different types of existing and future combustors. The NO_x indices might therefore not be accurate representations of the actual NO_x reduction.
- The ideal jet velocity ratio V18/v8 takes on a non-realistic value for some of the given combinations of BPR, FPR, OPR and T_{t4} in literature. Optimisation towards a desired ratio < 1 proved to be impossible by only changing some of the unspecified design parameters. As V18/V8 is very sensitive to a change in T_{t4}, this required a deviation of the presented value in [27] for GTF-2050.
- The software does not consider engine weight and drag increase for a larger fan diameter (as a result of a larger BPR) on the total aircraft, which would influence the TSFC and emissions in real scenarios.

2.2.4. Architecture comparison conclusion

In this analysis, the IRA has the smallest improvement compared to the GTF-2015B in terms of TSFC, the OR the largest. This was expected as this is in accordance with the TSFCs given in the associated studies. The WET engine shows the greatest improvement potential in terms of NO_x emissions, the CCE performs the worst. Taking T_{t4} into account by using the EI_{NO_x} metric, both CCE and IRA show a significant increase in NO_x emissions. The actual effect of the higher combustion inlet temperature due to recuperation is not taken into account for the IRA, so in reality the increase would be even greater. Although the IRA engine shows some improvement compared to GTF-2015B in terms of TSFC, IRA is only expected to be applied to engines with a lower OPR. Also, as mentioned in [27], the TSFC and NO_x decrease depend highly on the configuration. The IRA used in this analysis was based on a high-heat-exchanger-effectiveness with ITB concept. A slight change in heat exchanger effectiveness can be very dominant for the overall performance of this concept, making the option less desirable.

The UHBPR shows a similar TSFC reduction compared to the CCE and WET. Since all architectures are expected to be introduced between 2030-2035, the analysis also shows how competitive the concepts might be to each other on the market. As was stated in [24] and Section 2.2.3, the total NO_x emissions of the OR might be higher than the UHBPR due to the higher cruise emissions. The UHBPR is also more suitable to fly longer distances compared to the OR due to lower noise levels and might ease aircraft integration compared to both OR and WET, as these alternative architectures require changes to the engine itself (with a weight penalty) and the airframe for installation. Although the UHBPR does not rival the NO_x reduction of the WET in this analysis, combining the aforementioned benefits with low emissions technology like lean direct injection or steam injection, the UHBPR could rival the proposed alternative architectures. As of today, there has been no publication on such a combination of several future engine technologies. It would therefore be valuable to perform a study on this to determine whether the future iteration of the conventional turbofan is able to rival the performance of alternative architectures, or whether the engine design direction should shift towards alternatives.

3
Methodology

The conflicting design choices for an engine design with a lower TSFC and an engine with lower NO_x emissions calls for a combination of novel aero-engine technologies capable of achieving both design goals. This chapter describes the approach towards the design of an engine model with a combination of such technologies. First, the software in which the engine models were made is explained in Section 3.1. The state-of-the-art reference engines against which the future engine models will be compared later are introduced in Section 3.2. Next, Section 3.3 elaborates upon the current, environmental and future engine design drivers. Lastly, Section 3.4 discusses which future low-NO_x combustion techniques will be employed in the future engine models and how their NO_x performance can be measured.

3.1. Gas turbine modelling software

There are several tools available for engine modelling. Gas turbine modelling software GasTurb allows for optimisation of completely pre-programmed gas turbine models, such as single and multi-spool aero-engines or industrial gas turbines [28]. The Gas Turbine Simulation Program (GSP) is a gas turbine modelling software that allows for modular engine design, where pre-defined components such as inlet, fan, compressor, combustor, turbine and exhaust can be connected by the user, either directly or through ducts. Additionally, GSP offers a library with control components that can be used to control design values, off-design outputs and more. Both programs use a zero-dimensional modelling approach and a Newton-Raphson based iteration solver, which solves the non-linear differential equations for the conservation of mass, energy and momentum. The working gas properties are modelled according to the ideal gas law.

GasTurb

One feature that makes GasTurb very suitable for modelling the baseline future engines (BF-models) is the optimisation tool. This tool requires the input of variables and constraints between certain ranges and an optimisation parameter set by the user. The program then searches for a design by means of iteration for the optimisation parameter that is also set by the user. There are several optimisation options. By choosing the 'endless random' option, GasTurb randomly selects a starting point around the best solution found previously and adapts variables within their set ranges to provide a result that does not violate the constraints, while moving towards a minimum or maximum of the optimisation parameter. After an optimum is found, this option selects a new point away from the present point automatically and endlessly. By choosing the 'systematic' optimisation option, GasTurb systematically combines the variables starting with the design values until a minimum or maximum is reached. Choosing the 'systematic' option immediately might cause the program to find a local minimum and not the overall minimum. It was therefore chosen to apply the 'endless random' option until the design appeared to have reached close to the overall minimum. When the provisional minimum did not appear to change after many new random starting points, the optimisation was stopped. Then, to move closer to that local and apparent overall minimum, a new optimisation can be performed with the 'systematic' option, which is a gradient search, until that minimum is found. This ensures a design that was a close to or equal to the actual optimum. The parameters that are optimised are thoroughly explained in section 4.1.2. After the optimised BF-models are constructed, the off-design performance can be evaluated in GasTurb as well.

GasTurb uses station numbering as illustrated in Figure 3.1, which will be used throughout the entire thesis.

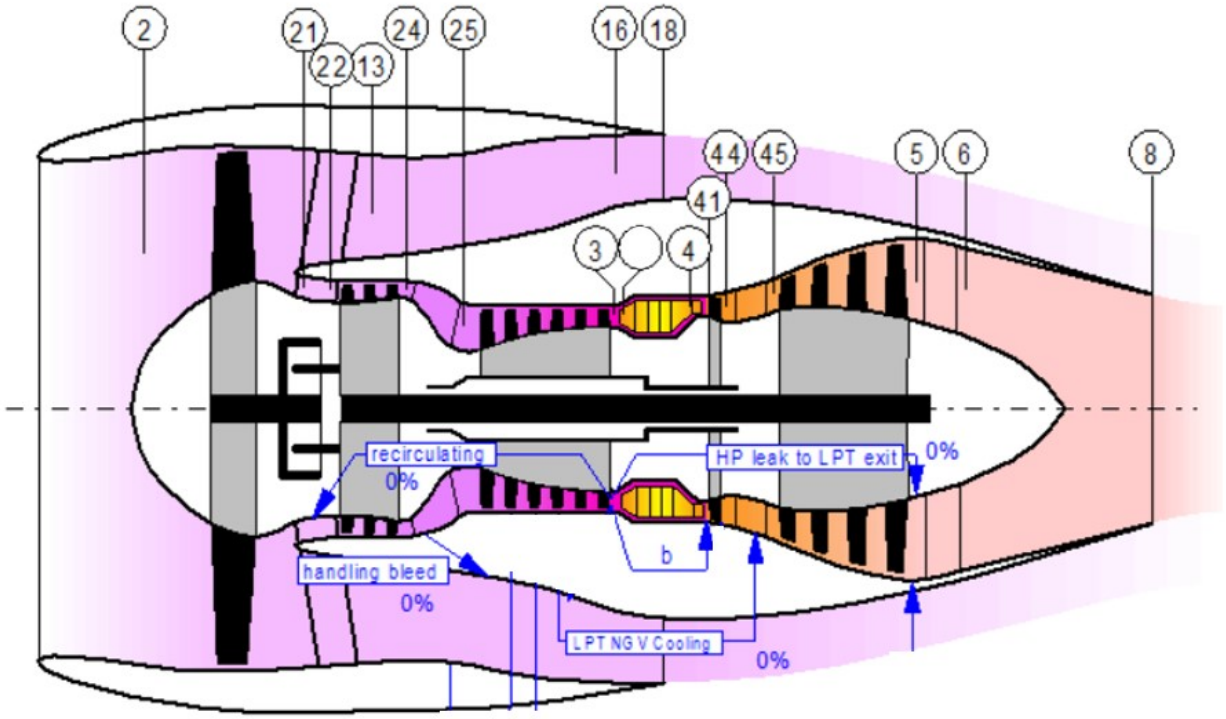

Figure 3.1: Numbering conventions for thermodynamic stations (modified from [28])

GSP

The features of GasTurb are not sufficient for making the upgraded future engine models (UF-models). An ITB aero-engine is not available in the GasTurb library and water injection can only be done in the 1-spool, 3-spool or geared mixed turbofan option from the GasTurb library. The BF-models from GasTurb can be recreated in GSP, after which design and off-design calculations can be performed to match them with the results of GasTurb. As the standard component maps for GSP are different than for GasTurb, the component maps from GasTurb should be loaded into GSP to reproduce the GasTurb off-design results as accurately as possible. A series of off-design calculations can then be performed with the future low-NO_x techniques implemented to review their performance under different conditions.

3.2. Reference engines & baseline models

To evaluate the performance of a combined-technology future turbofan engine in 2035 and 2050, first two state-of-the-art baseline models (B-models) should be constructed. It was chosen to model the direct-drive variant according to the CFM LEAP-1A26 engine, which currently powers the Airbus A320 family. This aircraft, along with the Boeing 737 MAX variants, is expected to dominate the single-aisle aircraft fleet until at least 2035. The other engine option for the Airbus A320 family is a geared variant: the Pratt & Whitney PW1127G, which can be used as the baseline for the GTF. This section describes the comparison of the state-of-the-art baseline models to their real-life counterparts in terms of performance in Section 3.2.1 and in terms of emissions in Section 3.2.2.

3.2.1. Baseline engine performance

There is limited information available on modern engines. However, EASA type certificate data sheets and the ICAO emissions databank provide some manufacturer information and ground testing data for take-off (T/O), climb out, approach and idle conditions. The engine specifications for the LEAP-1A26 and PW1127G can be found in Table 3.1 [37], [38]:

Table 3.1: Publicly available engine specifications of the LEAP-1A and PW1100G

Engine specifications (at T/O)	LEAP-1A26	PW1127G
OPR [-]	33.3	31.7
BPR [-]	11.1	12.3
Net thrust [kN]	120.64	120.43
Fuel flow [kg/s]	0.861	0.800
Fan diameter [cm]	198	206
Max. LPT inlet temperature [K]	1333	1356
Gear ratio [-]	N/A	3.0625
Maximum LP spool speed [rpm]	3894	10047
Minimum LP spool speed [rpm]	-	1801
Maximum HP spool speed [rpm]	19391	22300
Minimum HP spool speed [rpm]	-	12400
Fan-IPC-HPC-HPT-LPT stages	1-3-10-2-7	1-3-8-2-3
Power offtake [kW]	0	0
Overboard bleed [kg/s]	0	0

The state-of-the-art baseline engine models (B-models) were made in gas turbine modelling software GasTurb [28]. Using the values from Table 3.1 as off-design specifications, the engine models were translated to a top of climb (TOC) design condition (altitude = 10668 m, Mach = 0.78, ΔT from ISA = +10 K) by iteration. The TOC design parameters were adjusted until a satisfying correlation with the T/O condition was achieved. Starting values for component efficiencies, pressure ratios and TIT were based on engines with a similar thrust output and were translated and iterated to match the current technology level and T/O engine specifications. As GasTurb uses modelling assumptions, an error margin of <2% (with the publicly available engine specifications from Table 3.1) was deemed sufficient to accurately represent the LEAP-1A and PW1100G engines. Table 3.2 shows the difference between the B-models (suffix -B) and their real-life counterparts. A full overview of the B-models parameters can be found in Appendix A

Table 3.2: Comparison of B-models with the LEAP-1A26 and PW1127G at T/O

Engine specifications (at T/O)	DDTF-B	diff. [%]	GTF-B	diff. [%]
OPR [-]	33.3	0	31.7	0
BPR [-]	11.1	0	12.3	0
Net thrust [kN]	120.64	0	120.43	0
Fuel flow [kg/s]	0.874	1.51	0.814	1.75
Fan diameter [cm]	194	-1.86	205	-0.7
Gear ratio [-]	N/A	N/A	3.06	0
Power offtake [kW]	0	0	0	0
Overboard bleed [kg/s]	0	0	0	0

An important output from the TOC design point calculations was the net thrust for both engines, such that the future models can be compared to the B-models for the same thrust output. For the B-models, a selection of important engine characteristics at TOC is given in Table 3.3. Since the geared option (GTF-B) and the direct-driven option (DDTF-B) have a close TOC net thrust, a comparison between these options will be more meaningful.

Table 3.3: Selection of design characteristics at TOC of the GTF and DDTF state-of-the-art baseline models (suffix -B)

	DDTF-B	GTF-B
F_N [kN]	25.99	26.60
TSFC [g/kNs]	14.96	14.40
OPR [-]	41.07	41.60
BPR [-]	10.9	12.1
F_S [m/s]	126.5	120.2

3.2.2. Baseline engine emissions

There are many different semi-empirical NO_x correlation equations for different types of combustion. Kaiser et al. evaluated an upgraded version of the WET engine that was discussed in Section 2.1.3 and mention seven different NO_x emissions correlations from multiple sources that can be based on an offset, technology factor, mass flow, residence time, humidity/water-to-air ratio (WAR), temperature(s) and/or pressure(s) [19]. They also formulate a new NO_x

correlation specifically suitable for a WET engine. In an attempt to identify what equation fits best for the specific type of engines that will be used in this thesis, a test was performed with the following equations:

$$EI_{NO_x} = 32 \cdot EXP\left(\frac{T_{t3}-826}{194}\right) \cdot \frac{P_{t3}}{100 \cdot 29.65} \cdot TF \cdot EXP\left(\frac{-0.2465 \cdot WAR^2 - 0.915 \cdot WAR}{WAR^2 + 0.0156}\right) \tag{3.1}$$

$$EI_{NO_x} = 32 \cdot EXP\left(\frac{T_{t3}-826}{194} + \frac{6.29 - 100 \cdot WAR}{53.2}\right)\left(\frac{P_{t3}}{29.65}\right)^{0.4} \tag{3.2}$$

$$EI_{NO_x} = 23 \cdot EXP\left(\frac{T_{t3}-826}{194} + \frac{6.29 - 100 \cdot WAR}{53.2}\right)\left(\frac{P_{t3}}{29.65}\right)^{0.4} \tag{3.3}$$

$$EI_{NO_x} = 2.2 + 0.1235 \cdot EXP\left(\frac{T_{t3}}{194.4}\right) \cdot P_{t3}^{0.4} \tag{3.4}$$

$$EI_{NO_x} = (8.4 + 0.0209) \cdot EXP\,(0.0082 \cdot T_{t3})\left(\frac{P_{t3}}{30}\right)^{0.4} \cdot EXP\,(19(0.006344 - WAR))\left(\frac{T_{t4}-T_{t3}}{300}\right)^{TF} \tag{3.5}$$

In all equations, EI_{NO_x} is the NO_x emissions index in g/kg, T_3 and P_{t3} are the combustor total inlet temperature (in K) and pressure (in bar), T_{t4} is the turbine inlet temperature, WAR is the water-to-air ratio and TF is a technology factor that is dependent on the thermodynamic cycle and can be adjusted to represent more aggressive future cycles. Both Equation (3.1) and Equation (3.5) allow for a modification with the TF to account for the use of more aggressive, high pressure ratio cycles in the future.

To determine which correlation fits best with the EI_{NO_x} for modern-day engines, all correlations should be evaluated and compared to emissions data from [39]. The PW1127G employs an RQL combustor, while the LEAP-1A26 makes use of the TAPS II lean burning combustor. The RQL combustor of the PW1127G currently has a lower EI_{NO_x} during landing and take-off cycles, so the emissions cycle data from this combustor were used as a reference to determine the best fit between the different NO_x correlations. Table 3.4 shows the differences between the EI_{NO_x} calculated with the respective equations and the original values from [39]. The best values are indicated in bold.

Table 3.4: Evaluation of several NO_x correlations with a modern RQL combustor

PW1127G	Ground test value [g/kg]	Eq. 3.1 [%]	Eq. 3.2 [%]	Eq. 3.3 [%]	Eq. 3.4 [%]	Eq. 3.5 [%]
Take-off	20.81	-16.98	39.04	**-0.07**	24.35	**0.79**
Climb out	16.95	-24.04	38.32	**-0.58**	26.20	**0.41**
Approach	10.59	-51.17	22.28	-12.11	25.97	**0.79**
Idle	5.20	-87.27	-30.47	-50.03	**1.04**	**1.43**

Equation (3.1), Equation (3.2) and Equation (3.4) all deviate more than 20% on average from the original values when compared to the modern day GTF engine model. Although Equation (3.3) shows a good correlation with the take-off and climb out results, the approach and idle phases have a deviation of 12% and 50% respectively. Equation (3.5) fits almost perfectly within the ranges of the ambient test conditions of the PW1127G. This makes sense, as this equation was formulated to be especially suitable for RQL combustors. With the option of adapting this equation for future cycles by means of the technology factor TF, this correlation shows the most promise for evaluation of the NO_x emissions for the future engine models.

3.3. Engine design drivers

There are several trends that can describe modern engine design. Historical trends like increasing the OPR and TIT have shown a steady increase in thermal efficiency, while increasing the BPR contributes to the propulsive efficiency, leading to a higher overall engine efficiency. This has a positive influence on the economical and environmental desire to decrease the TSFC and therefore also the CO_2 emissions. However, the climate impact caused by other exhaust gases are shifting the focus from engine performance enhancement to total emissions reduction. To get a good understanding of the required design direction, it is important to know what drives engine design. This section describes the engine design drivers based on a parametric study performed on an engine model of a modern turbofan in Section 3.3.1 and the newest environmental goals set by European and international aviation organisations in Section 3.3.2. Section 3.3.3 concludes which of the design drivers are to be taken into account for future engine design and which technologies should be used for the upgraded future engine models.

3.3.1. Parametric design drivers

Although an aero-engine has many different design parameters, changing some have greater influence on the engine performance than changing others. It is well known that a high OPR and TIT contribute to a the thermal efficiency, while a large BPR has a positive influence on the propulsive efficiency. To examine which design parameters have the largest influences on certain performance characteristics, a parametric study was performed to asses the effect of changing several design parameters on TSFC, NO_x emissions index, specific thrust F_s, thermal efficiency η_{th} and propulsive efficiency η_p. The parametric study was performed by varying the outer fan pressure ratio (OFPR), inner fan pressure ratio (IFPR), intermediate pressure compressor pressure ratio (IPR), high pressure compressor pressure ratio (HPR), bypass ratio (BPR), turbine inlet temperature (TIT) and cooling percentage of the HPT by 5% and 10% in both directions. The B-model for the geared turbofan (GTF-B) was used for this analysis.

The parametric study was evaluated by taking the absolutes of the largest percentual differences of each parameter. For the IFPR, IPR, HPR, BPR and cooling percentage of the HPT, the largest difference was between -10% and +10%, which is as expected. The ideal jet velocity ratio $\left(\frac{V18}{V8}\right)_{id}$ is very sensitive to changes in the OFPR and TIT, causing invalid runs for the OFPR +10% and the TIT -10% cases. These cases were therefore not taken into account in the parametric study.

The results of the study can be found in the form Table 3.5, where the effect of increasing each parameter is shown, and in the form of spider plots in Figure 3.2. In Table 3.5, a parameter that is both the most dominant parameter and has a positive effect is marked in green. A parameter that is both the most dominant parameter and has a negative effect is marked in red. If a parameter is both the most dominant parameter and has a negative effect, it is marked in red. It should be noted that all values in Figure 3.2 are absolute values, thus it does not have to signify an increase in both a parameter and a characteristic. For example, decreasing the IFPR by 10% increases the TSFC by 1.77%, while increasing the IFPR by 10% decreases the TSFC by 1.53%. The total effect of the IFPR on the TSFC is thus 3.30%, which is the given value in Figure 3.2a for the IFPR.

Table 3.5: Effect of increasing each parameter on certain engine characteristics

Parameter	TSFC	NO_x	η_{th}	η_p	η_{tot}	Sp. Thr.
HPR↑	↓	↑	↑	↑	↑	↓
IPR↑	↓	↑	↑	↑	↑	↓
BPR↑	↓	-	-	↑	↑	↓
IFPR↑	↓	↑	↑	↑	↑	↓
OFPR↑	↓	-	-	↓	↓	↑
TIT↑	↑	↑	↑	↓	↓	↑
Cooling↑	↓	-	↓	↑	↓	↓

It can be observed in Figure 3.2b, Figure 3.2d and Figure 3.2e that the TIT is the most dominant parameter for the propulsive efficiency, thermal efficiency and specific thrust respectively. Specific thrust is marked in orange, as both high and low specific thrust can be beneficial. High specific thrust indicates a low inlet mass flow for a certain thrust output (thus a smaller inlet area and overall engine size), but low specific thrust engines are more fuel efficient. Generally, for large transportation aircraft, a lower specific thrust is more favourable. In terms of the overall efficiency, shown in Figure 3.2f, the BPR is the most dominant parameter. This is due to the contradicting effect of increasing the TIT, where the thermal efficiency increases as well, but the propulsive efficiency reduces. Therefore, the TIT is not the most dominant parameter for the total efficiency. When looking at the TSFC in Figure 3.2a, the OFPR is the dominant parameter. Adjusting the cooling percentage shows the least effect in all cases. This is because the cooling percentage mainly influences the efficiency of just one component and causes a much smaller gas temperature change than the TIT.

3.3.2. Environmental design drivers

The environmental design drivers are a result of European and international guidelines on CO_2 and NO_x emissions stated in Chapter 1.

CO_2

CO_2 emissions are directly related to the fuel consumption of the aircraft and can be be lowered by making the aircraft more fuel efficient. As was shown in Figure 3.2a and Table 3.5, an increase in OFPR lowers the TSFC the most. Increasing the OFPR increases the exhaust velocity of the bypass. It has been shown that the optimal TSFC is often achieved when the ratio between the bypass and core exhaust is around 0.75-0.8. Thus, to achieve its optimal TSFC, the TIT should be increased to achieve this. This can be aided by increasing the OPR. Section 1.2 states and 55% CO_2 emissions reduction in 2030 in the EU while also achieving a 2% fuel efficiency improvement per annum up to 2050.

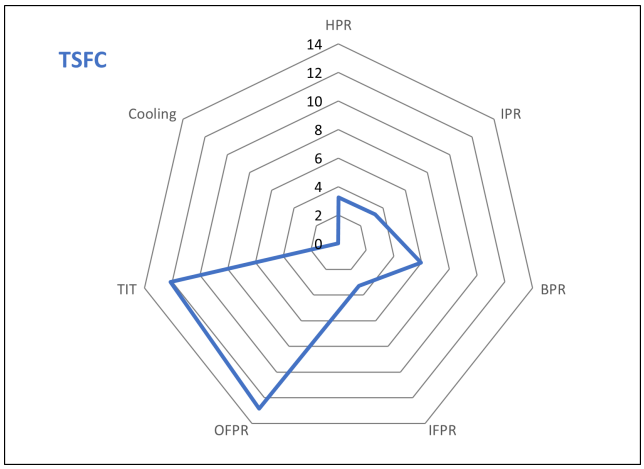

(a) TSFC

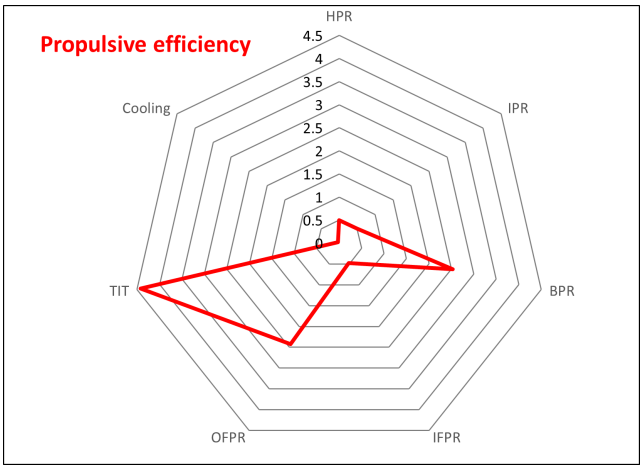

(b) Propulsive efficiency

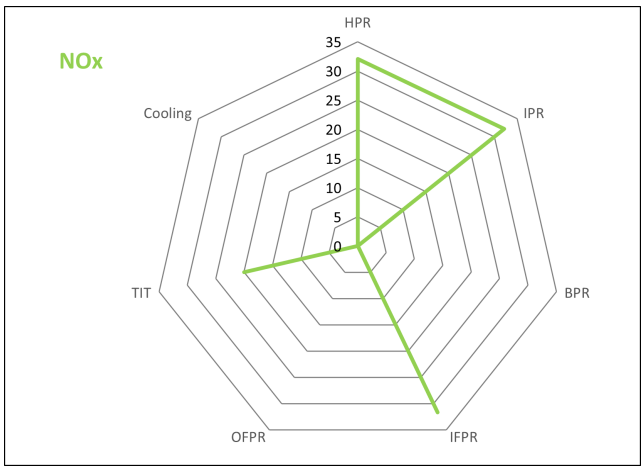

(c) S_{NO_x}

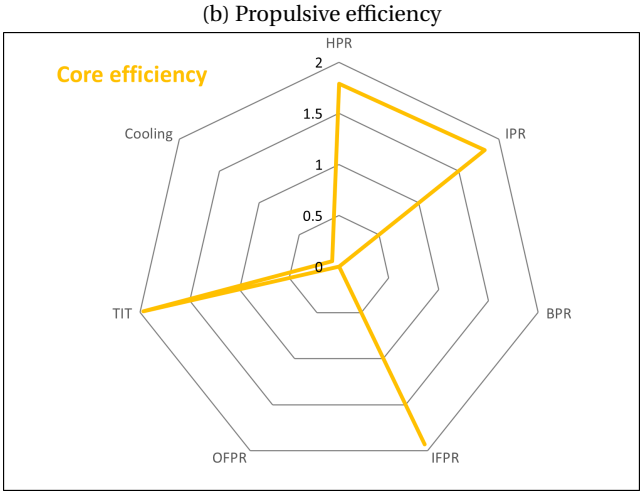

(d) Thermal efficiency

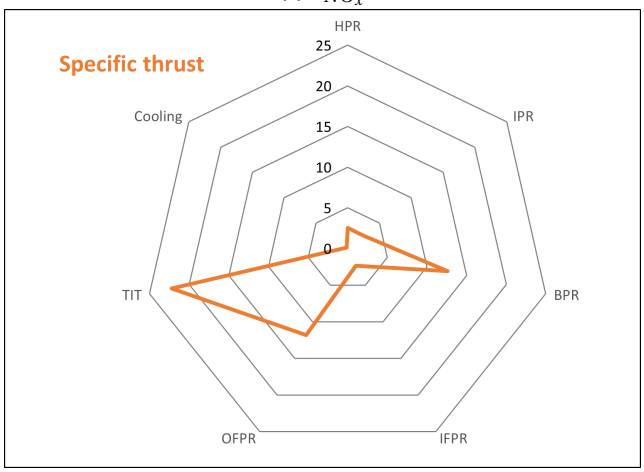

(e) Specific thrust

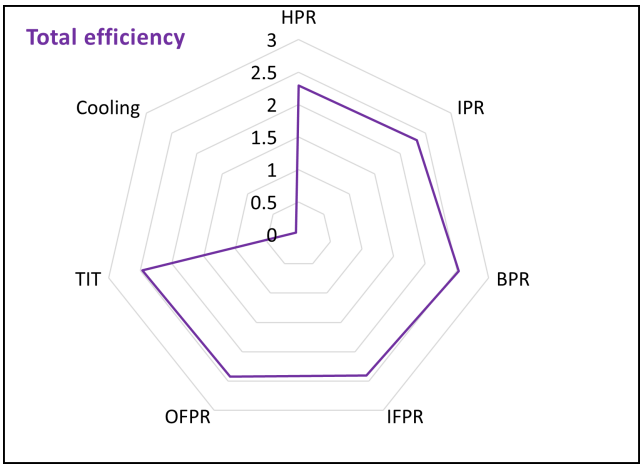

(f) Efficiency

Figure 3.2: Results of the parametric study. The values represent the sensitivity (in %) of the engine characteristics to a percentual change in each of the parameters ranging from -10% to +10%.

From 2050 onward, the CO_2 emissions should be net-zero. It was estimated that in 2035, a fuel efficiency improvement of 22% can be achieved for single-aisle aircraft, taking into account a 10% efficiency improvement of the engine [15]. Following the 2% per annum, the fuel improvement in 2035 should be around 26% compared to today's engines, requiring an even higher engine improvement percentage to achieve this climate goal. This means that the TIT and OPR would ideally be increased considerably.

NO_x

From Figure 3.2c and Table 3.5 it can be seen that such an increase in TIT and OPR is detrimental for the NO_x emissions. Even though NO_x emissions would naturally decrease slightly with decreasing fuel burn, more thermal NO_x is formed when the combustion temperature is increased, offsetting the reductions from a lower fuel burn. Thus, achieving the NO_x emission goals from Section 1.2 would require additional effort. While the options to decrease CO_2 emissions from the engine exhaust are limited, there are more options for NO_x emission reductions in the forms of low-NO_x combustion techniques. These techniques are already listed in Table 2.2. The efficiency of these techniques on NO_x reduction would be dependent on the engine design characteristics, but generally a lower OPR and TIT are the most influential.

3.3.3. Future design drivers

Engine design can be driven by different goals. To achieve the climate goals stated in Section 3.3.2 the TIT and OPR should be simultaneously decreased to keep NO_x emissions to a minimum, while these must be increased to minimise CO_2 emissions. Section 3.3.1 showed that increasing the OFPR is most critical for decreasing the TSFC, but is often combined with a higher TIT and OPR. This also increases η_{th}. A higher BPR has a positive impact on the TSFC, F_s and η_p. Combining these conclusion with the trends in Section 3.3.2 shows that a good balance is required between these parameters. A means to achieve both the emission and performance goals is by implementing low-NO_x technologies into a high-BPR high-OPR engine. There were several low-NO_x technologies explored in Section 2.1.2 that are expected to reach TRL 9 at the first climate-goals milestone point of 2030-2035. In this thesis four future technologies will be explored that could prove useful in achieving these climate goals:

- Ultra high BPR (UHBPR)
- Water injection (WI)
- Inter-turbine burning (ITB)
- Lean burning combustion chamber (LBCC)

The UHBPR engine can serve as the baseline model in which the other technologies can be implemented, either separately or combined. To assess the effect of combining these technologies in a future engine, four baseline models should be constructed:

- 2035 technology level direct-drive turbofan (DDTF): DD-2035BF
- 2035 technology level geared turbofan (GTF): GTF-2035BF
- 2050 technology level DDTF: DD-2050BF
- 2050 technology level GTF: GTF-2050BF

The DDTF and GTF both have advantages and disadvantages, which is why it would be valuable to model both. The DDTF is generally lighter and has a lower maximum OPR, which would be better for NO_x emissions. The GTF produces less noise due to the lower fan speed and has a lower TSFC. After the optimised baseline models are established, low-NO_x combustion techniques should be implemented. The implementation of these technologies are likely to have an influence on the engine design characteristics of the optimised baseline models.

3.4. Future low-NOx combustion technologies

In Section 3.3.3, the future low-NO_x combustion techniques that will be investigated in this thesis were mentioned. This section elaborates upon the effect of those techniques on the engine performance and emissions. Section 3.4.1 describes the effects of water injection, Section 3.4.2 of inter-turbine burning and Section 3.4.3 of a lean burning combustion chamber.

3.4.1. Water injection

The architecture of a water injection engine and the effect on the thermodynamic cycle performance were already discussed in Section 2.1.3. The effect of water injection has been proven already for aviation, but it has only seen application during take-off for commercial flights. When water injection is applied, the water can enter the combustor either mixed with the fuel, mixed with the air or directly into the primary zone. The different pathways are illustrated in Figure 3.3.

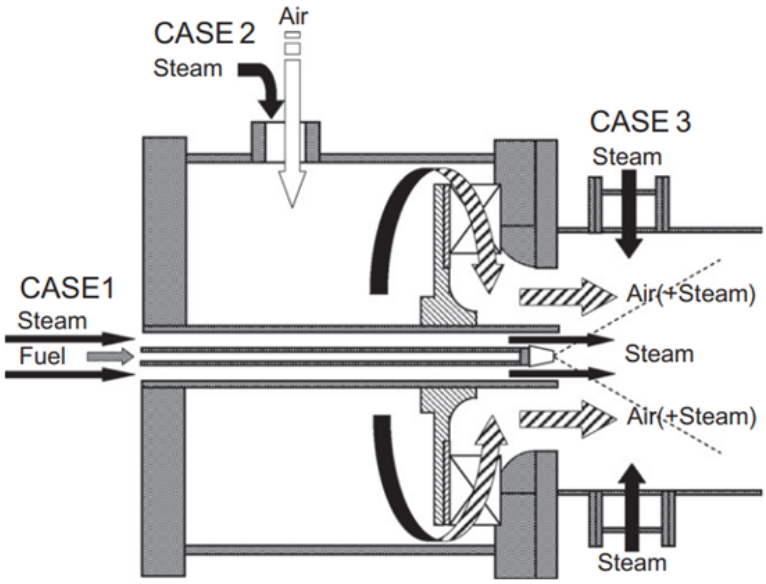

Figure 3.3: Steam addition pathways into the combustor [40]

The trade-off between the water injection rate, the TSFC and emissions reduction and engine weight will all play a role to determine the optimum configuration for a water injecting engine.

Performance

Looking at the engine alone, increasing the water content in the gas increases the mass flow and reduces the gas temperature, generating more thrust. This means that less fuel has to be used to generate the same amount of thrust, lowering the engine's fuel consumption. This directly decreases CO_2 emissions. How much the fuel consumption is reduced is dependent on the water-to-air ratio (WAR) and the OPR. A visualisation of this relation is given in Figure 3.4. The power that is augmented by water injection means that the inlet flow can be decreased to achieve the same amount of thrust, which will effectively decrease the engine weight. Using water injection could improve the TSFC by around 15%, decreasing the CO_2 emissions by the same percentage [19], [41].

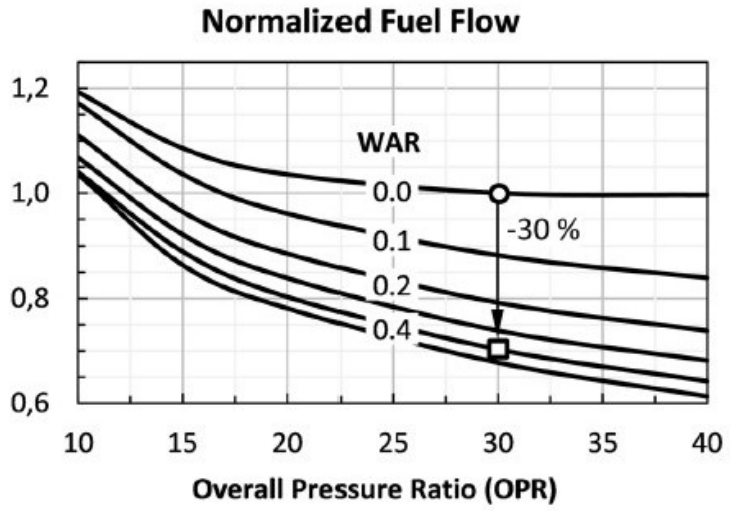

Figure 3.4: Normalised fuel flow for different values of WAR and OPR (adapted from [41]

NO_x and CO

Water injection has proven to decrease NO_x emissions significantly. Heat absorption by the water molecules decreases peak temperatures in the combustor, as well as decreasing the residence time. It is expected that water injection can reduce the NO_x emissions almost entirely, with decreases calculated to reach 84-95% [19]. The water is injected in the form of superheated steam and can be injected either before or directly into the combustor, as seen in Figure 3.3. An experimental study on the steam addition pathways has shown that pre-mixing the steam with the

fuel provides the largest NO_x reduction, but increases the CO concentration sharply with increasing water flow rate. Injection directly into the combustion chamber shows a lower NO_x reduction, but has almost no influence on the CO concentration at a water-to-combustion air ratio of 0.1-0.3 [40].

No correlation mentioned in Section 3.2.2 takes the injection pathway into account. As there is also no feature in GSP that modifies the injection location, the effect of the injection location on the NO_x emissions cannot be taken into account in this thesis. As water injection makes the fuel mixture leaner in the primary zone, a future variant of a lean burning combustor like the TAPS II used in the LEAP-1A engine might suffer from a lean blowout when too much water is injected. Therefore, a correlation based on an RQL combustor is better suited. Equation (3.5) showed an almost perfect correlation for a modern day RQL combustor, has a water-to-air ratio term and includes a technology factor that can be adjusted to represent more aggressive future cycles. Therefore, this equation will be used to represent the NO_x emissions for the water injection engine models.

H_2O and contrails

As the water content in the flow increases, H_2O emissions become more abundant. Water from the exhaust and the ambient can form droplets around other emitted combustion particles, after which they freeze into ice crystals and create contrails. The contrails themselves and contrail-induced clouds trap radiation from the Earth, contributing to the negative climate impact. This can however be prevented by water recovery in the exhaust. Theoretically, more than 100% water can be recovered due to ambient humidity and the H_2O that forms as a product of jet-fuel combustion. For this thesis, it will be assumed that 100% of the injected water is recovered, thus only the water that is initially on board will contribute to the additional weight and remains constant. The influence of H_2O and contrails was therefore not studied.

3.4.2. Inter turbine burning

Inter turbine burning, also known as sequential combustion, adds another combustor between the HPT and LPT. While multistage combustion could be possible, this thesis only focuses on one additional combustor. The additional power provided by the second combustor allows for lowering the first combustor exit temperature. This requires less HPT cooling, increasing the HPT efficiency, and decreases the formation of thermal NO_x emissions. A disadvantage of this technology is the additional weight to accommodate the second combustor and LPT cooling, reducing the LPT efficiency. The TIT is from here on referred to as T_{t4} to prevent confusion with the LPT inlet temperature after the second combustor. The exit temperature of the second combustor is referred to as T_{t46}.

Performance

Just like water injection, ITB is a means of power augmentation and therefore provides similar benefits. At high power conditions, the second combustor can deliver a higher fraction of the total energy, reducing the required inlet air mass flow. This decreases the size of the engine, which has a positive effect on the aircraft's TSFC. Additionally, the design point conditions at high altitude don't have to be adjusted to comply with the off-design requirements. This allows the engine to operate at more optimal conditions, increasing the engine efficiency while minimising the fuel flow. When the second burner isn't active it causes pressure losses and therefore decreases the efficiency.

NO_x

The first reason for the decreases NO_x emissions is the lower combustion temperature. For both combustors, the peak flame temperature is lower than for a regular turbofan. Secondly, after combustion in the first burner the gas has a lower oxygen concentration, which also discourages NO_x formation. Lastly, re-burning the gas mixture with NO_x particles in the second burner aids in the dissociation process, reducing NO_x emissions even more. The effect of these processes is dependent on the energy fraction the second burner delivers. For an engine that uses the same fuel for both combustors, the energy fraction is simply equal to the fuel flow of the second combustor divided by the total fuel flow. The effect of the energy fraction on the NO_x emission can be seen in Figure 3.5.

The formation of NO_x can be approximated by Equation (3.6), which has been derived from experimental testing [42].

$$EI_{NO_x} = EI^0_{NO_x}\left[y^{1.5} + (1-y)^{1.5} EXP\left(\frac{T_{t44} - T_3}{250} - 8.1 \cdot \alpha\right)\right] \tag{3.6}$$

$$y = \frac{FAR_1}{FAR_1 + FAR_2} \qquad \alpha = \frac{FAR_2(1 + FAR_s)}{FAR_s - FAR_2}$$

$EI^0_{NO_x}$ is the emissions index of the engine with a single combustion process, which will be calculated according to Equation (3.5). α is the vitiated air mass ratio, where FAR_1, FAR_2 and FAR_s are the first combustor, second combustor and stoichiometric fuel-to-air ratio. T_{t44} is the second combustor inlet temperature.

3.4.3. Lean burning combustion chamber

There are several actual and conceptual lean burning combustion chambers (LBCCs). As mentioned in Section 3.4.1, the LEAP-1A currently uses a lean burning combustor. The environmental effect of these combustor types is especially

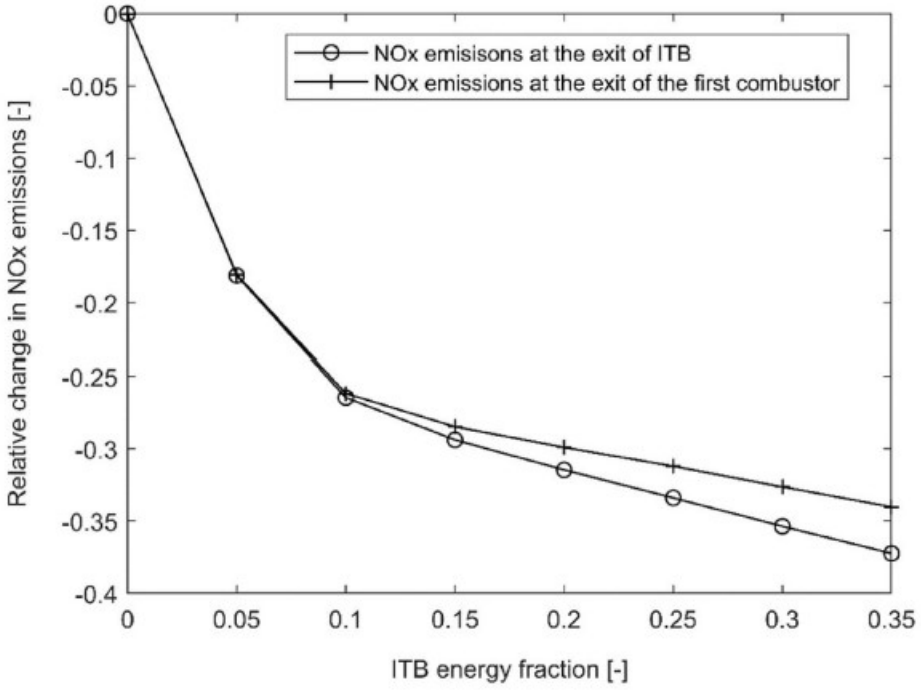

Figure 3.5: Effect of increasing the ITB energy fraction on the NO_x emissions [8]

visible during climb out and low power conditions, where the TAPS II combustor of the LEAP-1A achieves a 20% lower EI_{NO_x} than that of an RQL combustor from the PW-1127G [39].

Performance

Although an LBCC does not augment thrust like water injection or inter turbine burning, the leaner combustion suggests a lower fuel flow and might be beneficial for the TSFC. This is however not necessarily the case, as it can be seen from Table 3.1 that the PW1127G has a lower fuel consumption at take-off than the LEAP-1A26 for approximately the same amount of thrust. The TSFC and therefore CO_2 performance are thus case dependent.

NO_x

In an attempt to drastically reduce NO_x emissions, future engines could make use of an extremely lean burning combustion chamber, such as a MPLDI combustor. Figure 3.6 shows the difference in chamber architecture compared to an RQL combustor.

In a MPLDI combustor, fuel is directly injected into the primary zone by means of multiple fuel injectors at an equivalence ratio close to the lean blow-out limit. The difference with other combustors is that for (MP)LDI the fuel enters the combustor chamber with a very high swirl velocity by means of multiple fuel injection points, such that the fuel is atomised and mixed rapidly with the incoming air flow. The use of more injection points stimulates the mixing process and increases a more uniform air-fuel distribution, lowering the peak temperatures in the combustor. Next to this, the residence time is also decreased due to the fuel inlet velocity. Both of these occurrences contribute to lower NO_x formation specifically. The rate of NO_x emissions reduction is only lightly influenced by the inlet pressure and temperature. Figure 3.7 shows that at a constant pressure, the lines for different combustor inlet and exit temperatures are approximately parallel. It also shows that for an inlet pressure of 1.725 MPa and temperature of 811 K (similar to TOC inlet conditions for an engine with high OPR), the EI_{NO_x} can be reduced to almost 5 g/kg. The reference engines were tested at 17.0 and 13.38 g/kg for the same conditions, showing an improvement potential of up to 30%. This is a single case, but improvements of up to 53% compared to a modern day lean burning engine are possible [15].

Based on experimental data at relatively low T_{t4} and P_{t3}, the MPLDI combustor was shown to have a combustion efficiency of more than 99% at fuel-to-air ratios (FAR) of at least 0.012 [44]. As T_{t3}, P_{t3} and FAR for the future engine models will likely be higher than the experimental data, the combustion efficiency for MPLDI will be assumed equal to the 'regular' combustion efficiency of the RQL combustor. The implementation of MPLDI in the future engine models shall be evaluated only by new correlation for NO_x, which was formulated through different MPLDI experiments where $\frac{\Delta P}{P}$ denotes the pressure loss in the combustor [44]–[46]:

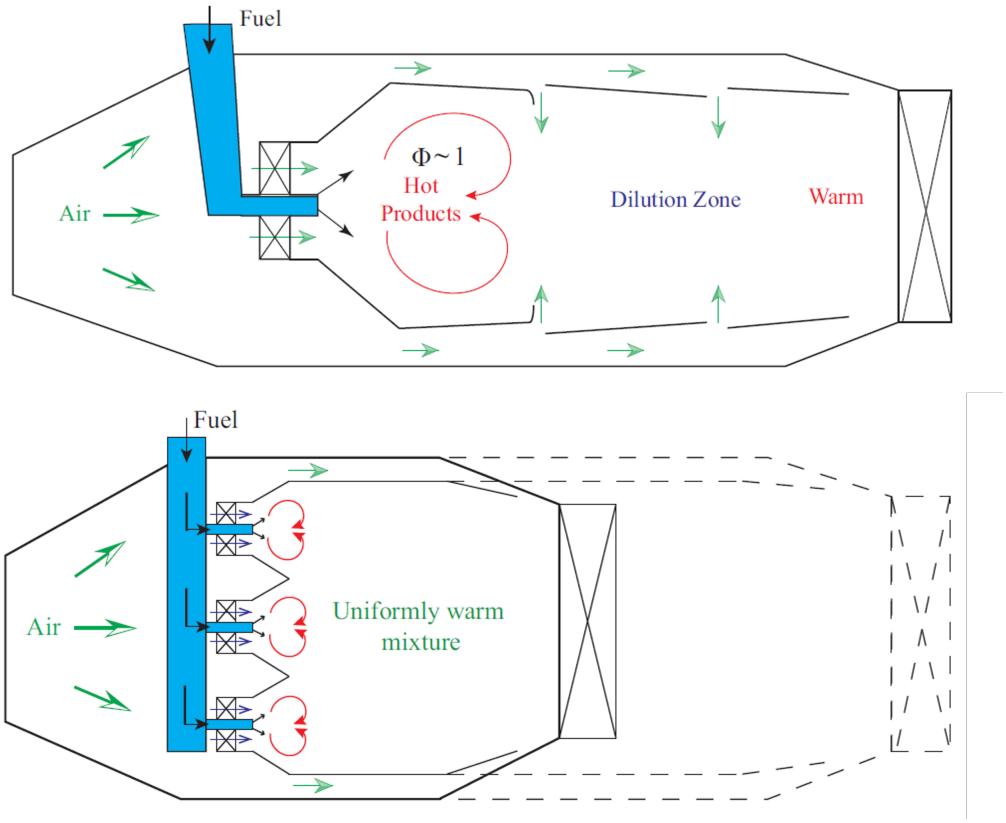

Figure 3.6: Conventional RQL combustor (top) vs MPLDI combustor (bottom)[43]

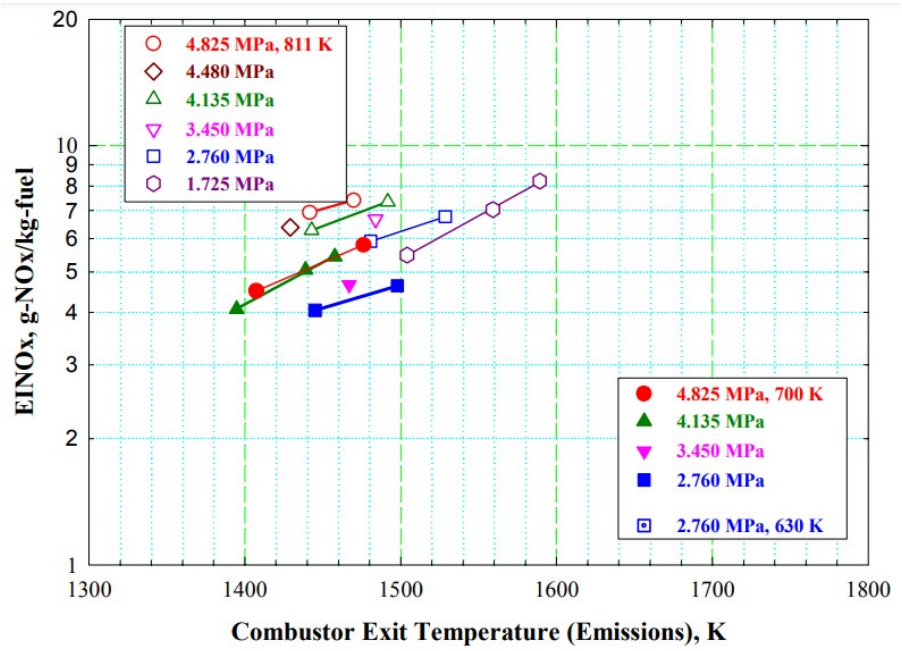

Figure 3.7: EI_{NO_x} reduction as a function of combustor inlet total pressure, inlet total temperature and exit total temperature [44]. The open and closed markers are representative of a combustor inlet total temperature of 811 K and 700 K respectively.

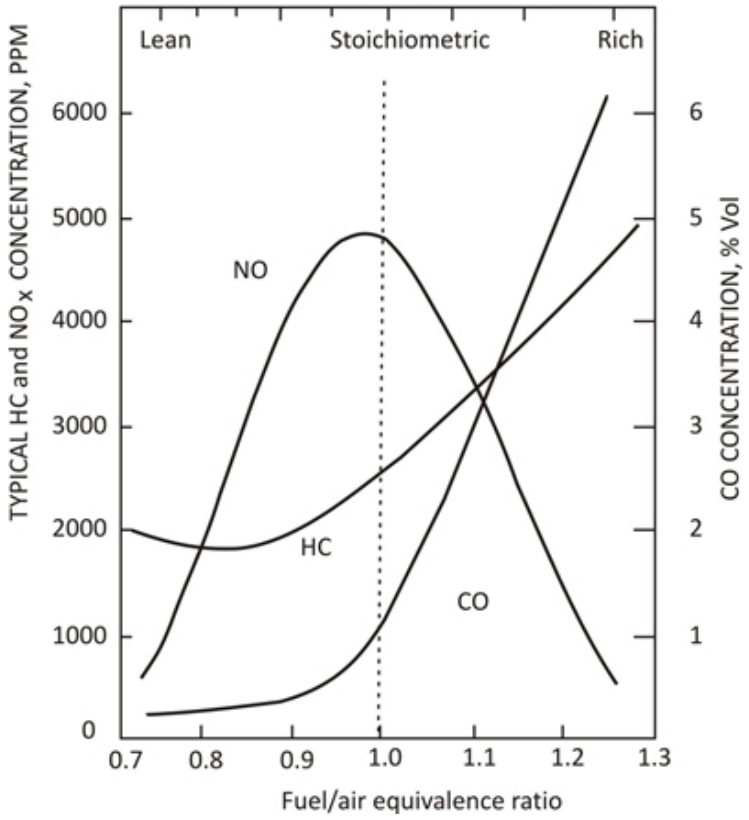

Figure 3.8: Effect of FAR on emissions production

$$EI_{NO_x} = a \cdot P_{t3}^{b} \cdot e^{T_3/c} FAR^{d} \left(\frac{\Delta P}{P}\right)^{e} \tag{3.7}$$

These different experiments have shown that the NO_x emissions for MPLDI are very case dependent and as such, the variables a, b, c and d can be adjusted to fit the experimental data. A different number of injectors, combinations of P3 and T3 and the value for the fixed pressure loss determine show different slopes for EI_{NO_x} as a function of FAR or T_{t4}. Therefore, the variables should be chosen to match the conditions as accurately as possible. For this thesis, the variables were set in accordance with Eq. 2 from [45], as this showed a good correlation for both medium and high pressure scenarios. Here, a = 1.359, b = 0.595, c = 194, d = 1.69 and e = -0.565.

CO and UHC

As the FAR decreases, so do the CO emissions. Figure 3.8 illustrates the effect of the FAR on the exhaust emissions of an aero engine. As the mixture gets leaner, the CO emissions decrease rapidly. For UHCs, a decrease can first be observed towards leaner mixtures, but at around 0.8 the (U)HC concentration increases. Although it would be valuable to asses the total climate impact from all exhaust emission, this thesis focuses on NO_x only.

4
Future engine modelling

Implementing low-NOx combustion technologies into an engines of the future requires first the construction of baseline future engine models (BF-models). This first part of this chapter (Section 4.1) describes the process of constructing these BF-models through an optimisation process and reviewing their off-design performance with GasTurb. The second part of this chapter (Section 4.2) focuses on the transfer of the baseline models into GSP, where the low-NOx combustion technologies are added.

4.1. Baseline future engine models

The BF-models will receive several updates compared to modern day engines in terms of component efficiencies, materials and pressure losses before being put through the optimisation process. These will be summarised in Section 4.1.1. After receiving these updates, the engines will be optimised in GasTurb with the integrated optimisation tool. This process in explained in Section 4.1.2. To ensure that the engine models are feasible, several design constraints had to be set, which are elaborated upon in Section 4.1.3. Finally, the off-design performance of the BF-models is reviewed in Section 4.1.3.

4.1.1. Future engine features compared to modern day engines

Previously, the future technologies that were talked about focused on the performance enhancement and emissions reduction of several components, mainly the combustor. However, other components and engine features are also expected to develop further:

- The expected lower pressure ratio of the fan and improved shaping and manufacturing of the blades will increase the efficiency of the fan. Many research papers regarding future engine technology assume a fan polytropic efficiency of around 0.95. Additionally, the IPC and HPC efficiencies are also expected to rise up to around 0.923 polytropic efficiency for geared turbofans [47]–[49].
- Shape optimisation of the ducts leads to a lower total pressure loss [50], [51].
- The combustor efficiency is expected to increase due to improved cooling and swirler technology [15].
- The efficiency of the HPT and LPT are expected to improve due to the use of advanced materials (such as ceramic matrix composites) with improved cooling technology [15]. These materials are expected to be have a temperature capability of up to 1711 K, assuming they are coated with a so called environmental barrier coating and are capable of trailing edge cooling [52]. As most or all of the cooling is supplied to the HPT, this would be especially beneficial for this component.
- Improved materials also decrease the weight of the engine and are more resistant to deformation under high stress conditions. Material properties such as density, Young's modulus and thermal expansion coefficient can be adjusted with the geometry function in GasTurb so they can be taken into account for the geometry calculations. These materials can replace the ones currently used for certain casings [52], fan blades [53] and LPT blades [54].

4.1.2. Optimisation in GasTurb

The next step was to make the four baseline future engine models (BF-models). Trends with respect to component efficiencies, pressure ratios and T_{t4} were taken from literature where the approximate same technology level and TOC thrust was used for the engine design. For 2035, the biggest difference was a higher specific work contribution from the IPC and a lower FPR to accommodate the higher BPR [47]–[49]. Design for 2050 technology engines showed a continuation of the FPR and BPR trend, but the IPR is not increased as significantly compared to the 2015-2035 time frame. Also, the component efficiencies are expected to reach values close to their theoretical maximum [51]. After upgrading the modern engine models with the future component efficiencies, certain ranges were set in which GasTurb was allowed to optimise the BF-models to ensure a feasible engine design. These ranges can be found in Table 4.1. The reasoning behind these ranges is explained in Section 4.1.3.

Table 4.1: Optimisation variables and constraints for the BF-models

	2035		2050	
Variables	Lower limit	Upper limit	Lower limit	Upper limit
OFPR [-]	1.45	-	-	-
IFPR [-]	1.18	≤ OFPR	-	≤ OFPR
IPR [-]	-	3 (DDTF) / 3.6 (GTF)	-	3 (DDTF) / 3.6 (GTF)
Spool speeds [rpm]	1801	22300	1801	22300
Gear ratio [-]	-	4	-	4
Cooling percentage [-]	-	20	-	20
Stator outlet temperature [K]	-	1589	-	1589
Constraints				
Blade height last stage HPC [cm]	2	-	2	-
Fan tip radius [cm]	-	113	-	-

Within these ranges, the optimisation function of GasTurb was used to calculate the engine design characteristics at TOC, with TSFC as the optimisation parameter. As the engine optimises for the TSFC, the EI_{NO_x} will worsen. However, the low-NO_x combustion techniques that will be implemented later are expected to solve this, which is why the TSFC was chosen as the optimisation parameter for the BF-models. The most important engine design characteristics can be found in Table 4.2. A complete overview of engine design parameters for the baseline and BF-models can be found in Appendix A.

Table 4.2: Optimised design characteristics at TOC condition for the BF-models

Engine characteristics	GTF-2035BF	GTF-2050BF	DD-2035BF	DD-2050BF
Net thrust [kN]	26.60	26.60	25.99	25.99
Fuel flow [kg/s]	0.348	0.325	0.354	0.330
TSFC [g/kNs]	13.07	12.21	13.63	12.72
EI_{NO_x} [g/kg]	22.58	17.63	22.32	15.70
Specific thrust [m/s]	108	86	103	94
OPR [-]	52.25	56.45	42.81	42.97
BPR [-]	14.29	15.61	14.30	15.99
OFPR [-]	1.48	1.35	1.45	1.39
IFPR [-]	1.35	1.33	1.42	1.38
IPR [-]	3.60	3.53	2.49	3.00
HPR [-]	11.16	12.35	12.56	10.69
T_{t4} [K]	1609	1523	1644	1560
d_{fan} [cm]	226	254	226	238
Gear ratio [-]	2.13	2.01	N/A	N/A
Mass []kg]	2268	2951	2306	2371

There are some future design trends visible that are in line with expectations, such as an increasing OPR, BPR and fan size from 2035 to 2050. The lower specific thrust for the 2050 BF-models combined with the higher component efficiencies result in a lower TSFC for the same thrust output. Although the OPR and BPR increase, the combustor outlet temperature decreases, which is not in line with previous engine design trends. The reason for this is that the 2050 models were optimized with a thrust limitation. The large BPR and high OPR are able to produce more thrust than the required 26.60 kN and 25.99 kN at higher temperatures. To make a meaningful comparison with state-of-the-art engines, the thrust was limited for these future models, and thus a lower T_{t4} is required to achieve this thrust.

The geometry of the BF-models can be seen in Figure 4.1 and Figure 4.2. The geared turbofans are shorter than their direct drive counterparts due to having fewer HPC and LPT stages. The fan diameter was limited for the 2035 models, leading to a maximum diameter of 1.13 m for both models. The 2050 BF-models had an unrestricted fan size, which allowed the geared version to achieve a higher fan diameter due to a lower fan tip speed.

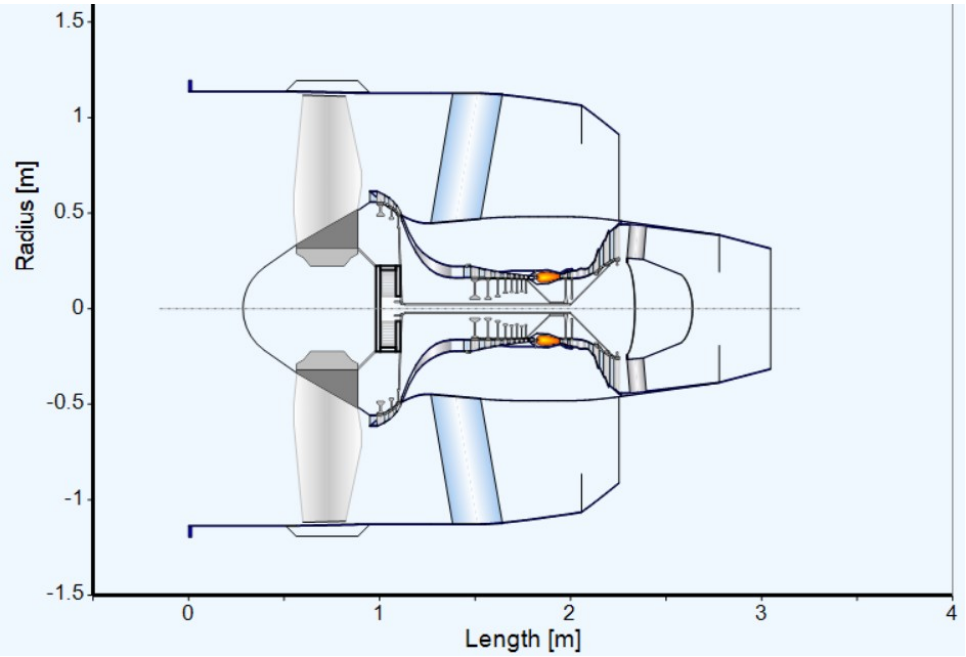

(a) GTF-2035BF

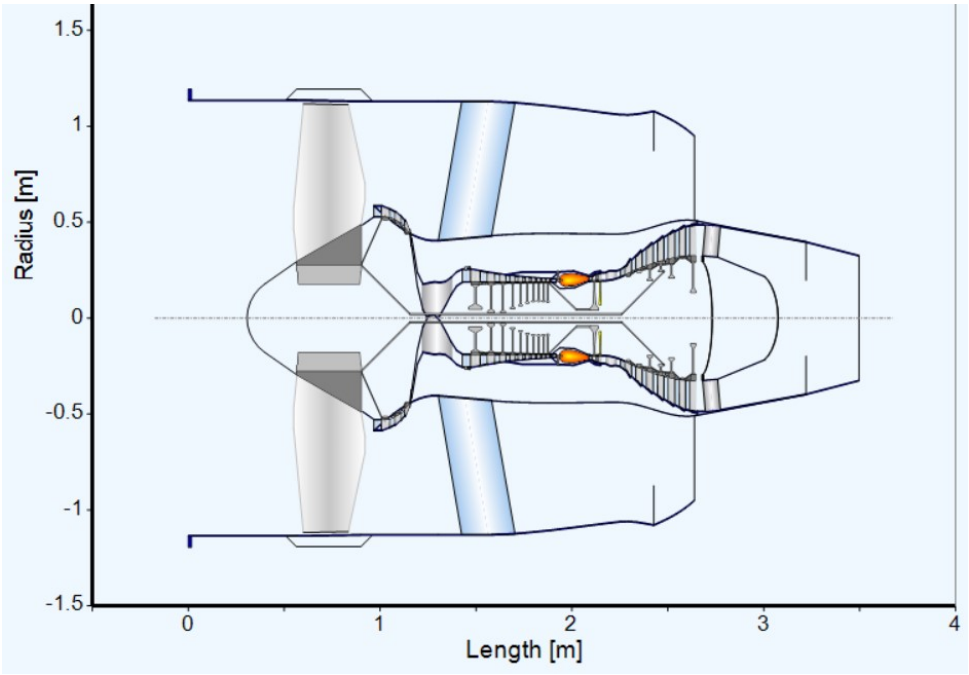

(b) DD-2035BF

Figure 4.1: Geometry of the 2035 BF-models

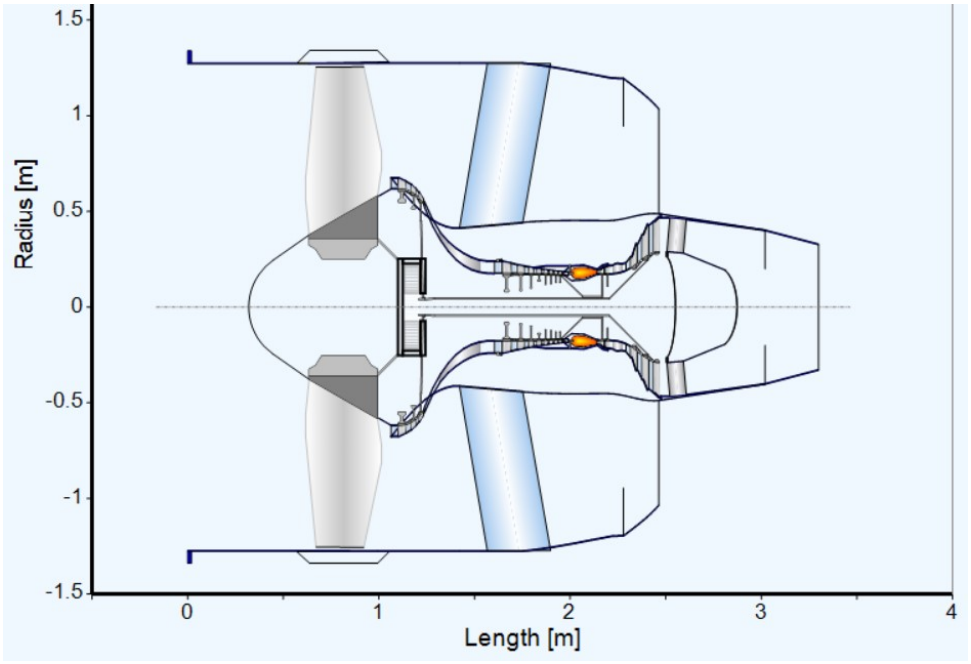

(a) GTF-2035BF

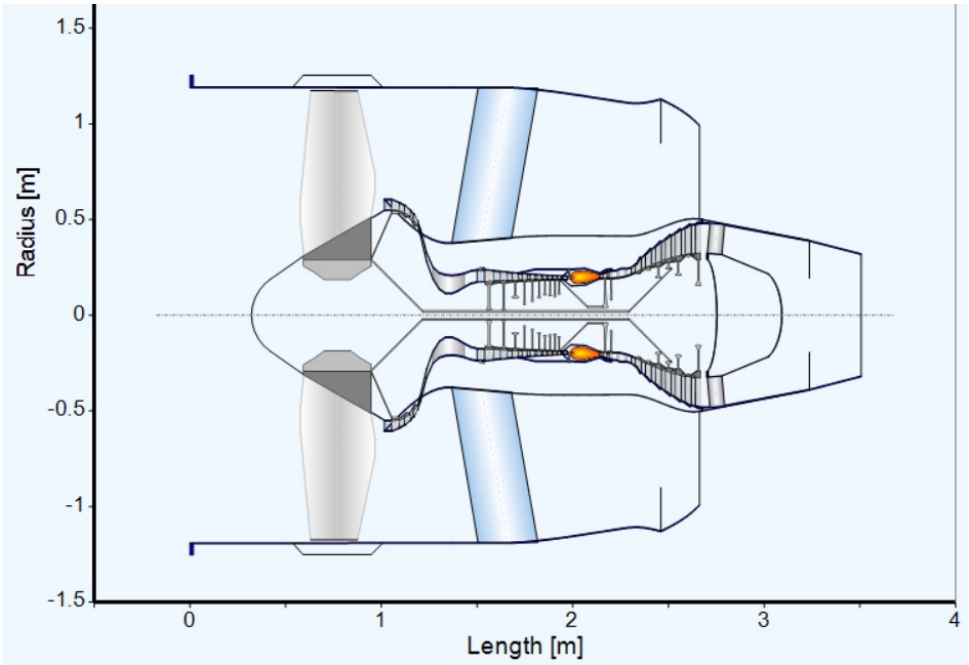

(b) DD-2050BF

Figure 4.2: Geometry of the 2050 BF-models

A comparison of the BF-models with their respective state-of-the-art baseline engine model (B-model) from Section 3.2 can be seen in Table 4.3.

Table 4.3: Differences of the BF-models with their respective state-of-the-art baseline engine model

Δ with B-model [%]	GTF-2035BF	DD-2035BF	GTF-2050BF	DD-2050BF
TSFC	-9.20	-8.88	-15.19	-14.97
EI_{NO_x}	36.83	1.90	35.47	-9.01
OPR	25.62	4.23	35.70	4.62
T_{t4}	1.86	0.80	-3.59	-4.28
BPR	18.10	31.20	29.00	46.67
d_{fan}	7.54	11.88	21.05	17.70
F_s	-10.41	-18.55	-28.70	-26.11
Mass	-12.57	-5.73	13.77	-3.09

The performance improvement of the UHBPR concept can already be seen from Table 4.3. The steep OPR and BPR increase for the geared options result in a promising TSFC reduction, but come at the cost of a large increase in EI_{NO_x} as expected. The direct drive BF-models show an even larger increase in BPR, which is very beneficial for the propulsive efficiency. The smaller rise of OPR results in a TSFC reduction that is almost equal, but slightly lower than the improvement of the GTFs. Also, looking at the absolute values in Table 4.2, it is evident that the GTF has a better TSFC performance. All engine models show a significant in specific thrust (Fs) reduction as well due to the additional thrust generated by the bypass flows.

4.1.3. Validation

The upper and lower limit for the design variables and constraints during the optimisation process were not selected arbitrarily. Research into 2035 and 2050 future engine design showed a range of values for design point parameters suitable for that point in time. This included not only updated component efficiencies, but also material properties of those used for the engine. For the take-off (T/O) conditions, it is important that the engine is able to generate enough thrust without exceeding temperature and spool speed limits.

Design point – TOC

The optimization ranges from Table 4.1 were imposed to ensure a feasible engine design before the low-NO_x combustion techniques are added in GSP. The reasoning behind these ranges is the following:

- **OFPR:** The OFPR is limited by the BPR and the incoming airflow. To sustain the incoming airflow without the use of a variable area nozzle (VAN) in the bypass, the OFPR should not be lower than 1.45 for a high-BPR engine [55]. For the 2035 technology level, a normal bypass nozzle was assumed. For the 2050 technology level, a VAN was assumed, allowing for removal of the lower limit for the OFPR.
- **IFPR:** The IFPR can be lower than the OFPR due to twisted blade design. In the design of similar future engines, the IFPR is between 80-90% of the OFPR, with a minimum of 1.18 [47]–[49]. This was chosen as the lower limit for the IFPR. The upper limit was chosen such that the IFPR does not exceed the OFPR.
- **IPR:** As was mentioned before, future engines see a trend of an increased contribution of the IPC to the OPR. For the GTFs, the upper limit was set to 3.6 to match the trend future of IPC design [47], [49], [56]. However, for the DDTF case, the spool speed of the IPC and thus the IPR is limited by the fan tip speed. The upper limit for the IPR was therefore set to 3 for the DDTFs.
- **OPR:** The OPR is limited by the rotor blade height of the last stage of the HPC (HC10). Although in reality the lower design limit is around 2 cm, it was chosen to lower this to 1.3 cm for all future engine models. This value was taken from the geometry calculation by GasTurb for the PW1100G engine model, where the last stage blade height was calculated to be 1.3 cm. It is likely that the geometry calculation by GasTurb does not reflect real geometry design accurately, which is why this was chosen as an acceptable lower blade height limit.
- **HPR:** The HPR was not limited, as the IFPR, IPR and HPC last stage blade height will determine the maximum HPR.
- **BPR:** The BPR is limited by the ratio between the fan diameter and the core size. The fan diameter upper limit was set at 2.26 m, which is based on the minimum allowable ground clearance for CS-25 aircraft. For 2050 it was assumed that a large part of today's fleet is replaced by new aircraft. The design of these aircraft is currently unknown, but it was assumed that, partly due to the possible introduction of unconventional airframes, there is no limit in the fan diameter. The core size is limited by the rotor blade height of HC10, which was set to a lower limit of 1.3 cm as previously mentioned.
- **Spool speeds:** The low pressure and high pressure spool limits were set to the same limits as the PW1127G and LEAP-1A limits, which can be found in Table 3.1. The combination of the spool speeds, the pressure ratios for the adjoined turbomachinery components and the geometry determine the stresses on the blades. Appropriate stress and burst margins were set according to the GasTurb manual to ensure a feasible geometry design [36].
- **Gear ratio:** The PW1127G has a gear ratio of 3.0625. The upper limit for the gear ratio was set to 4, based on [49].
- **Cooling percentage:** Cooling for both the first stator and the first rotor of the HPT were set to a combined maximum of 20% of the core mass flow (pre-combustor), in accordance with the cooling factors in [47] and [56].
- **SOT:** The stator outlet temperature (SOT) was set to a maximum of 1589 K, which is the maximum allowable tem-

perature of the composite material that was chosen for the HPT blades. Although the composite used in the analysis is coated with a layer that can withstand up to 1711 K, it was chosen to set the maximum to 1589 K to ensure material integrity at high loads and during the long engine life cycle [54].

Off-design performance – T/O

Meeting the same take-off requirements as the PW1127G and LEAP-1A26 shows if the future engine designs could power the next fleet of single-aisle aircraft. The take-off thrust for these engines was specified in Table 3.1. This thrust rating is defined at standard static conditions (altitude = 0 m, temperature = 298.15 K, Mach = 0), also know as sea-level static conditions (SLS). Running the BF-models a this condition showed an excess thrust power for all models, especially for the 2050 models. This was expected, as the ultra high BPR and low OFPR allow for more thrust generation in the bypass.

It was discovered during the T/O calculations that the IPC map did not fit the future IPCs well. The map was scaled to fit the higher pressure-ratio IPCs, such that the maps from GasTurb can also be used in the T/O calculations in GSP. After scaling the map, the fuel flow of the BF-models was adapted to match the thrust rating of their respective baseline models. The off-design results can be found in Table 4.4.

Table 4.4: Off-design performance of the BF-models at sea-level static conditions

	GTF-2035BF	DD-2035BF	GTF-2050BF	DD-2050BF
Thrust [kN]	120.43	120.64	120.43	120.64
Fuel flow [kg/s]	0.730	0.759	0.636	0.687
TSFC [g/kNs]	6.05	6.29	5.28	5.70
EI_{NO_x} [g/kg]	27.28	22.15	25.18	19.07
OPR [-]	37.55	31.23	38.46	30.77
T_{t4} [K]	1630	1667	1522	1577
BPR [-]	15.15	14.78	15.98	16.39

The NOx emissions index formulated in Equation (3.5) was also evaluated with the off-design models, as it showed the best correlation with the modern day engine models. DD-2035BF and DD-2050BF have a similar but slightly lower OPR than the PW1127G during take-off and TOC, while the T_{t4} is higher for DD-2035BF. The TF from Equation (3.5) was adapted such that the NOx emissions for the high-OPR geared engine models were higher and the lower-OPR direct drive models was around the same value as the take-off and climb out values of the PW1127G (20.8 and 17.0 respectively), thereby assuming initially an RQL combustor for the future engines. The EI_{NO_x} in Table 4.2 was calculated with this TF as well.

4.2. Upgraded engine modelling

Now that the BF-models are established, they can be upgraded with the low-NO_x combustion techniques (water injection (WI), inter turbine burning (ITB) and lean burning combustor (MPLDI)) in GSP.

4.2.1. Transfer to GSP

A reference model for each BF-model was constructed and given the same inputs as the optimised versions of the engines in GasTurb. To keep the models as similar as possible, the design mass flow at the inlet was changed in GSP to match the inlet corrected flow in GasTurb, the cooling fractions were adjusted to match the LPT exit temperature and the duct losses were slightly altered to match the overall pressure ratio. All values were matched such that the net thrust and TSFC were matched with a less than 0.5% difference in the reference model. The reference model could then be used as a baseline before adding the low NO_x combustion techniques. The layout for the water injection and MPLDI did not have to be adjusted, as water injection is a feature of the combustor component in GSP and the effect of MPLDI can be viewed through the NO_x correlation from Equation (3.7). These engines were thus constructed as depicted in Figure 4.3. For ITB, an additional combustor had to be added between the HPT and LPT. This resulted in the engine construction seen in Figure 4.4.

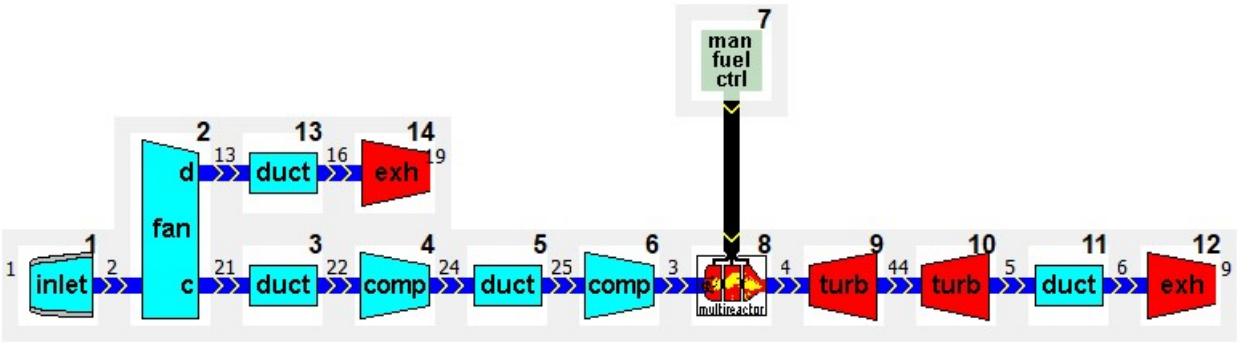

Figure 4.3: Water injection and LBCC engine model in GSP

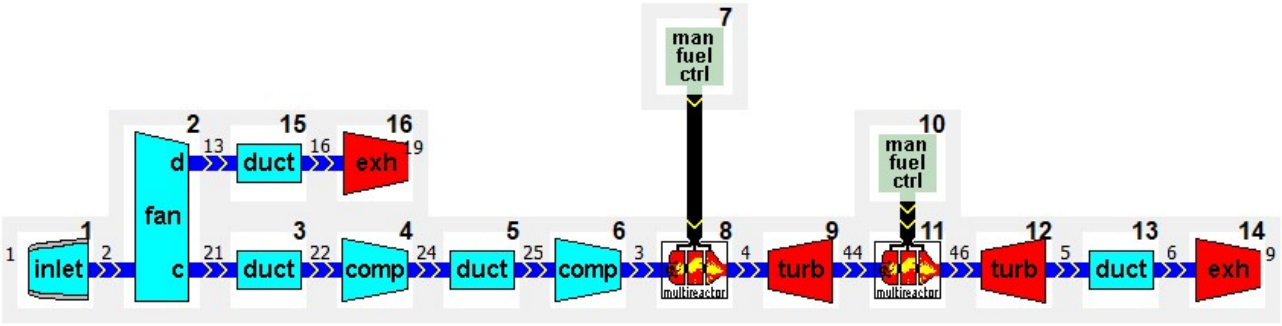

Figure 4.4: ITB engine model in GSP

4.2.2. Definition of design space

With the low-NO_x combustion technologies added to the BF-models, certain parameters can be adjusted to evaluate their performance within a new design space. The optimisation of the BF-models towards the lowest possible TSFC has pushed the OPR towards a theoretical maximum. For the GTFs, this value is much higher due to the higher rotational speed of the IPC. Changing the number of stages and the gear ratio might push this to an even higher number, although this might have a negative effect on the engine weight. For the DD-models, the limit is seemingly being approached. Because the OPR cannot be increased without adjusting the BPR due to the limit on the size of HC10, and the configuration of the BF-models was optimised for the lowest TSFC, it was chosen not to increase the OPR any further.

Water injection

Water injection is a standard feature of the combustor component in GSP. In proposals for a water injection engine, the exhaust heat from the core is used to evaporated the water into superheated steam before it is injected in the combustion chamber. Lowering the OPR of the engine results in a higher LPT exit temperature, which can be used for evaporation of water in the gas mixture. Since a lower OPR is also beneficial for reducing the NOx emissions, the OPR was reduced by a maximum of -10%. As water injection allows for higher specific work by the turbines for the same expansion ratio, the T_{t4} could be decreased as well. It was chosen to decrease the T_{t4} with a maximum of 10% as a means to obtain a significant NOx benefit, The water-to-air ratio (WAR) and energy percentage of the second burner (E%) were both varied between 0-30% with the range of OPRs and combustor outlet temperatures to obtain numerous design and off-design points. A higher percentage of water might decrease the FAR too much to sustain stable combustion. These point can then be evaluated by means of a trade-off that will asses all performance aspects of the engine.

ITB

The addition of the second combustor allows LPT to extract more work from the air mass flow, so T_{t4} can be lowered again. This will decrease the maximum work extraction by the HPT, thus the OPR should be decreased as well. The right side of Figure 2.4 shows the thermodynamic cycle of an ITB engine. Lowering T_{t4} with the addition of the heat from the second combustor (Q_{ITB}) maintains the thermal efficiency while lowering the NOx emissions, which is what is desired for the design of the futures engines. Therefore, like with WI, the OPR and T_{t4} were lowered up to 10%. The energy contribution of the second combustor E% was varied to a maximum of 30% as a safe margin, as a combination of MPLDI and ITB might push FAR1 towards the lean blowout limit.

MPLDI

For multi-point lean direct injection there is no change in design conditions. The combination of MPLDI with water injection and ITB was evaluated by applying an NOx correction and removing the designs with a fuel-to-air ratio below the lean blowout limit.

5
Results and discussion

This chapter contains the results of the upgraded future engine model (UF-model) simulations. First, the effect of water injection (WI) is evaluated in Section 5.1 during both the design and off-design conditions. Secondly, the performance of the ITB UF-models is evaluated in Section 5.2. The performance of both the WI and ITB UF-models are then evaluated with an LBCC combustor in Section 5.3. The results of all UF-models is summarised in Section 5.4. The design options are then compared to each other and evaluated with trade-off in Section 5.5. Then, the final designs are compared to the alternative architectures in Section 5.7. Lastly, some limitations for the simulations are discussed in Section 5.8.

The design point simulations were done at TOC (h = 10668m (35000 ft), M = 0.78, ΔISA = 10K), the off-design simulations at SLS condition. The UF-models that use WI are stylised with suffix -WI and the ITB models are stylised with suffix -ITB. For all simulations, an appropriate step size was chosen to visualise the possibilities within the design space. There are however more design possibilities within the minima and maxima of the adjusted variables, so the densities of displayed points might vary. The isolines for minimum and maximum T_{t4} and OPR show the actual design space boundaries, which coincide (approximately) with the outer edges of the contours. Anything within this space is a possible design point.

It should be noted that several design points were removed from the design spaces of the UF-models, as not every combination of OPR and T_{t4} within their range of up to -10% is able to provide a feasible or realistic design:

- At low OPR, low T_{t4} and low WAR/E%, the exhaust velocity of the core is much lower than the flight speed and as such contributes almost no net thrust. The optimum TSFC for a turbofan at TOC lies around a jet velocity ratio $\left(\frac{V_{18}}{V_8}\right)$ of 0.7-0.85 at TOC conditions [36], [57]. If $\left(\frac{V_{18}}{V_8}\right)$ is larger than 1, the turbofan behaves more like a propeller engine.
- For the 2035 cases, combinations of parameters that produced less thrust than the modern day variants (26.60 kN and 25.99 kN) would not be adequate as they would require a larger inlet mass flow to achieve the desired thrust and would therefore exceed the fan diameter limit.
- For the 2050 cases, a fan limit was previously assumed to be non-existent due to the possibility of different airframes with a larger clearance margin. However, a thrust output lower than that of the BF-models would require a larger inlet diameter, increasing the wetted area of the engine and hence the drag exponentially, and would increase the weight.

The design points that fit one of the descriptions above were filtered from the simulation outputs before the remaining design points are evaluated.

5.1. Water injection

This section describes the performance of the WI UF-models. The results of the design point simulations are shown in Section 5.1.1 and those of the off-design simulations in Section 5.1.2. In some figures, isolines are given for clarity. Black isolines correspond to a constant OPR, while red dotted isolines correspond to a constant T_{t4}.

5.1.1. Design point

The results from the DP calculations showed a very large design space. As an example, the design space of GTF-2050WI is shown in Figure 5.1. Dark blue indicates a low WAR, while yellow indicates a high WAR (0-30%). Due to the thrust augmentation by water injection, this also indicates an increase in net thrust. Every black dot indicates a unique design point. The design point for the associated BF-model is indicated with a yellow star.

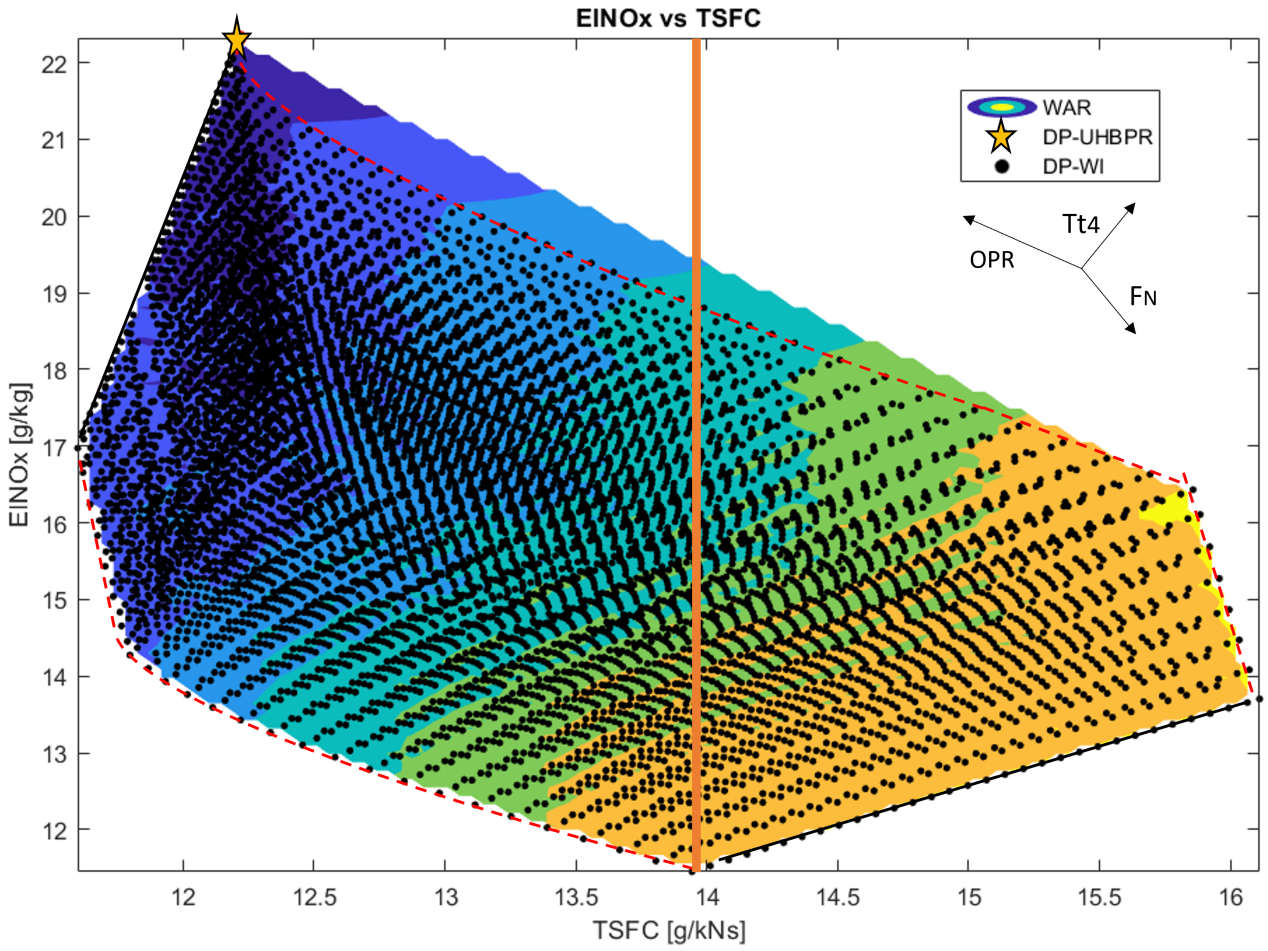

Figure 5.1: Simulation results within the entire design space of GTF-2050WI at TOC. The orange line is placed at the point of minimum TSFC to indicate the less favourable design options on the right side of line. The arrows in the upper right corner indicate the direction of increase for the combustion outlet temperature T_{t4}, overall pressure ratio (OPR) and net thrust F_N.

When evaluating the effect of changing the variables separately, several general trends can be observed for all UF-models:

1. As the OPR increases, the TSFC goes down while EI_{NO_x} goes up.
2. As the T_{t4} increases, both TSFC and EI_{NO_x} go up. At higher OPRs with lower WAR, the EI_{NO_x} rises faster for the same increase in T_{t4} compared to at higher wARs.
3. As the WAR increases, TSFC goes up while EI_{NO_x} goes down.

What is also visible from Figure 5.1 is that for any design point value of EI_{NO_x} on the right side of the thick orange line (slightly to the left of TSFC = 14 g/kNs), there exists a design point with an equal EI_{NO_x} but a lower TSFC on the left side. The designs on the right side of that line are thus not interesting to explore. This phenomena is visible in all UF-models. Discarding the unfavourable points, the favourable design options for all UF-models are shown in Figure 5.2.

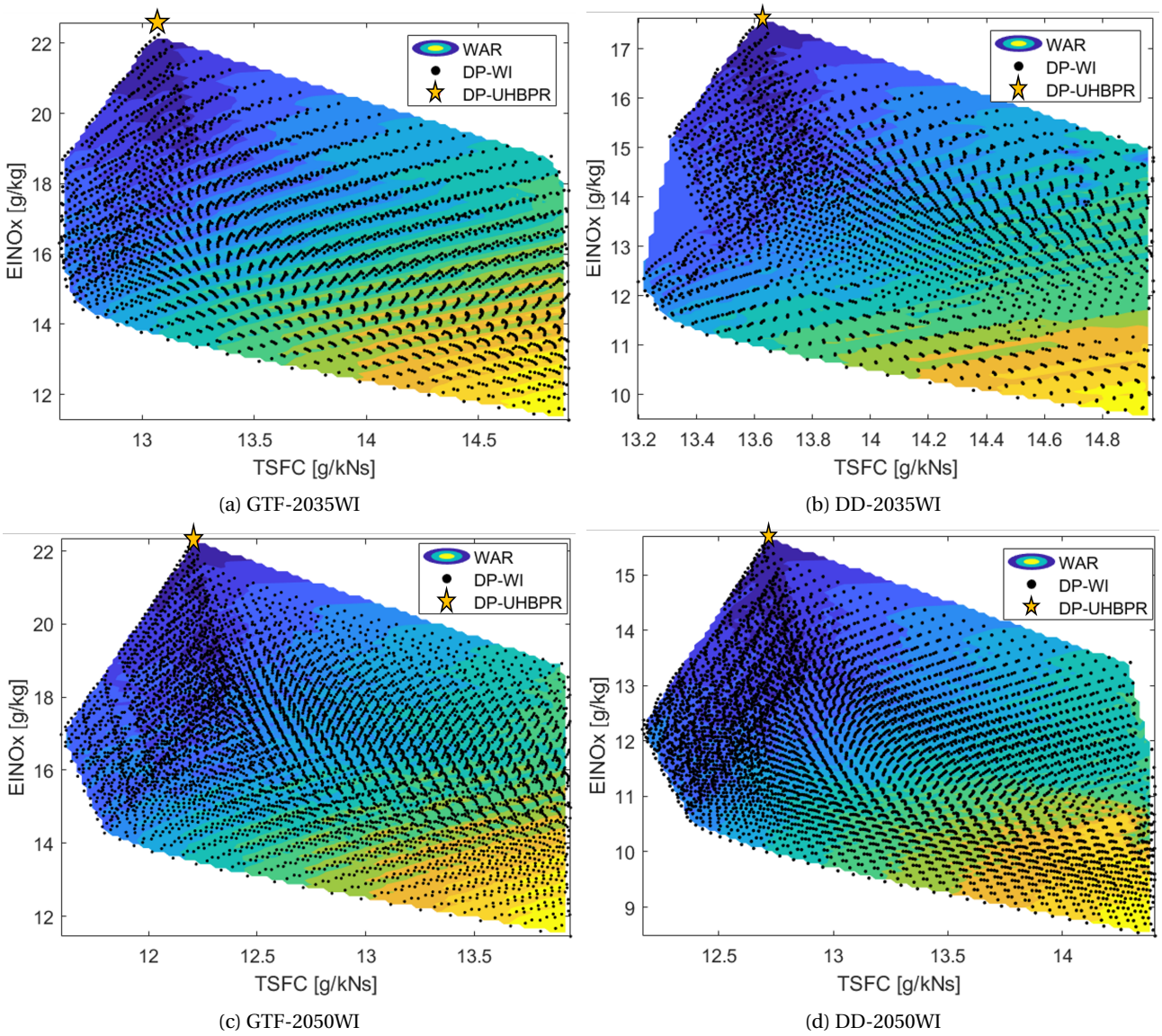

(a) GTF-2035WI

(b) DD-2035WI

(c) GTF-2050WI

(d) DD-2050WI

Figure 5.2: Water injection design points for all UF-models compared to BF-models at TOC

The aforementioned trends remain the same for the filtered design spaces. The change in performance of the UF-models with a change is OPR is as expected. Higher inlet temperatures and pressures at the combustor inlet require less fuel to be added to the system to achieve the same T_{t4}, therefore decreasing the TSFC. EI_{NO_x} is a function of the OPR and T_{t4} (as described by Equation (3.5)), which shows that for a higher OPR and equal T_{t4}, the EI_{NO_x} increases. The other way around this also holds. Also, for a fixed OPR, increasing the T_{t4} would require a higher fuel flow to achieve a higher combustion temperature, increasing the TSFC. As for the WAR, one would expect that the TSFC would go down due to the augmented thrust provided by the water. This is the case for lower WARs (the upper left corners of Figure 5.2, but as the OPR decreases, the engine requires a higher WAR to achieve the required thrust. The temperature inside the combustor decreases as the WAR rises. This is beneficial for the EI_{NO_x}, but as another result of this lower temperature, additional fuel is now needed to achieve the same T_{t4} as before. This becomes more severe as the OPR decreases and the T_{t4} increases, producing the less desirable results on the right side of the thick orange line in Figure 5.1.

When the objective is to keep the thrust constant for a certain amount of injected water, the thrust provided by the injected water allows for a decrease in T_{t4} and therefore fuel mass flow to compensate for this, lowering the TSFC. This effect can be seen in Figure 5.3. Dark blue indicates a low WAR, while yellow indicates a higher WAR (0 to ~ 7%). Also visible are the isolines of the OPRs and T_{t4}s. As the OPR and T_{t4} were varied step-wise, the design points coincide here with the isolines. However, as mentioned in the introduction of this section, any design point within the maximum and minimum OPR, T_{t4} and WAR is a solution. The design points of the BF-models are again indicated with a yellow star.

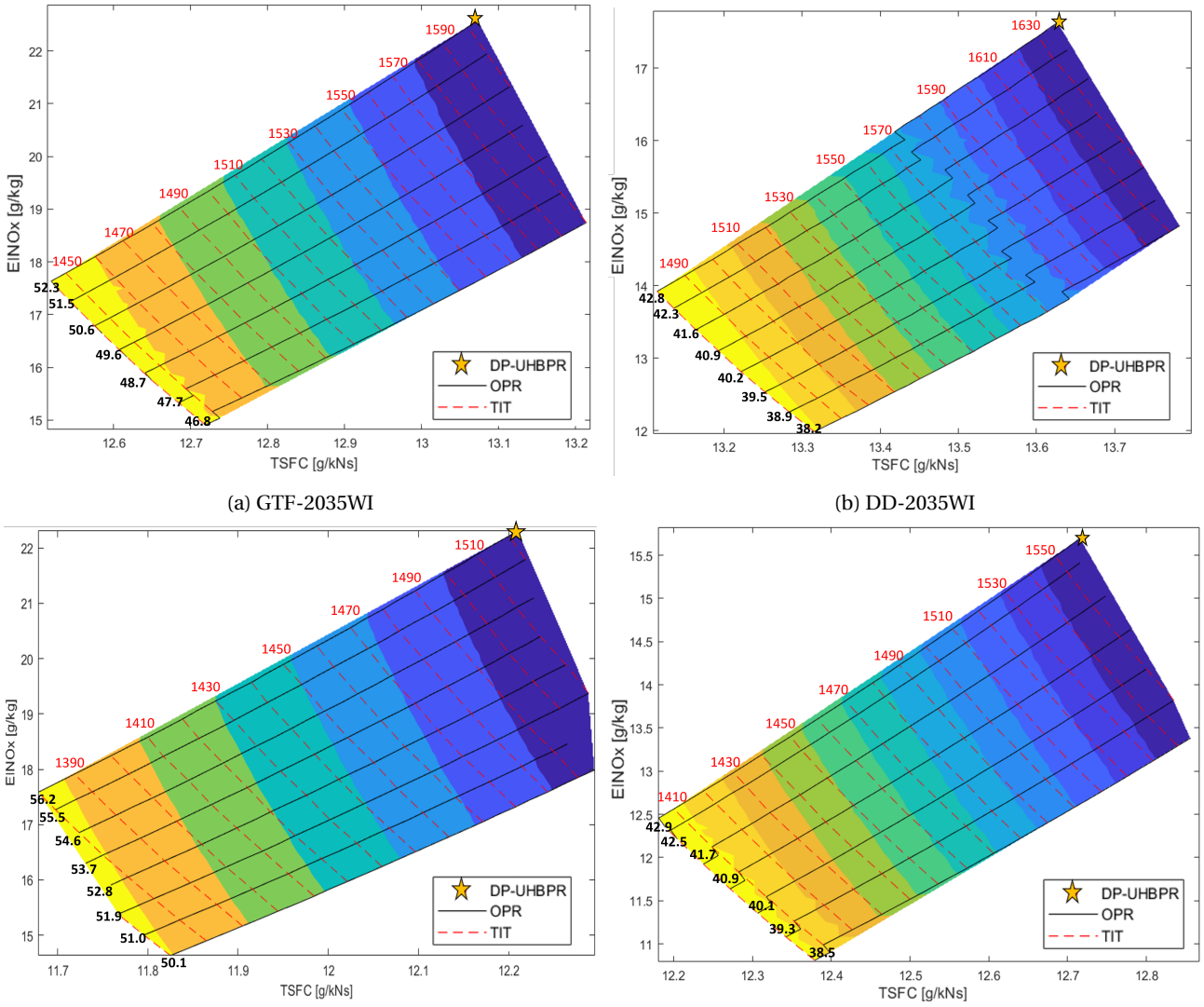

(a) GTF-2035WI

(b) DD-2035WI

(c) GTF-2050WI

(d) DD-2050WI

Figure 5.3: EI_{NO_x} vs TSFC at a constant thrust with varying WAR, OPR and T_{t4} at TOC

Although the entire lower Pareto front (coinciding with the red isoline for lowest T_{t4}) of Figure 5.1 is an interesting space to explore for EI_{NO_x} reduction, a TSFC reduction is limited to the upper left side of the design space. Here, the WAR is high enough to provide additional thrust while not decreasing the combustion temperature too much. Figure 5.3a through Figure 5.3d are essentially close-ups of the upper left corners of the associated design spaces in Figure 5.2. Figure 5.2 already illustrates that there exist a design space with significant TSFC and EI_{NO_x} improvements by decreasing the T_{t4}, but another way to keep the thrust constant would be by decreasing the inlet mass flow. This might be the most beneficial change in terms of TSFC, as this would mean the inlet diameter can be decreased. This would save weight, decrease drag, and thus require less fuel mass flow to achieve the required thrust. How much the inlet mass flow can be decreased depends on the take-off requirement.

There are improvements in both TSFC and EI_{NO_x} possible, but all sub-figures show that there is a design range for the associated UF-model that has to compromise on either NO_x emissions or fuel consumption by selecting a certain OPR, T_{t4} and water injection percentage. Certain combinations of these parameters at TOC might not provide a sufficient off-design performance at SLS, thus this has be assessed first.

5.1.2. Off-design

One of the state parameters for off-design was the output thrust. The required take-off thrust was kept the same as for the baseline models and BF-models, being 120.64 kN and 120.43 kN for the DD and GTF UF-models respectively. This way, the improvement of the take-off performance compared to modern engines in terms of TSFC and EI_{NO_x} is more obvious. With the output thrust as a state parameter, only WAR and the fuel flow were varied. Due to the step-wise decrease of the fuel flow while keeping the thrust constant, Figure 5.4 shows a decrease in EI_{NO_x} for constant values of TSFC. Any combination of fuel flow and water injection percentage that provides enough thrust is however a possible configuration and would fall within the contours of the sub-figures in Figure 5.4.

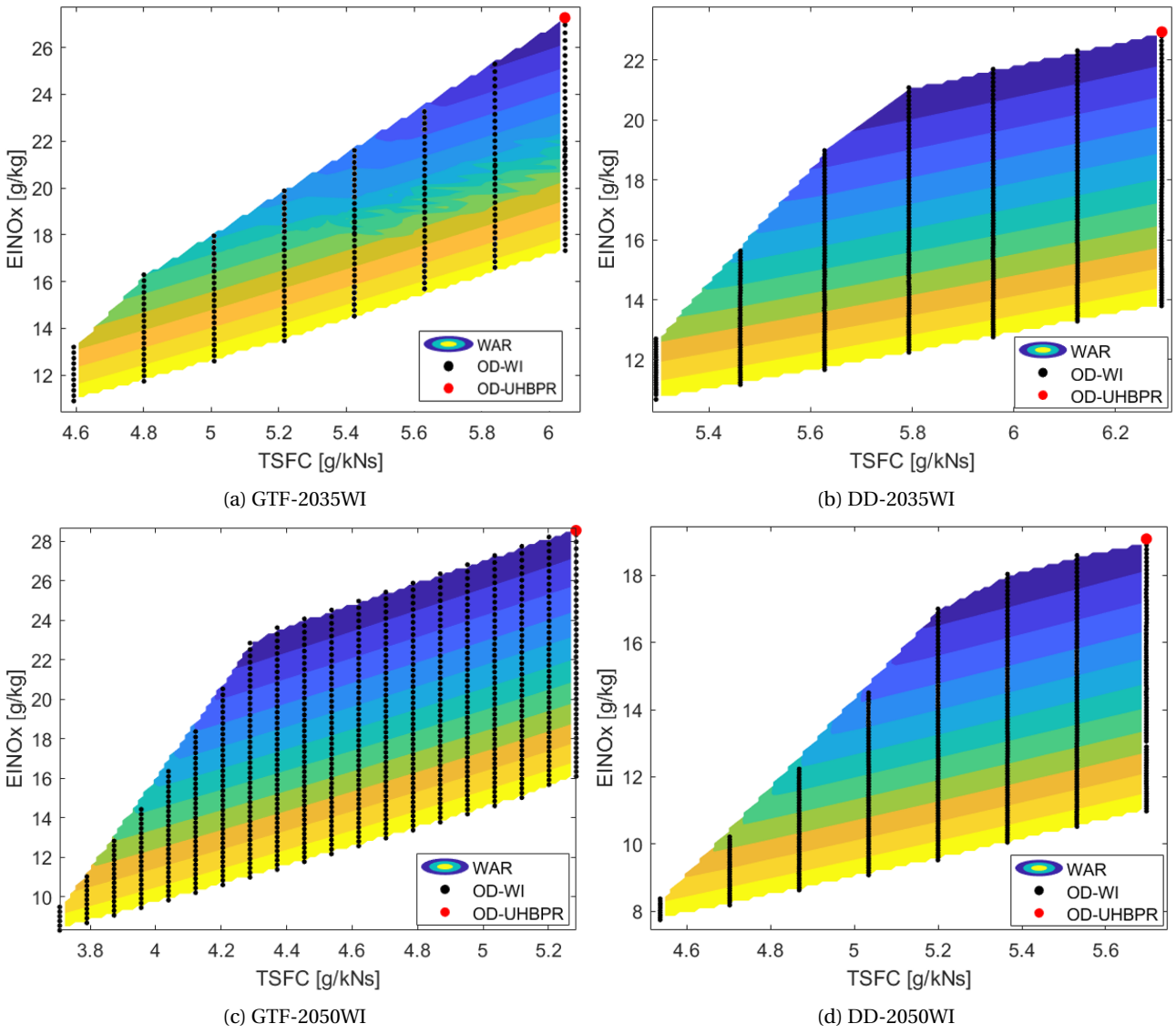

(a) GTF-2035WI

(b) DD-2035WI

(c) GTF-2050WI

(d) DD-2050WI

Figure 5.4: Off-design points for all WI UF-models compared to BF-models

There is a different trend visible for off-design conditions than for design conditions, being that the optimum point at off-design coincides with both a minimum TSFC and a minimum EI_{NO_x}. Due to there being no required T_{t4} to achieve, the cooling of the combustion chamber by the added water now doesn't need to be compensated by an increase in fuel mass flow. Achieving the same output thrust for a lower fuel flow requires a higher WAR. A higher WAR simultaneously decreases NO_x formation, leading to an optimal design at the lowest possible T_{t4} with the highest WAR.

5.2. Inter turbine burning

ITB had the same design approach as WI. OPR, T_{t4} and second combustor energy percentage E% were varied and the results were filtered according to the same standards as mentioned in the introduction of this chapter. The initial 'design point' of the ITB in GSP with the same design parameters as the BF-models would show a slightly higher TSFC than the BF-models, as the second combustor causes some pressure loss when it is not used. Compensating this pressure loss by adding more power to one of the combustors means adding more fuel and thus increasing the TSFC. So, contrary to the WI models, there exists no point in the design space that provides a better fuel performance than the associated UHBPR BF-model. Nevertheless, the performance improvement of ITB lies mainly in its contribution to take-off power and decrease in NO_x emissions. The results of the design point simulations are shown in Section 5.2.1 and those of the off-design simulations in Section 5.2.2.

5.2.1. Design point

The design space of ITB, like that of WI, is very large. An example of the design space of the DD-2050ITB is shown in Figure 5.5. The contour indicates the E% of the second combustor, where dark blue is a lower contribution and bright yellow a higher contribution. The red dotted line is one isoline of the T_{t4}, the black lines are some isolines of the OPR.

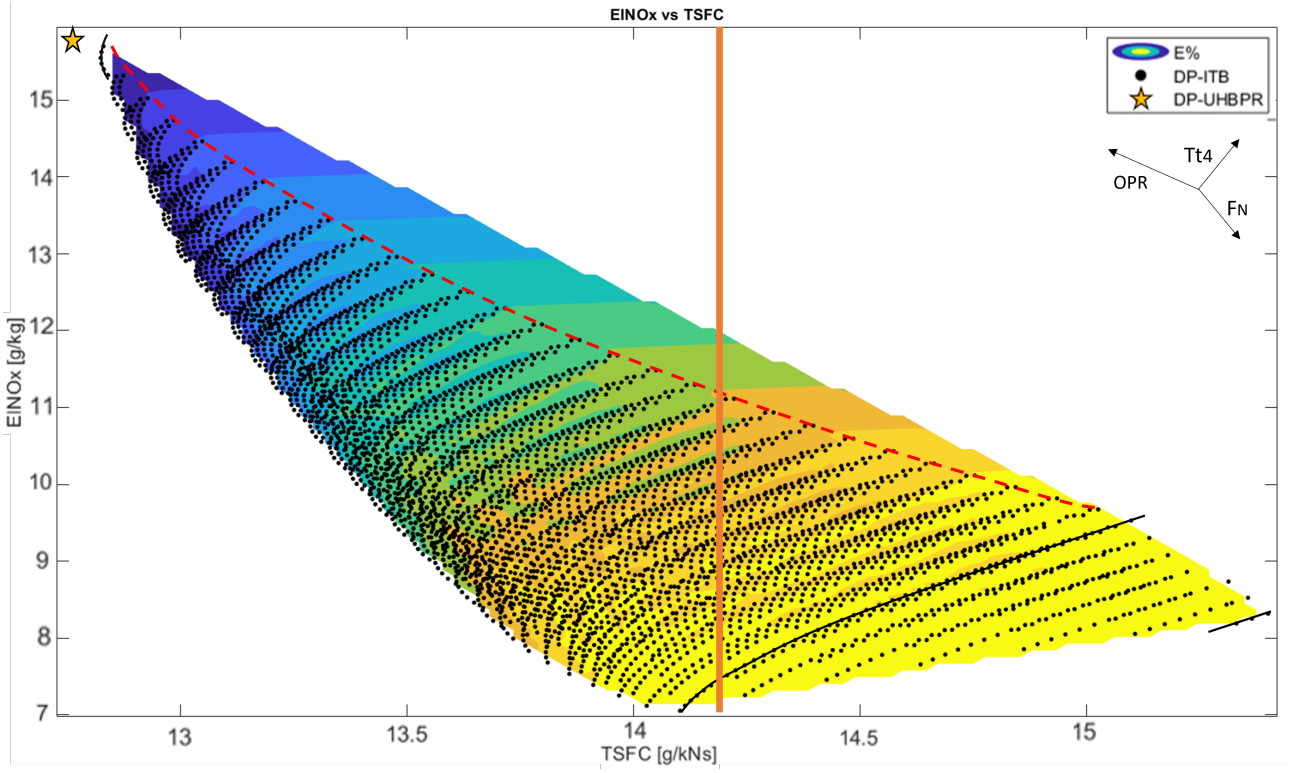

Figure 5.5: Simulation results within the entire design space of DD-2050ITB. The orange line is placed at the point of minimum TSFC to indicate the less favourable design options on the right side of line. The arrows in the upper right corner indicate the direction of increase for the combustion outlet temperature T_{t4}, overall pressure ratio (OPR) and net thrust F_N.

All ITB UF-models show the same general trends as the ones in Figure 5.5. Evaluating the design variables separately, the following conclusions can be drawn:

1. As the OPR increases, the TSFC goes down while the EI_{NO_x} goes up.
2. As the T_{t4} increases, both the TSFC and EI_{NO_x} go up.
3. As the E% increases, the TSFC goes up while the EI_{NO_x} goes down.

Although the graphs from Figure 5.6 and Figure 5.1 look different, the trends remain the same. Trend 1 and 2 occur due to the same principles as explained in Section 5.1.1. The third trend is similar, expect the effect on TSFC and EI_{NO_x} are dependent on the E% instead of the WAR. At higher E%, the fuel flow in the main combustor is lower than the design case. This leads to a lower main combustor outlet temperature. Combining this with a low OPR provides the great NO_x reduction that can be observed in the lower right corners of Figure 5.6. As all cases follow the same general trend as DD-2050ITB, all design points on the right side of the minimum EI_{NO_x} point in all cases (visualised as the thick orange line in Figure 5.5) were omitted here. Although the second combustor produces NO_x as well, this value is much lower as the flow is already partially expanded after the first combustor and the combustion temperature is lower.

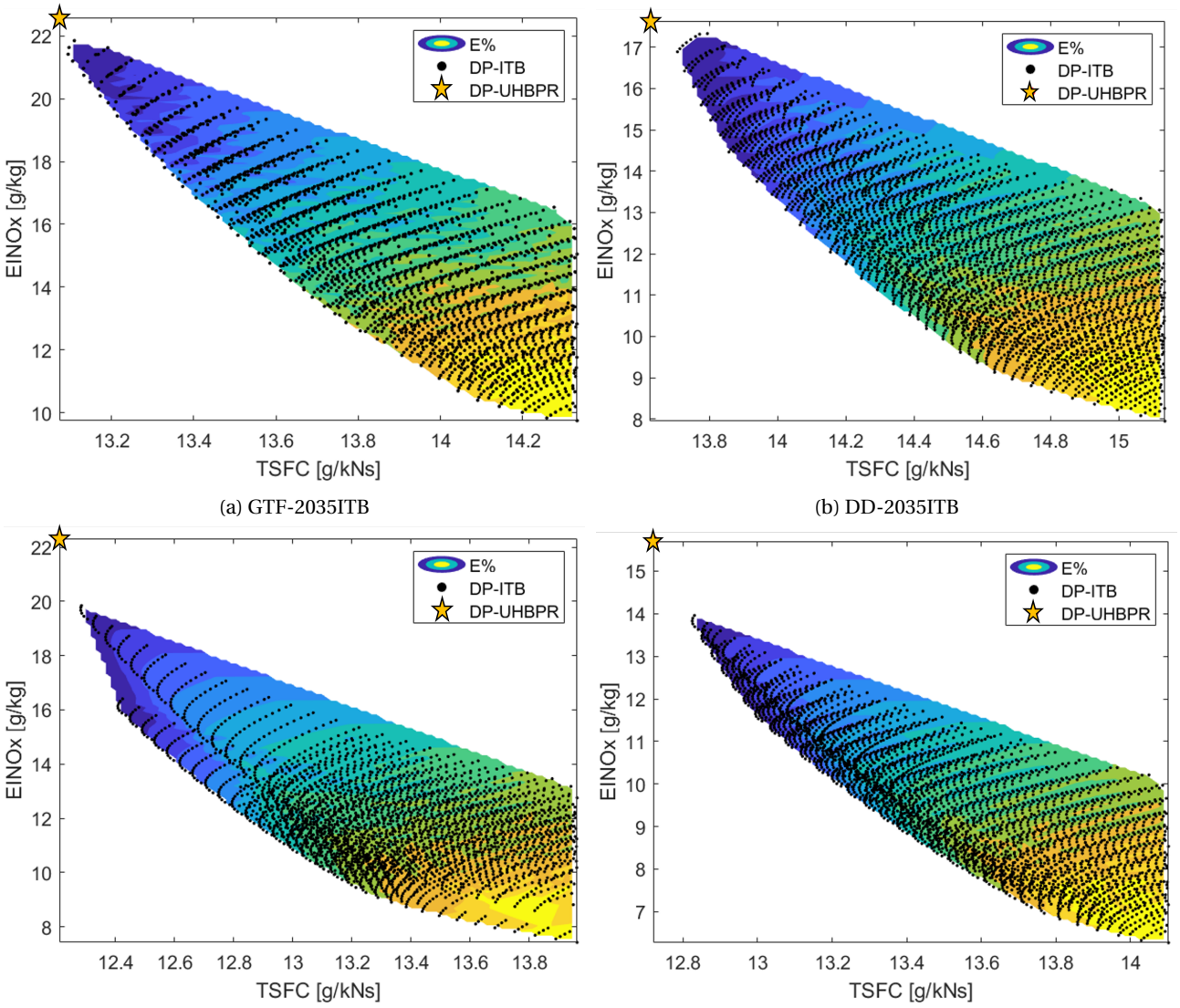

(a) GTF-2035ITB

(b) DD-2035ITB

(c) GTF-2050ITB

(d) DD-2050ITB

Figure 5.6: ITB design points for all UF-models compared to BF-models

The increase in TSFC for higher E% comes with an increase in net thrust. This means that the inlet mass flow can be decreased while still achieving the required thrust. A lower inlet mass flow would lead to a smaller engine, which would be beneficial for the weight. Like with WI, the decrease in inlet diameter would be dependent on the take-off requirement and the limit of HC10. As such, the off-design performance will be analysed next.

5.2.2. Off-design

For the off-design series, the thrust output was set to the same value as the baseline models. The input parameters are the fuel flow of the first ($\dot{m}_{f1}$) and second combustor ($\dot{m}_{f2}$). Starting with the fuel flow output from the off-design case of the BF-models, $\dot{m}_{f1}$ was decreased while $\dot{m}_{f2}$ was increased. The results in Figure 5.7 show that there is a region where there is both an improvement in EI_{NO_x} and in TSFC, contrary to the design case. For the EI_{NO_x}, the same holds as for the design condition, where a lower OPR and T_{t4} decrease the EI_{NO_x} significantly. Due to the additional thrust by the second combustor, T_{t4} can be decreased considerably. This leads to a lower $\dot{m}_{f1}$ and subsequently a lower TSFC. The effect of adding ITB to an engine is thus most beneficial during the take-off condition with moderate second burner contribution.

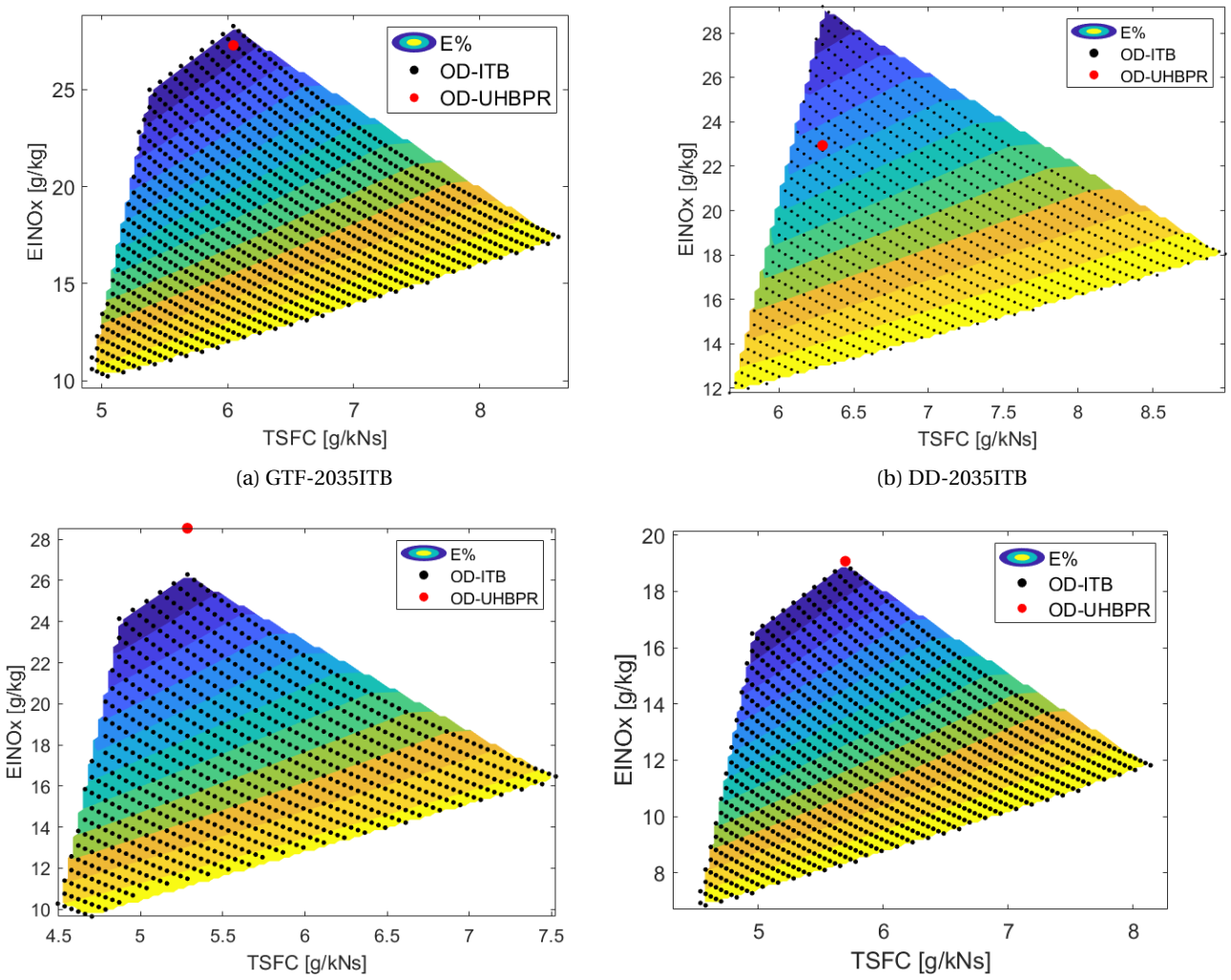

(a) GTF-2035ITB

(b) DD-2035ITB

(c) GTF-2050ITB

(d) DD-2050ITB

Figure 5.7: Off-design points for all ITB UF-models compared to BF-models

The design trend of a lower EI_{NO_x} and TSFC for a higher E% is obvious for every model. However, the design space is not equal, especially for DD-2035ITB. This is due to an off-design mismatch between GasTurb and GSP, where the off-design outputs are not similar for equal inputs. To incorporate ITB in the DD-2035BF model, some off-design parameters had to be changed in GSP, which recalculated the combustor inlet temperature, pressure and turbine inlet temperature. Since all these factors affect EI_{NO_x}, the trend here is different. If the less desirable combinations of fuel flow and energy percentage are removed (upper right section Figure 5.7b, the trend is the same as for the other engines. The combinations of fuel flow and E% that remain are real design options calculated by GSP and are suitable for this ITB engine model, thus the results can be evaluated nonetheless. For GTF-2050ITB the offset between the point of OD-UHBPR and the 'top' of the graph that is visible in Figure 5.7d is caused by the same phenomenon as for DD-2035ITB as described above, but less severe. The trend is therefore exactly the same as for GTF-2035ITB and DD-2050ITB and can also be evaluated as is.

5.3. Multi-point lean direct injection

As was mentioned earlier, the use of a lean burning combustor is likely for the time frames that are assessed here. The benefits of combining such a combustor with WI or ITB could lead to an even larger decrease in NO_x emissions, provided the combustion is stable. This would also mean that a design can be chosen from within the design space that has a more favourable TSFC performance, while achieving additional NO_x benefits from the LBCC. Section 3.4.3 mentioned the prerequisites for efficient combustion at very low FARs. The FARs of the different designs were therefore adjusted as if an MPLDI combustor was used instead of an RQL combustor. The incoming air flow that enters the primary zone is much larger than that of an RQL combustor. Even with enough mass flow for liner cooling, the incoming mass flow is about three times as high in the primary zone as for an RQL. At too low equivalence ratios, the lean blow out limit can be reached. Experiments with MPLDI at different inlet temperatures and pressures has shown stable and high efficiency combustion for FARs of <0.02 at TOC and T/O inlet conditions (medium and high P3, high T3) [44]. A follow up study with an improved 36-point MPLDI showed stable combustion up to a FAR of ~ 0.017 at high

P3 and T3 inlet conditions [45]. This is well below the usual blow out limit of a turbofan. The test facility limitations in terms of inlet conditions cannot however guarantee stable operation over the entire engine operating envelope.

Several assumptions had to be made to apply an MPLDI to the WI and ITB UF-models:

1. With relatively low combustion temperatures and advanced future materials, 15% of the incoming air was assumed to be used for liner cooling, hence 85% of the flow was assumed to enter the combustion zone.
2. Due to the low FAR in the second combustor of an ITB engine, efficient combustion cannot be guaranteed here. Therefore, an MPLDI combustor is only installed as the first combustor in the ITB engines. The second combustors remains an RQL.
3. The water injection was also assumed to be injected immediately at the front of the combustor.
4. For the calculation with Equation (3.7), it also has to be assumed that the fuel, water and air are instantaneously mixed to base the FAR on the combination of all three mass flows.
5. For a wide range of inlet pressure testing conditions, the minimum FAR for stable operation was shown to be around 0.02. Although lower FARs (up to around 0.017) have shown stable operation, design and off-design points with a FAR lower than 0.02 were disregarded.

The trends for the effect of employing an MPLDI combustor are the same for all UF-models. Therefore, only one example per UF-model is shown to discuss the general trends. The MPLDI combustor combined with water injection is shown in Figure 5.8.

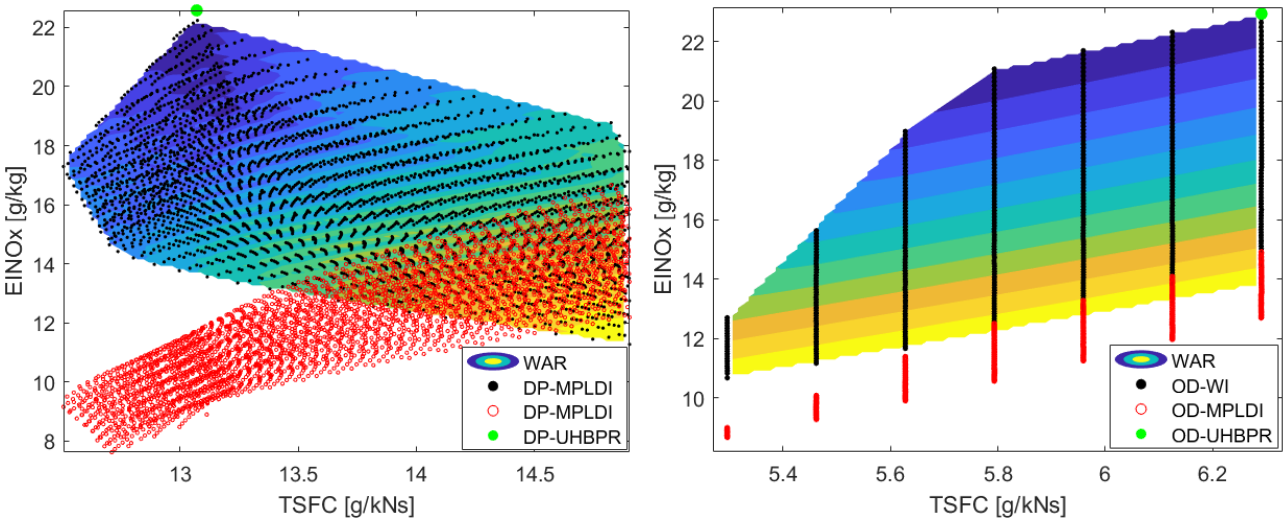

(a) GTF-2035WI-MPLDI

(b) DD-2035WI-MPLDI

Figure 5.8: Comparison between the EI_{NO_x} of an RQL combustor (black dots) and a MPLDI combustor (red circles) with water injection at design condition (left) and off-design condition (right)

It can be seen that a higher WAR is not as beneficial anymore for the EI_{NO_x} reduction as it was for solely WI at the design condition. With MPLDI the point of lowest EI_{NO_x} can be found at the combination of minimum OPR, minimum T_{t4} and minimum WAR. For WI, this was the case at minimum OPR and minimum T_{t4}, but at maximum WAR. For the MPLDI combustor, the FAR should be as low as possible. As was explained in Section 5.1.1, a low OPR with high WAR requires more fuel to achieve the same T_{t4}. Even though the FAR is initially decreased due to the higher water content, the contribution of the water to the overall air mass flow is small. Thus, the increase in WAR is proportionally larger than the increase in water content, increasing the FAR. Therefore, a lower WAR is desirable when using an MPLDI combustor. This is why the trend is visible in Figure 5.8a that for a constant OPR and T_{t4} and increasing WAR, the EI_{NO_x} goes up. Nevertheless, the water injection is necessary to allow the turbines to extract enough power from the exhaust gas at such low OPRs and T_{t4}. The combined improvement is thus very great. For the off-design condition, the same reasoning for MPLDI improvement applies as for the case with solely WI, explained in Section 5.1.2.

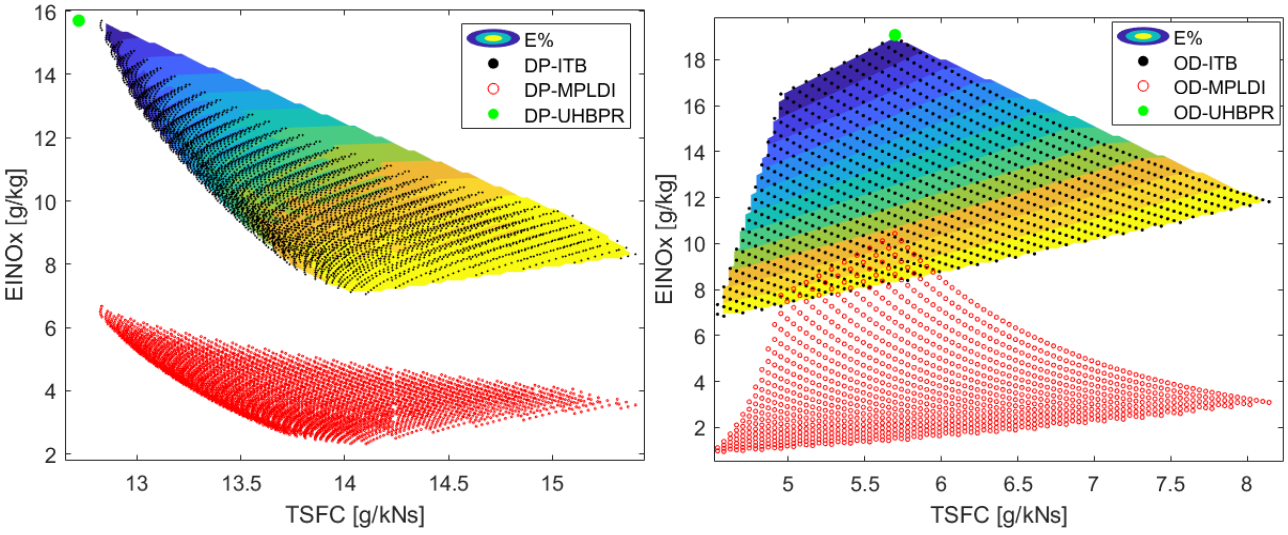

(a) DD-2050ITB-MPLDI

(b) DD-2050ITB-MPLDI

Figure 5.9: Comparison between the EI_{NO_x} of an RQL combustor (black dots) and a MPLDI combustor (red circles) with inter turbine burning at design condition (left) and off-design condition (right)

For ITB, the employment of the MPLDI combustor shifts the design and off-design points almost linearly downward. The first combustor of the ITB achieves a lower FAR and thus a large decrease in EI_{NO_x}, but there is no additional mass flow content (like with WI) to offset this. The graph of the ITB with MPLDI will thus, contrary to WI, follow the same trend as the ITB with RQL. To calculate the total NO_x emissions, Equation (3.6) was used again. The first term in Equation (3.6) was described as the emission index of an engine with a single combustion process, thus substituting this for Equation (3.7) gives an approximation for the total EI_{NO_x} emissions. However, the validity of manipulating Equation (3.6) to describe an ITB-MPLDI with regular second combustor is uncertain. For off-design, the change in EI_{NO_x} for a higher energy percentage decreases, which is a result of the decreased contribution of the MPLDI combustor to the total NO_x emissions.

5.4. Results summary

Before making the trade-off, a summary of the results of all models can be seen in Table 5.1. Horizontally, the UF-models are evaluated at their lowest TSFC point and at their lowest EI_{NO_x} point. As was shown in Section 5.1 and Section 5.2 these points do not coincide, except at the off-design condition with water injection. For both the lowest TSFC point and the lowest EI_{NO_x} point, the associated values for TSFC and EI_{NO_x} are given in the columns normalised against the baseline models. The actual values can be view in Appendix B. For clarity, the values in bold indicate a reduction.

Table 5.1: Summary of results for lowest TSFC and lowest EI_{NO_x} values for all models compared to the baseline models.

			GTF-2035		DD-2035		GTF-2050		DD-2050	
			TSFC	EI_{NO_x}	TSFC	EI_{NO_x}	TSFC	EI_{NO_x}	TSFC	EI_{NO_x}
BF	DP		**-9.24**	32.20	**-8.89**	31.76	**-15.21**	30.68	**-14.97**	17.34
	OD		**-8.92**	31.20	**-11.87**	**-25.52**	**-20.52**	37.21	**-20.13**	**-38.08**
WI	DP	Min TSFC	**-13.19**	1.23	**-12.37**	4.04	**-19.51**	**-0.64**	**-18.65**	**-8.74**
		Min EI_{NO_x}	3.47	**-34.02**	**0.53**	**-36.55**	**-3.19**	**-32.96**	**-3.68**	**-36.62**
	DP-MPLDI	Min TSFC	**-13.19**	**-53.28**	**-12.37**	**-50.60**	**-19.51**	**-59.66**	**-18.65**	**-59.79**
		Min EI_{NO_x}	**-11.74**	**-61.18**	**-10.96**	**-58.22**	**-17.15**	**-68.56**	**-16.98**	**-67.71**
	OD	Min TSFC	**-30.90**	**-47.64**	**-25.74**	**-65.36**	**-44.30**	**-60.05**	**-36.39**	**-74.84**
		Min EI_{NO_x}	**-30.90**	**-47.64**	**-25.74**	**-65.36**	**-44.30**	**-60.05**	**-36.39**	**-74.84**
	OD-MPLDI	Min TSFC	**-21.57**	**-48.03**	**-25.74**	**-72.82**	**-31.66**	**-57.45**	**-31.76**	**-78.05**
		Min EI_{NO_x}	**-21.57**	**-48.03**	**-25.74**	**-72.82**	**-31.66**	**-57.45**	**-31.76**	**-78.05**
ITB	DP	Min TSFC	**-9.10**	25.41	**-8.36**	26.23	**-14.72**	15.16	**-14.30**	16.22
		Min EI_{NO_x}	**-0.49**	**-42.97**	1.20	**-40.58**	**-3.06**	**-56.56**	**-5.75**	**-47.31**
	DP-MPLDI	Min TSFC	**-9.10**	**-51.64**	**-8.36**	**-44.62**	**-14.72**	**-53.86**	**-14.30**	**-53.51**
		Min EI_{NO_x}	**-0.49**	**-91.33**	**1.20**	**-90.13**	**-3.68**	**-91.57**	**-5.75**	**-92.23**
	OD	Min TSFC	**-25.79**	**-46.25**	**-20.55**	**-61.75**	**-32.26**	**-50.58**	**-36.39**	**-77.53**
		Min EI_{NO_x}	**-23.98**	**-50.87**	**-20.55**	**-61.75**	**-29.25**	**-53.56**	**-35.83**	**-77.79**
	OD-MPLDI	Min TSFC	**-25.79**	**-91.01**	**-20.55**	**-93.93**	**-32.26**	**-93.22**	**-36.39**	**-96.82**
		Min EI_{NO_x}	**-23.98**	**-92.60**	**-20.55**	**-93.93**	**-29.25**	**-94.09**	**-35.83**	**-96.88**

At a few conditions the BF-models and UF-models do not outperform the baseline models:

- For the BF-models, it was already discussed that the EI_{NO_x} at design point (DP) is higher due to the increase in OPR compared to the baseline models. For the off-design (OD) points, this is not the case for DD-2035BF and DD-2050BF as the use of the RQL combustor improves the EI_{NO_x} compared to the lean-burning TAPS II used in the baseline.
- For GTF-2035WI and DD-2035WI at DP, the minimum TSFC only has a small EI_{NO_x} improvement that is not able to overcome the 30% increase due to the higher OPRs compared to the baseline, as the TSFC improvement is mainly achieved by decreasing T_{t4}. For GTF-2050WI, the improvement is only marginal for the same reason. DD-2050 has approximately the same OPR as DD-2035, but a much lower T_{t4}. Therefore, the EI_{NO_x} for DD-2050 is able to reach an improvement with WI at DP.
- The minimum TSFC at ITB DP is found at an E% of zero. This means that for all models, there is no NO_x benefit at this point.
- Moving towards a lower EI_{NO_x} at ITB DP always increases the TSFC, so the TSFC improvement made with the BF-models is decreased. For DD-2035ITB, this off-sets the entire TSFC improvement and for GTF-2035ITB it almost does. The TSFC margin for GTF-2050BF and DD-2050BF are large enough compared to the baseline to ensure when the TSFC moves up for the ITB DP cases, it does not surpass the baseline TSFC values.

The rest of the points within the design spaces show an improvement compared to the baseline engines. With just WI and ITB, the EI_{NO_x} can be improved with at least 30% for all engine models. With the addition of MPLDI, the improvements range from around 50% to a maximum of almost 97%. Although values of 50-60% are not a surprising improvement compared to experimental tests with MPLDI, values of 80-97% seem unrealistic. This magnitude of improvement is only visible at the ITB cases, which probably suggests that the EI_{NO_x} correction used here does not describe the effect of the MPLDI combustor in an sequential combustion set-up very well. The improvement potential of an MPLDI combustor has been estimated at around 53% compared to modern day lean burning engines [15]. Using solely ITB shows an improvement potential between ~ 35-70%. At the lowest improvement margin, this could be combined to 65% improvement, while for the most extreme case the combined improvement should be around 83%. A more accurate representation of NO_x emissions through ITB with a MPLDI combustor is thus required to be able to evaluate these results. The expected improvements for TSFC and EI_{NO_x} from Section 3.4.1 with WI are not entirely in line with the results in Table 5.1. The TSFC reduction is only minimal, but the effect of decreasing the engine size was not taken into account in this evaluation. The NO_x emissions were predicted to decrease up to around 90%, but the maximum improvement here is 75% from solely the WI. However, a lower fuel consumption does contribute to lower NO_x emissions as well. The combined improvement can, for the lowest EI_{NO_x} cases, approach this 90%. At off-design conditions this is especially visible.

It was previously explained why the TSFC during take-off would specifically benefit from the use of WI and ITB. This is reflected in the results in Appendix B, where the TSFC improvements at OD add an additional 15-25% of TSFC improvement on top of the TSFC reduction by the BF-models. For the WI OD cases, the large amount of injected water

at take-off for additional thrust decreases the FAR already. When combined with an MPLDI combustor, the FAR might be too low to ensure stable combustion. Omitting these design options can result in a smaller TSFC improvement compared to the OD case with just WI.

5.5. Trade-off

To determine the overall best engine configuration, a trade-off can be done. For the trade-off, several things should be considered before deciding on an optimal design. This section explores what affects the choice for the optimal design. As was previously mentioned, engine size plays a role on the aircraft level, thus this is explored in Section 5.5.1. The fuel consumption versus emissions is always a trade-off for engine design. Ideally, the engine models would be able to achieve the emissions goals stated in Section 1.2 while showing an improved fuel performance compared to current day engines. This is discussed in Section 5.5.2.

5.5.1. Engine size

Contrary to regular engine design, the engine models are actually "oversized" for TOC condition rather than T/O, This is the result of the increase in BPR for the BF-models while the thrust requirement stays the same as for the baseline engines. The augmented thrust provided by water injection and inter turbine burning dismiss the need for additional thrust by a larger inlet mass flow (W_1). A numerical experiment was conducted where W_1 at TOC was varied for different values of OPR, T_{t4} and WAR/E%. There stills exist a large design space for an engine with enough power to also comply with the take-off requirement, assuming that WI/ITB is always available. An example of such a design space can be seen in Figure 5.10. The contour is replaced by a contour for W_1, where yellow indicates a higher mass flow and blue a lower mass flow.

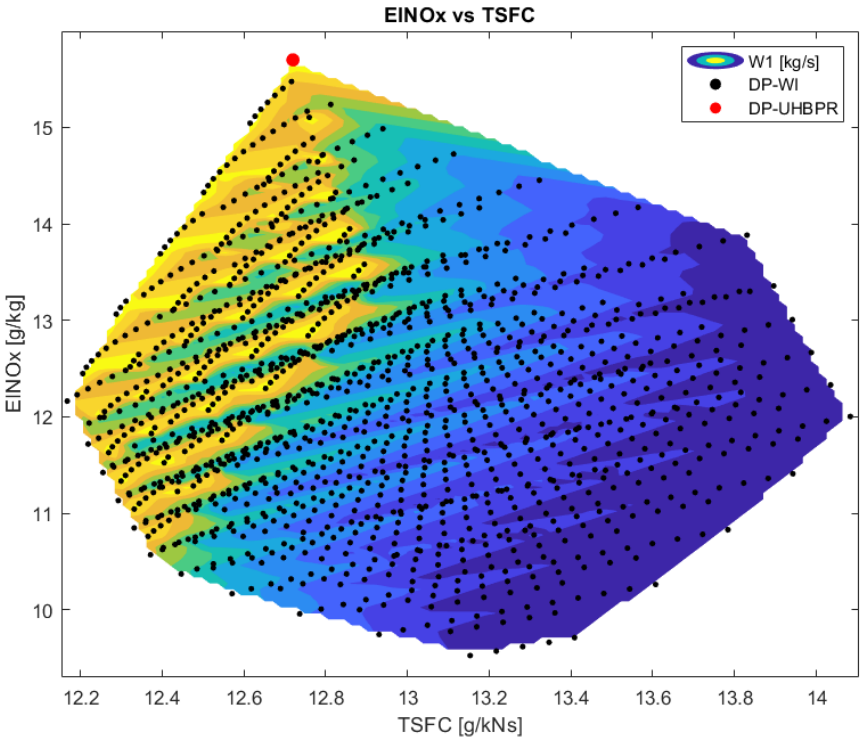

Figure 5.10: Design space for DD-2050WI with a varying inlet mass flow to achieve the required thrust

It can be seen from Figure 5.10 that the EI_{NO_x} improvement is similar to Figure 5.2d, although somewhat lower as a result of high-WAR designs decreasing the inlet diameter beyond what is required at minimum for take-off. The TSFC improvement is the same, but that does not take into account the weight savings on the entire aircraft. Since both a water injection system and a second burner add weight to the engine, it would be interesting to explore how this would balance each other. This is especially relevant for water injection. For water injection to be effective on long distances, a lot of the water that is injected has to be recovered from the exhaust stream. Otherwise, the weight of the water adding to the total weight of the aircraft will eventually offset the TSFC improvement. These designs are only possible when the BPR is kept constant, which means that the core would shrink along with the engine. The BF-models were optimised such that HC10 would reach its minimum value. Changing the core size significantly might

affect this constraint as well. As GSP offers no internal geometry calculations, it cannot be said if these design would be feasible. Therefore, this option is not considered for the trade-off. It would be valuable to explore this in further research, but performing geometry calculations for every point in this design space would be beyond the scope of this thesis.

5.5.2. Performance versus emissions

With the addition of an LBCC, a trade-off between TSFC and EI_{NO_x} is made easier. The design point for the maximum TSFC improvement gives a 10-15% TSFC reduction for the 2035 UF-models and a 15-20% reduction for the 2050 UF-models. Combined with an LBCC, the EI_{NO_x} can be reduced by at least 45% for the lowest TSFC option compared to the modern day baseline models. As was stated in Section 1.2, there are several goals for emissions reductions in 2035 and 2050:

- ACARE states "a 30% reduction in non-CO_2 climate effects [...] relative to the 1990 baseline" for 2035.
- The ICAO states a 60% reduction in NO_x emissions compared to their 2008 reference for 2030 and a 2% fuel efficiency improvement per annum from 2020-2050.
- Both aspire net-zero CO_2 emissions by 2050.

The NO_x improvement of at least 45% would make a large contribution to the 30% reduction of non-CO_2 climate effects. A 60% NO_x improvement in 2035 is attainable for both the GTF-2035WI and DD-2035WI when looking at the combined TSFC and EI_{NO_x} improvement. Especially LTO NO_x emissions can be reduced drastically for the DD-2035WI. The major decrease in T_{t4}, especially at take-off condition, is very beneficial for the prevention of thermal NO_x formation, but has a negative effect on the CO, UHC and soot emissions. However, the low equivalence ratio in the MPLDI combustor is beneficial for CO emissions. These emissions have been ignored thus far, but for future research there would need to be an assessment of the climate impact of all exhaust emissions to evaluate the total climate improvement of the UF-models to be able to compare it to the ACARE goal.

According to [15], the contributions of the engine to the total fuel efficiency of the engine in 2035 and 2050 are 10% (out of 30%) and 16% (out of 53%) respectively. As stated there, the law of diminishing returns and non-linear influence on the fuel burn decreases the total improvements of all technology improvements to 22% and 38%. To achieve the 2% annual fuel efficiency improvement, the total fuel burn improvement should be 26% for 2035 and 51% for 2050. This means that the efficiency of the technologies contributing to the fuel efficiency should be more than predicted now. As there are no TSFC improvements at DP for ITB, this will not provide the additional fuel burn improvements that are required. With WI however, the improvements at DP exceed the prediction made in [15]. Additionally, although a smaller part of the overall flight envelope, the improvements at OD are 2.5 to 4.5 times as large. The combined contribution of this to the total flight fuel savings moves the total fuel improvement of the 2035 engines close to the 26%. For the more fuel-efficient GTF-2035, it is likely that this percentage can be reached in 2035. For 2050, the fuel burn improvements of both GTF-2050 and DD-2050 are not great enough to achieve the 51% fuel burn improvement in 2050. To achieve this, the contribution of other technologies such as the airframe have to improve significantly as well compared to the current prediction. Advanced airframes such as the blended wing-body might achieve a fuel burn improvement of 30% per passenger kilometre for medium to long range aircraft [58]. Achieving a 55% reduction in CO_2 emissions for EU flights will not only be dependent on the fuel efficiency of the engine, but also on the effort into carbon off-setting by means of, for example, using sustainable aviation fuels.

5.6. Final designs

The only engine that appears to have a sufficient combination of TSFC and EI_{NO_x} characteristics such that it is able to reach the climate goals for the appropriate time frame is the GTF-2035WI. Its combination of low TSFC and EI_{NO_x} at design point and off-design conditions shows sufficient improvement in both fuel consumption and NO_x emissions to achieve the desired milestones in 2035. For ITB, the lack of TSFC improvement during TOC compared to a regular, optimised UHBPR engine makes this combination of technologies not suitable for achieving the fuel burn improvement goals. The NO_x improvement is very significant, especially combined with the MPLDI. However, the actual improvement of this combination should be investigated further as the current correlation does not appear to accurately describe the combined potential. For 2050, the goal of maintaining a 2% annual fuel burn improvement from 2020 is not likely to be met. The combinations of technologies show a maximum TSFC improvement of approximately 19% at TOC for WI and 15% at TOC for ITB. The NO_x characteristic of both 2050 UF-models are better than their 2035 counterparts, but it also shows that more innovation is needed to obtain a larger margin. Looking at the absolute values in Appendix B, the GTF-2050 has a better TSFC performance for any combination of technologies, the DD-2050 has a better NO_x performance for any combination of technologies. GTF-2050BF is the only BF-model with a higher engine mass than its associated baseline engine. DD-2050BF is slightly lighter than its associated baseline engine, making it a better candidate for the implementation of the future technologies than GTF-2050 when looking at the aircraft level. Part of the TSFC improvements in Table 5.1 will be off-set by the additional weight of the WI and ITB systems, so a lighter engine would mean a smaller offset. The DD-2050UF would therefore be the preferred engine for the 2050 scenario. The engine characteristics of the final designs can be seen in Table 5.2.

Table 5.2: Engine characteristics of the final designs

	GTF-2035WI-MPLDI		**DD-2050WI-MPLDI**	
	DP	OD	DP	OD
Thrust [kN]	26.60	120.43	25.98	120.63
Fuel flow [kg/s]	0.333	0.653	0.316	0.587
TSFC [g/kNs]	12.52	5.42	12.18	4.87
EI_{NO_x} [g/kg]	7.78	11.52	5.22	6.76
OFPR [-]	1.48	1.36	1.39	1.28
IFPR [-]	1.35	1.26	1.38	1.28
BPR [-]	14.29	9.25	15.99	14.71
$\eta_{p_{fan_c}}$	0.935	0.936	0.935	0.918
$\eta_{p_{fan_d}}$	0.932	0.933	0.932	0.915
IPR [-]	3.60	2.83	3.00	2.38
$\eta_{p_{IPC}}$	0.915	0.913	0.908	0.919
HPR [-]	11.164	11.63	10.694	10.84
$\eta_{p_{HPC}}$	0.918	0.921	0.925	0.929
OPR [-]	52.25	40.34	42.89	32.14
T_{t4} [K]	1450	1301	1405	1263
WAR [-]	0.067	0.175	0.067	0.139
$\eta_{p_{HPT}}$	0.908	0.907	0.910	0.908
$\eta_{p_{LPT}}$	0.924	0.922	0.930	0.929

Cruise condition

All engines have so far only been analysed at two flight conditions: top of climb and sea-level static conditions (take-off). These two points can be seen as the aerodynamic design point and the thermal design point. Another important flight condition is cruise, as a short-to-medium range aircraft will spend most of their flight time in this condition. This point can be seen as the energy design point. Here, the components should operate at their maximum efficiency and therefore generally operate at slightly lower pressure ratios to achieve the highest fuel efficiency, This means that the thrust output at cruise is lower than at TOC, usually in the range of 85-90%. Top of climb is the transition from climb phase to cruise flight, so the altitude (10668 m) and Mach number (0.78) of the aircraft during cruise are the same as at TOC. However, for cruise ΔT from ISA is set to 0 K. This change in temperature affects the inlet conditions and thus the engine performance. It was previously established that the most promising future engine models for a combination of design point and off-design performance are the GTF-2035WI-MPLDI for 2035 and the DD-2050WI-MPLDI for 2050. Therefore, only these engines are analysed at cruise.

The cruise condition for both engines should be derived from the state-of-the-art baseline models (B-models) first, The cruise conditions for the B-models define the thrust output for the future models and will serve as the baseline to compare the cruise performance of the future with. The engine characteristics at cruise condition for the B-models can be found in Table 5.3. The thrust output at cruise for the B-models was used to calculate the engine characteristics of the baseline future engine models (BF-models), such that the future engines can be compared to the state-of-the-art engines in terms of TSFC. This is the same procedure that was done for both TOC and take-off. The results of the BF-models can also be found in Table 5.3. The BF-models at cruise condition formed the starting point for the upgraded future engine models (GTF-2035WI-MPLDI and DD-2050WI-MPLDI). The discussion of the design point calculations at TOC in Section 5.1.1 showed that the point of lowest TSFC can be found by varying the OPR and T_{t4}, while automatically adjusting the WAR to achieve the required thrust. An EI_{NO_x} correction can then be applied to see the effect of replacing the normal RQL combustor with an MPLDI combustor. The performance results of the GTF-2035WI-MPLDI and the DD-2050WI-MPLDI can be seen in Figure 5.11a and Figure 5.11b respectively.

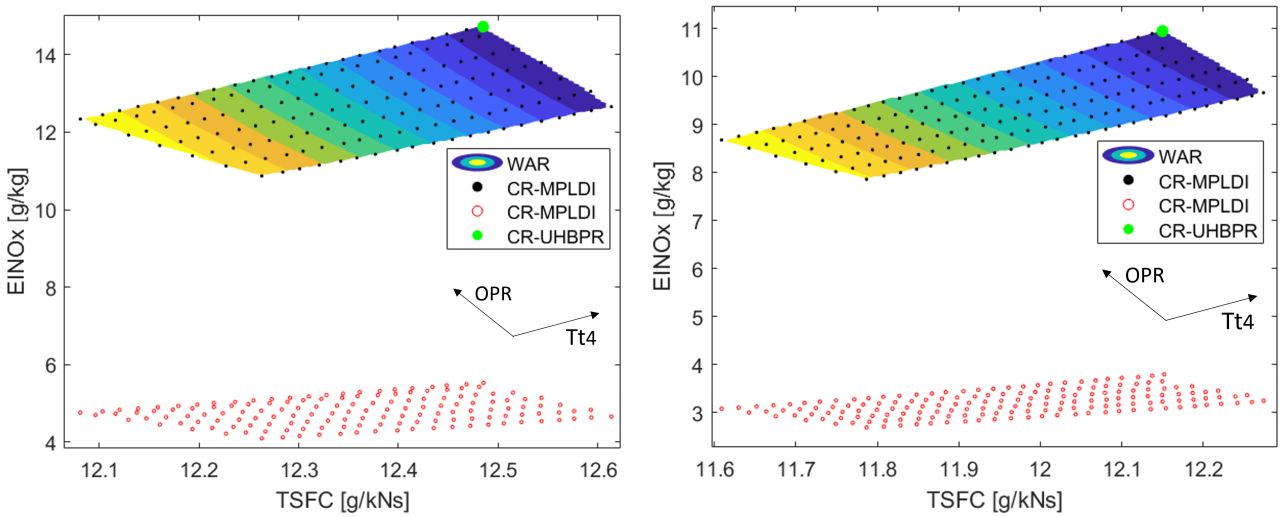

(a) GTF-2035WI-MPLDI

(b) DD-2050WI-MPLDI

Figure 5.11: Comparison between the EI_{NO_x} of an RQL combustor (black dots) and a MPLDI combustor (red circles) with water injection at cruise conditions for the final design options. The arrows on the right side in the figures indicate the direction of increasing OPR and T_{t4}.

The same trends are visible for the cruise condition as for the TOC condition that were presented in Figure 5.3. A high WAR, high OPR and low T_{t4} provide the biggest TSFC improvement. The large diameter of the engine and subsequent inlet mass flow combined with the augmented thrust by water injection provide enough thrust at low T_{t4} to provide the same amount of thrust as a state-of-the-art engine, leading to an improvement in EI_{NO_x}. The addition of the MPLDI provides an even more drastic EI_{NO_x} reduction, like at TOC and take-off condition. The same trade-off as discussed before between performance and emissions can also be applied here: the MPLDI provides such an EI_{NO_x} reduction that the point of minimum TSFC is the most interesting point within the design space to evaluate. The engine characteristics of the GTF-2035WI-MPLDI and DD-2050WI-MPLDI at the point of lowest TSFC are therefore visible in Table 5.3 for comparison to their respective B-model and BF-model.

Table 5.3: Engine characteristics at cruise condition for the B-models, BF-models and selected UF-models(GTF-2035WI-MPLDI and DD-2050WI-MPLDI)

	GTF-B	**GTF-2035BF**	**GTF-2035WI-MPLDI**	**DDTF-B**	**DD-2035BF**	**DD-2050WI-MPLDI**
	CR	CR	CR (min TSFC)	CR	CR	CR (min TSFC)
Thrust [kN]	23.90	23.90	23.90	23.40	23.40	23.40
Fuel flow [kg/s]	0.327	0.298	0.289	0.334	0.284	0.268
TSFC [g/kNs]	13.70	12.48	12.08	14.29	12.15	11.61
EI_{NO_x}	15.54	14.74	4.77	11.83	10.94	3.08
OFPR [-]	1.43	1.44	1.44	1.50	1.36	1.36
IFPR [-]	1.29	1.32	1.32	1.33	1.35	1.35
BPR [-]	12.61	14.93	14.93	11.35	16.67	16.67
η_{fan_c}	0.943	0.959	0.959	0.923	0.956	0.956
η_{fan_d}	0.942	0.956	0.956	0.922	0.953	0.953
IPR [-]	2.49	3.47	3.47	1.95	2.92	2.92
$\eta_{p_{IPC}}$	0.908	0.922	0.922	0.89	0.915	0.915
HPR [-]	12.34	10.84	10.84	15.08	10.37	10.37
$\eta_{p_{HPC}}$	0.909	0.921	0.921	0.909	0.928	0.928
OPR [-]	38.36	48.10	48.10	37.91	39.72	39.72
T_{t4} [K]	1452	1486	1376	1503	1440	1295
WAR	0	0	0.049	0	0	0.069
$\eta_{p_{HPT}}$	0.897	0.906	0.906	0.900	0.908	0.908
$\eta_{p_{LPT}}$	0.914	0.923	0.923	0.900	0.929	0.929

When the engine characteristics of the B-models and BF-models at TOC (see Appendix A) are compared to the characteristics at cruise condition, the aforementioned trends become visible. The same holds for the UF-models when comparing them to Table 5.1. The OPRs are slightly lower, while the efficiencies of the compressors are higher. There is a different trend for the turbines however, as the efficiencies lower slightly. This is likely a result of the cooling flows,

as these were not adjusted accordingly for the lower combustion temperatures within the design space. The TSFC performance and EI_{NO_x} at cruise are better than for TOC for all models, as was expected due to the higher component efficiencies, lower OPR and T_{t4}. The BPR at cruise is also slightly higher, contributing to a higher propulsive efficiency.

Overall, the cruise performance of the UF-models compared to the B-models is significantly better. The TSFC is improved by 12% for the the final 2035 model and by 19% for the 2050 model. NO_x emission are reduced by almost 70% for the 2035 model and 74% for the 2050 model. The TSFC improvement at cruise is almost the same as at TOC, but the NO_x improvement is greater. Since the aircraft spends most of its time in cruise, this has a positive influence on the NO_x emissions analysis conducted in Section 5.5.2. However, the negative effect of the even lower combustion temperatures on the formation of CO, UHC and soot offsets part of the positive influence of the EI_{NO_x} on the total climate impact.

5.7. Comparison to alternative architectures

The upgraded future engine models were a means to try and evaluate how realistic it would be to reach the climate goals with conventional engine technology. Alternative engine architectures like the WET, CCE, IRA and OR are being researched as the technology improvement of the conventional turbofan seems to be reaching an asymptote. Their biggest conventional competitor was the UHBPR, but it was evaluated in Chapter 2 that this engine could not compete with NO_x reductions of the WET and OR, while having a lower TSFC than the OR, CCE and WET. Employing the same technique as the WET engine by using water injection, upgrading the exhaust with an additional combustor and employing an LBCC were means to rival these alternative architectures. Even though the UF-models would require some internal architectural changes, they are not as severe as for example the WET engine and the CCE.

To assess the different architectures, the UF-models can be compared in the same manner as the other engine architectures in Table 2.8. For this purpose, the GTF-2035WI-MPLDI and DD-2050WI-MPLDI are evaluated for the same thrust requirement as the baseline model from the literature review (GTF-2015B) and added to Table 2.8. The TSFC and NO_x performance of the alternative architectures in literature are all evaluated at TOC. Therefore, the performance of the GTF-2035WI-MPLDI and the DD-2050WI-MPLDI are also measured at TOC.

Table 5.4: Comparison between GTF-2015B and all different engine architectures

	ΔTSFC [%]		ΔS_{NO_x} [%]		ΔEI_{NO_x}
	Associated GTF	GTF-2015B	Associated GTF	GTF-2015B	GTF-2015B
OR	-13.4	**-19.7**	-35.4	-35.3	-26.6
CCE	-18.2	-16.3	-10.0	-0.3	+17.4
WET	-13.0	-16.8	-90.0	**-90.3**	**-90.2**
IRA	-7.3	-10.0	-10.0	-12.0	+7.8
UHBPR	-23.9	-16.1	N/A	-12.9	-1.12
GTF-2035WI-MPLDI	-13.2	-17.4			-67.2
DD-2050WI-MPLDI	-18.7	-19.4			-78.9

The competitiveness of the WI-MPLDI models can be read from Table 5.4. Where first the UHBPR only offered a similar or lower TSFC improvement as the alternative architectures without any additional technologies, it now performs second best. For EI_{NO_x}, the improvement is marginal for an UHBPR engine, but with the additional low-NO_x combustion technologies the future UHBPR engines approach the NO_x improvement of the advanced WET engine.

5.8. Limitations

There were several limitations that influence the results described in this chapter:

- The step sizes for the simulations defined the lower limits for the design space in terms of T_{t4} and fuel flow. For smaller step sizes, more solutions can possibly be found that provide even better performance. This is visible in for example Figure 5.4, where the smaller step size of the GTF-2050WI and the coincidentally well chosen step sizes for the DD-2050 show more convergence towards a single minimum than the GTF-2035WI and DD-2035WI. Another example of this is Figure 5.6a.
- One of the main advantages of a lower combustion temperature is the reduced cooling requirement for the HPT. Larger WAR and E% both contribute to a lower combustion outlet temperature, so for both cases the cooling would ideally be adjusted as a function of these parameters. Determining a cooling schedule for all different design options would take a lot of time, and GSP does not adjust the cooling flow depending on T_{t4}, so the cooling fraction was kept constant. The HPT efficiency and subsequent overall efficiency are negatively influenced by this.
- The design space was limited to a 10% OPR and T_{t4} decrease in design conditions and a maximum WAR and E% of

30%. There also exist several, if not many, points outside this design space that can still be explored and could have an even better performance than the UF-models have currently.

- The EI_{NO_x} for an inter-turbine burning engine with a multi-point lean direct injection combustor as main combustor was calculated by combining Equation (3.6) with Equation (3.7). Evaluation of the results in Section 5.4 showed that this method likely over-predicts the effect on NO_x emissions and the lack of experimental data for such an engine option means that this calculation method cannot be validated.
- It was explained in Section 3.4.1 that the injection pathway of the water influences the NO_x reduction that can be achieved. GSP offers no options to change the injection pathway and as such, the NO_x emissions reduction is only described for one fixed (unknown) injection pathway.

6
Conclusions

The goal of this thesis was to evaluate the performance of a conventional turbofan engine for short-to-medium range aircraft, upgraded with future engine technologies that compromise between a fuel burn decrease and a decrease of in-flight exhaust emissions. This chapter concludes the findings of this thesis and makes recommendations for future work.

The proposed sub-questions in Section 1.4 serve as a guideline to answer the main research question of this thesis and in doing so provide several conclusions from this work. Therefore, the sub-questions are answered first:

1. What are the main drivers for engine design in the future? The main driver for engine design in the future is to find the balance between TSFC improvement (performance) and NO_x emissions (environmental). The effect of the engine design parameters are closely linked to one another, thus there exists no perfect combination. A solution would be to employ low-NO_x combustion techniques into a high-BPR high-OPR engine in an attempt to achieve the fuel burn improvement and emission reduction goals stated by international aviation organisations. More detail on the environmental and performance drivers are explained in the sub-sub-questions below.

- **1a. What are the required fuel burn and emission reductions of the propulsion unit based on its contribution to the total aircraft fuel efficiency?** According to the climate guidelines of several international aviation organisations, the fuel efficiency should increase with 2% per annum from 2020 to 2050. This should provide a 26% fuel burn improvement by 2035 and a 52% improvement by 2050. For 2035, the current outlook estimates a 10% fuel burn improvement from the engine (33% of sum of the total fuel burn improvements in combination with other technologies) for a total fuel burn improvement of 22%. This total takes into account the effect of diminishing returns and non-linear fuel improvement. For 2050, the estimate is a 16% fuel burn improvement from the engine (30% of the total fuel burn improvement) to achieve 38% total fuel burn improvement. Assuming the contribution of the engine remains constant, a fuel burn improvement of at least 13% is required for 2035 engines and 25% for 2050 engines. Non-CO_2 emissions are not directly related to fuel burn, but are largely dependent on the type of combustor. For non-CO_2 emissions, there is only an environmental milestone in 2030-2035 that aims to reduce the non-CO_2 climate impact by 30% for EU flights compared to 1990 and the NO_x emissions by 60% compared to 2008. A 60% reduction in NO_x emissions for future engines compared to modern engines would suffice to reach this goal.
- **1b. What is the effect of adjusting engine component characteristics on engine performance and emissions?** The engine parameters with the biggest influence on engine performance are the bypass ratio (BPR), outer fan pressure ratio (OFPR) and combustor outlet total temperature (T_{t4}). Increasing the BPR is especially beneficial for the propulsive efficiency, increasing the T_{t4} for the thermal efficiency and increasing the OFPR for the fuel efficiency. However, high BPRs are often paired with lower OFPRs to increase the propulsive efficiency even more and high T_{t4}s are paired with an increased overall pressure ratio. The increased OPR has, together with the increased T_{t4}, the largest negative influence on NO_x emissions. This contradicting design requirement is very difficult to balance on its own. Aiming for a low TSFC by means of a high-BPR, high-OPR engine while employing low-NO_x combustion techniques should provide a good balance.

2. How can future conventional gas turbine achieve the required fuel burn characteristics on engine performance and emissions specified in sub-question 1? As already hinted in the precious sub-question, a high-BPR engine with high-OPR and low-NO_x combustion techniques could provide enough improvement to achieve both goals.

- **2a. What future engine technologies can be combined into the same engine?** It was chosen to start with an optimised UHBPR engine and add low-NO_x combustion techniques to this. With the available resources, it was chosen to combine water injection with a lean burning combustor and to combine inter turbine burning with a lean burning combustor. Since the working principle of the first combustor in a sequential combustion set-up does not change it is possible to apply a lean burning combustor here. For the second combustor and the water injection, the fuel-to-air ratio will determine if employing a lean burning combustor is possible. For the second combustor, it was found that the FAR was below the lean blowout limit. For water injection, several design points had to be omitted to ensure a stable flame, but for most design points the FAR was high enough to ensure stable and highly efficient combustion.
- **2b. What combination of future engine technologies provides the biggest improvement potential in TSFC and NO_x emissions?** When looking at the absolute values in Table B.1 for TSFC, the best result for TSFC was achieved

with water injection for the GTFs. This is a result of the much higher OPR than can be achieved by these engines due to the geared fan. The use of a multi-point lean direct injection (MPLDI) combustor does not affect the TSFC performance at the design point for any of the water injection models. DD-2035WI and DD-2050WI have a better EI_{NO_x} performance for both design and off-condition, which can be attributed to the much lower OPR of the DD models compared to the GTF models and the dependence of EI_{NO_x} on the inlet conditions as described by Equation (3.5). The NO_x performance of the ITB models is better than that of the WI models when evaluating the lowest EI_{NO_x} points in the design spaces. For MPLDI, the NO_x emissions of the ITB models are always lower than for WI. However, the EI_{NO_x} correlation used for the combination of ITB and MPLDI appears to be overestimating the NO_x reductions. The only engine that seems to be capable to achieve the climate goals in their time-frame is the GTF-2035WI. The DD-2050WI has the best improvement potential for the 2050 time-frame as it has a much lower weight than the GTF-2050. However, for both engines, the weight addition of the water injection and water recovery system have not been taken into account for the TSFC calculations. A possible decrease in engine size was also not evaluated, which might compensate for the weight that water injection adds.

2c. How does a future conventional turbofan with a combination of future engine technologies perform on different mission types and segments? Table 5.1 shows that the largest improvements for TSFC are obtained during take-off condition. The improvement compared to the associated baseline engines is in most cases doubled or even tripled. The use of MPLDI at take-off decreases the FAR to values below the stability limit, which requires several low TSFC design options to be omitted. The TSFC improvement is therefore not maximised with MPLDI at take-off. The EI_{NO_x} improvements for these higher TSFCs at take-off with MPLDI are still large enough to decrease the NO_x emissions with 1-40% compared to the cases where there is no MPLDI combustor employed. At TOC there are significant TSFC improvements for all cases, although for ITB the TSFC is actually higher than for just the optimised UHBPR version of that engine model due to the pressure loss when the second combustor is not in use. Also at TOC, the EI_{NO_x} improvement for all models is relatively low when the engine is designed for minimum TSFC, and vice versa. The addition of the MPLDI at the minimum TSFC design point shows a very large decrease of NO_x emissions, ranging from -55% to -70%. A cruise condition performance evaluation of the best 2035 and best 2050 engine design showed a 12% and 19% TSFC improvement respectively. This is approximately equal to the improvement at TOC. The improvement of the NO_x emissions were slightly higher than for the TOC condition, reducing by 70% for the 2035 engine design and 74% for 2050.

3. How does a future conventional gas turbine compare to different engine architectures and thermodynamic cycles? Comparing the two most promising designs from each time frame (GTF-2035WI-MPLDI and DD-2050WI-MPLDI) with the alternative architectures (see Table 5.4), it can be seen that the upgraded future engine models are very competitive in both TSFC performance and emissions reductions. The open rotor still shows the best improvement in terms of TSFC, but only shows a moderate EI_{NO_x} improvement. The WET engine promises a 90% emissions reduction that cannot be paralleled by any other existing or future technology. The 67 and 78% reduction of the GTF-2035WI-MPLDI and DD-2050WI-MPLDI do however come much closer than any other alternative architecture as a result of the low combustion temperatures. Additionally, the GTF-2035WI-MPLDI and DD-2050WI-MPLDI show very high TSFC improvements compared to the other alternative architectures due to their high bypass ratio.

4. What is the combined improvement potential of a future conventional gas turbine with advanced airframe technology in terms of fuel efficiency and NO_x? The expected fuel burn improvements from airframe technologies in 2035 and 2050 are currently estimated to be 12 and 18% respectively. With advanced airframes such as a blended wing-body, this could increase towards 30% savings per passenger kilometre for a long range 250 pax aircraft. For a conservative estimate of 18 and 24% fuel burn improvements by an advanced airframe and the fuel burn improvements from GTF-2035WI-MPLDI and DD-2050WI-MPLDI, the total fuel burn improvement (applying a non-linear and diminished fuel burn improvement) for 2035 is capable of reaching the 2% fuel burn improvement per annum goal with more certainty. For 2050 however, this goals still seems to be unattainable. The additional fuel burn improvement would also decrease the NO_x emissions slightly, providing an even greater margin for the 60% NO_x reduction goal.

The main research question can now be answered:
Are conventional turbofans still suitable as standard for short-to-medium-range aircraft in the future?
In terms of both TSFC improvements and NO_x emissions, a UHBPR, high-OPR future turbofan with low-NO_x combustion technologies shows very promising results. The TSFC improvements approach that of the highly efficient open rotor proposal, while the EI_{NO_x} improvement for this upgraded future conventional turbofan is the only improvement, compared to the evaluated alternative architectures, that comes somewhat close to the 90% NO_x reduction promised by the WET engine. Not only shows this a good market competitiveness, the improvements are also sufficient to reach at least the 2030-2035 climate goals set by ACARE and the ICAO. The 2050 goals however are unobtainable with only engine improvement and even when combined with an advanced airframe. Depending on the maximum carbon off-setting, net-zero CO_2 emissions might still call for (hybrid-)electric or hydrogen engines.

Recommendations

The results for the TSFC and EI_{NO_x} performance as a result of the analysis in this thesis can be improved upon for higher accuracy and different design considerations:

- The additional weight for the ITB and WI systems were not taken into account for the TSFC calculations. Depending on how much weight is added compared to how much weight is saved due to the optimisation of the BF-models should be investigated to more accurately represent the TSFC results. Weight can also be saved by decreased the size of the engine. It was shown that for every UF-WI-model, there exists a design space with a lower inlet mass flow that is still able to achieve all thrust requirements. The engine design parameters would however likely change as the limit for the blade height of the last rotor stage of the HPC would limit the OPR.
- A certain FAR was assumed to represent the stability limit for the water injected MPLDI based on a non-WI MPLDI. The actual FAR for which the combustion stability can be guaranteed might be higher. Additional research is needed to investigate this stability limit.
- The EI_{NO_x} correlation for ITB with an MPLDI was based on the EI_{NO_x} correlation for an MPLDI combustor combined with the EI_{NO_x} correlation for regular sequential combustion. The improvements of -95% EI_{NO_x} that are achieved in this thesis are likely an overestimation. A more suitable EI_{NO_x} correlation should be developed that would model the implications of combining an MPLDI main combustor with an RQL second combustor more accurately.
- The climate impact of an aero-engine is not only dictated by the CO_2 and NO_x emission, but also by H20 emissions, contrail formation, CO, UHC and soot, which were all omitted from evaluation. The effect of all emission on the climate impact would provide a more realistic conclusion on whether the desired 30% reduction by 2035 can be achieved.

Bibliography

[1] International Civil Aviation Organization, *Aircraft Engine Emissions*. [Online]. Available: https://www.icao.int/environmental-protection/pages/aircraft-engine-emissions.aspx.

[2] Boeing, *BLENDED WINGLETS*. [Online]. Available: https://www.boeing.com/commercial/aeromagazine/aero_17/winglets.pdf.

[3] R. Vos, *The technology behind the Flying-V*. [Online]. Available: https://www.tudelft.nl/lr/flying-v/technologie.

[4] European Federation for Transport and Environment AISBL, *Airplane pollution*, 2018. [Online]. Available: https://www.transportenvironment.org/challenges/planes/airplane-pollution/#:~:text=Emissions%20from%20aviation%20are%20a,altitude%20at%20which%20aircraft%20operate.

[5] V. Singh and S. K. Sharma, "Fuel consumption optimization in air transport: a review, classification, critique, simple meta-analysis, and future research implications," *European Transport Research Review*, vol. 7, no. 2, p. 12, Apr. 2015, ISSN: 1867-0717. DOI: 10.1007/s12544-015-0160-x.

[6] A. Kharina and D. Rutherford, "Fuel efficiency trends for new commercial jet aircraft: 1960 to 2014," Aug. 2015.

[7] Pratt & Whitney, *GTF Engine*, 2015. [Online]. Available: https://www.prattwhitney.com/en/products/commercial-engines/gtf.

[8] F. Yin and A. G. Rao, "A review of gas turbine engine with inter-stage turbine burner," *Progress in Aerospace Sciences*, vol. 121, p. 100 695, Feb. 2020, ISSN: 03760421. DOI: 10.1016/j.paerosci.2020.100695.

[9] D. Quattrochi, *6.9 Effect of Departures from Ideal Behavior – Real Cycle behavior*, Jun. 2006. [Online]. Available: http://web.mit.edu/16.unified/www/SPRING/propulsion/notes/node51.html.

[10] ACARE, *Achieving climate neutral air mobility*. [Online]. Available: https://www.acare4europe.org/acare-goals/.

[11] International Civil Aviation Organization (ICAO), *ON BOARD A SUSTAINABLE FUTURE*. [Online]. Available: https://www.icao.int/environmental-protection/Documents/ICAOEnvironmental_Brochure-1UP_Final.pdf.

[12] S. Dmytriyev, V. Loginov, T. Gusev, and T. Stepanova, "Analysis and forecast on changes in the level of harmful substance emissions from aviation gas turbine engines," in *EUCASS*, 2019. DOI: 10.13009/EUCASS2019-1056.

[13] ICAO, "ICAO LTAG Data to support States analysis," 2021. [Online]. Available: https://www.icao.int/environmental-protection/LTAG/Pages/LTAG-data-spreadsheet.aspx.

[14] Japan Aircraft Development Corporation, "Worldwide Market Forecast 2022-2041," JADC, Tech. Rep., Mar. 2022. [Online]. Available: http://www.jadc.jp/files/topics/174_ext_01_en_0.pdf.

[15] V. Grewe, A. Gangoli Rao, T. Grönstedt, *et al.*, "Evaluating the climate impact of aviation emission scenarios towards the Paris agreement including COVID-19 effects: supplementary material," *Nature Communications*, vol. 12, no. 1, p. 3841, Jun. 2021, ISSN: 2041-1723. DOI: 10.1038/s41467-021-24091-y.

[16] A. Bauen, N. Bitossi, L. German, A. Harris, and K. Leow, "Sustainable Aviation Fuels," *Johnson Matthey Technology Review*, 2020, ISSN: 2056-5135. DOI: 10.1595/205651320X15816756012040.

[17] A. Murray, T. Smith, E. Pittman, J. D. Moore, and G. A. Risha, "Development and Experimentation of a Lab-Scale Pulse Detonation Engine (PDE)," in *AIAA Propulsion and Energy 2019 Forum*, Reston, Virginia: American Institute of Aeronautics and Astronautics, Aug. 2019, ISBN: 978-1-62410-590-6. DOI: 10.2514/6.2019-3808.

[18] K. Ranasinghe, K. Guan, A. Gardi, and R. Sabatini, "Review of advanced low-emission technologies for sustainable aviation," *Energy*, vol. 188, p. 115 945, Dec. 2019, ISSN: 03605442. DOI: 10.1016/j.energy.2019.115945.

[19] S. Kaiser, O. Schmitz, P. Ziegler, and H. Klingels, "The Water-Enhanced Turbofan as Enabler for Climate-Neutral Aviation," *Applied Sciences*, vol. 12, no. 23, p. 12 431, Dec. 2022, ISSN: 2076-3417. DOI: 10.3390/app122312431.

[20] S. Kaiser, H. Kellermann, M. Nickl, A. Seitz, and Z. Vlahostergios, "A Composite Cycle Engine Concept for Year 2050," Conference: 31st Congress of the International Council of the Aeronautical Sciences, Belo Horizonte, Brazil, Tech. Rep., Sep. 2018.

[21] E. O. Osigwe, A. Gad-Briggs, T. Nikolaidis, S. Jafari, B. Sethi, and P. Pilidis, "Thermodynamic Performance and Creep Life Assessment Comparing Hydrogen- and Jet-Fueled Turbofan Aero Engine," *Applied Sciences*, vol. 11, no. 9, p. 3873, Apr. 2021, ISSN: 2076-3417. DOI: 10.3390/app11093873.

[22] A. Angrand, "Safran ponders open rotor options," *Air & Cosmos International Magazine*, pp. 22–23, May 2019. [Online]. Available: https://issuu.com/aircosmosinternational/docs/airandcosmosinternational_7.

[23] J. Bijewitz, A. Seitz, and M. Hornung, "Architectural comparison of advanced ultra-high bypass ratio turbofans for medium to long range application," Deutsche Gesellschaft fur Luft-und Raumfahrt-Lilienthal-Oberth eV, Tech. Rep., 2015.

[24] M. D. Guynn, J. J. Berton, W. J. Haller, E. S. Hendricks, and M. T. Tong, "Performance and Environmental Assessment of an Advanced Aircraft with Open Rotor Propulsion," NASA, Hampton, Tech. Rep., Oct. 2012.

[25] S. Kaiser, A. Seitz, S. Donnerhack, and A. Lundbladh, "Composite Cycle Engine Concept with Hectopressure Ratio," *Journal of Propulsion and Power*, vol. 32, no. 6, pp. 1413–1421, Nov. 2016, ISSN: 0748-4658. DOI: 10.2514/1.B35976. [Online]. Available: https://arc.aiaa.org/doi/10.2514/1.B35976.

[26] S. Boggia and K. Rüd, "Intercooled Recuperated Aero Engine," MTU Aero Engines, München, Tech. Rep., Mar. 2013.

[27] C. Salpingidou, Z. Vlahostergios, D. Misirlis, M. Flouros, F. Donus, and K. Yakinthos, "Investigation and Assessment of the Performance of Various Recuperative Cycles Based on the Intercooled Recuperation Concept," in *Volume 3: Coal, Biomass, and Alternative Fuels; Cycle Innovations; Electric Power; Industrial and Cogeneration; Organic Rankine Cycle Power Systems*, American Society of Mechanical Engineers, Jun. 2018, ISBN: 978-0-7918-5104-3. DOI: 10.1115/GT2018-76778.

[28] J. Kurzke, *GasTurb: Design and Off-Design Performance of Gas Turbines*, Germany, 2012.

[29] M. Rafiee, A. Siadatan, E. Afjei, and E. Abadi, "Utilizing TE pellet as the Condenser of Thermal Power Plant," *Sensors & Transducers Journal*, vol. 17, pp. 257–266, Jan. 2012.

[30] D. Y. Cheng and A. L. Nelson, "THE CHRONOLOGICAL DEVELOPMENT OF THE CHENG CYCLE STEAM INJECTED GAS TURBINE DURING THE PAST 25 YEARS," in *Proceedings of ASME TURBO EXPO 2002*, Amsterdam, Jun. 2002.

[31] D. L. Chase, "Combined-Cycle Development Evolution and Future," GE Power Systems, Tech. Rep., Apr. 2001.

[32] ElectricalWorkbook, *What is Dual Cycle? Process, Derivation, Diagram & Efficiency*, 2022. [Online]. Available: https://electricalworkbook.com/dual-cycle/.

[33] M. D. Guynn, J. J. Berton, K. L. Fisher, W. J. Haller, M. T. Tong, and D. R. Thurman, "Engine Concept Study for an Advanced Single-Aisle Transport," National Aeronautics and Space Administration (NASA), Hampton, Tech. Rep., Aug. 2009. [Online]. Available: http://www.sti.nasa.gov.

[34] EASA, *TYPE-CERTIFICATE DATA SHEET*, Nov. 2022. [Online]. Available: https://www.easa.europa.eu/en/downloads/20863/en.

[35] B. Fanzago, "Performance of modern unmixed turbofan engines: model simulation, analysis and optimization using GasTurb software," Ph.D. dissertation, Universita degli Studi di Padova, Padua, 2019.

[36] J. Kurzke, *GasTurb 12 Manual*, Germany, 2012.

[37] EASA, *TYPE-CERTIFICATE DATA SHEET LEAP-1A & LEAP 1C SERIES ENGINES*, Mar. 2016. [Online]. Available: https://www.easa.europa.eu/sites/default/files/dfu/EASA%20E%20110%20TCDS%20Issue%202%20LEAP-1A_1C_20161103_1.0.pdf.

[38] EASA, *TYPE-CERTIFICATE DATA SHEET*, Oct. 2022. [Online]. Available: https://www.easa.europa.eu/en/document-library/type-certificates/engine-cs-e/easaime093-pw1100g-jm-series-engines.

[39] European Union Aviation Safety Agency (EASA), *ICAO Aircraft Engine Emissions Databank*, Jun. 2023. [Online]. Available: https://www.easa.europa.eu/en/domains/environment/icao-aircraft-engine-emissions-databank.

[40] T. Furuhata, T. Kawata, N. Mizukoshi, and M. Arai, "Effect of steam addition pathways on NO reduction characteristics in a can-type spray combustor," *Fuel*, vol. 89, no. 10, pp. 3119–3126, Oct. 2010, ISSN: 00162361. DOI: 10.1016/j.fuel.2010.05.018.

[41] O. Schmitz, H. Klingels, and P. Kufner, "Aero Engine Concepts beyond 2030: Part 1-The Steam Injecting and Recovering Aero Engine," *Journal of Engineering for Gas Turbines and Power*, vol. 143, no. 2, Feb. 2021, ISSN: 15288919. DOI: 10.1115/1.4048985.

[42] D. A. Sullivan, "A Simple Gas Turbine Combustor NOx Correlation Including the Effect of Vitiated Air," *Journal of Engineering for Power*, vol. 99, no. 2, pp. 145–152, Apr. 1977, ISSN: 0022-0825. DOI: 10.1115/1.3446260.

[43] D. Dewanji, "Flow Characteristics in Lean Direct Injection Combustors," Ph.D. dissertation, TU Delft, Delft, Oct. 2012.

[44] R. Tacina, C. Wey, P. Laing, P. Hannifin, and A. Mansour, "SECTOR TESTS OF A LOW-NOX, LEAN-DIRECT-INJECTION, MULTIPOINT INTEGRATED MODULE COMBUSTOR CONCEPT," in *ASME Turbo Expo*, Amsterdam, Jun. 2002.

[45] C.-M. Lee, K. M. Tacina, and C. Wey, "HIGH PRESSURE LOW NOX EMISSIONS RESEARCH: RECENT PROGRESS AT NASA GLENN RESEARCH CENTER," NASA Glenn Research Center, Cleveland, Tech. Rep., 2007.

[46] Z. J. He, C. T. Chang, and C. E. Follen, "NOx Emmissions Performance and Correlation Equations for a Multipoint LDI injector," NASA Glenn Research Center, Cleveland, Ohio, Tech. Rep., 2014. [Online]. Available: https://ntrs.nasa.gov/api/citations/20140005329/downloads/20140005329.pdf.

[47] X. Zhao, S. Sahoo, K. Kyprianidis, J. Rantzer, and M. Sielemann, "Off-design performance analysis of hybridised aircraft gas turbine," *The Aeronautical Journal*, vol. 123, no. 1270, pp. 1999–2018, Dec. 2019, ISSN: 0001-9240. DOI: 10.1017/aer.2019.75.

[48] S. Samuelsson, K. G. Kyprianidis, and T. Grönstedt, "Consistent Conceptual Design and Performance Modeling of Aero Engines," in *Volume 3: Coal, Biomass and Alternative Fuels; Cycle Innovations; Electric Power; Industrial and Cogeneration*, American Society of Mechanical Engineers, Jun. 2015, ISBN: 978-0-7918-5667-3. DOI: 10.1115/GT2015-43331.

[49] A. Alexiou, N. Aretakis, I. Kolias, and K. Mathioudakis, "Novel Aero-Engine Multi-Disciplinary Preliminary Design Optimization Framework Accounting for Dynamic System Operation and Aircraft Mission Performance," *Aerospace*, vol. 8, no. 2, p. 49, Feb. 2021, ISSN: 2226-4310. DOI: 10.3390/aerospace8020049.

[50] C. Clemen, P. Albrecht, and S. Herzog, "SYSTEMATIC OPTIMISATION OF A TURBOFAN BYPASS DUCT SYSTEM," in *ASME Turbo Expo*, Copenhagen, 2012. [Online]. Available: http://www.asme.org/about-asme/terms-of-use.

[51] F. S. Mastropierro, J. Sebastiampillai, F. Jacob, and A. Rolt, "Modeling Geared Turbofan and Open Rotor Engine Performance for Year-2050 Long-Range and Short-Range Aircraft," *Journal of Engineering for Gas Turbines and Power*, vol. 142, no. 4, Apr. 2020, ISSN: 0742-4795. DOI: 10.1115/1.4045077.

[52] R. J. Boyle, A. H. Parikh, M. C. Halbig, and V. K. Nagpal, "Design Considerations for Ceramic Matrix Composite Vanes for High Pressure Turbine Applications," in *AMSE Turbo Expo*, San Antonio, Jun. 2013.

[53] S. Praveen kumar and K. Tejas, "Impact Simulation: Comparison of Composite Jet Engine Fan Blade with and without Leading Edge Reinforcement," *International Research Journal of Engineering and Technology (IRJET)*, vol. 8, no. 8, Aug. 2021.

[54] K. H. Khafagy, C. Sorini, T. Skinner, and A. Chattopadhyay, "Modeling creep behavior in ceramic matrix composites," *Ceramics International*, vol. 47, no. 9, pp. 12 651–12 660, May 2021.

[55] A. Epstein, *The Pratt & Whitney PurePower® Geared Turbofan™ Engine*, Paris, Sep. 2015. [Online]. Available: https://academieairespace.com/wp-content/uploads/2018/05/prattw.pdf.

[56] T. Grönstedt, C. Xisto, X. Zhao, *et al.*, *Multidisciplinary assessment of a year 2035 turbofan propulsion system*, 2022.

[57] A. Dik, N. Bitén, V. Zaccaria, I. Aslanidou, and K. Kyprianidis, "Conceptual Design of a 3-Shaft Turbofan Engine with Reduced Fuel Consumption for 2025," *Energy Procedia*, vol. 142, pp. 1728–1735, Dec. 2017, ISSN: 18766102. DOI: 10.1016/j.egypro.2017.12.556.

[58] M. Brown and R. Vos, "Conceptual Design and Evaluation of Blended-Wing Body Aircraft," in *2018 AIAA Aerospace Sciences Meeting*, Reston, Virginia: American Institute of Aeronautics and Astronautics, Jan. 2018, ISBN: 978-1-62410-524-1. DOI: 10.2514/6.2018-0522. [Online]. Available: https://pure.tudelft.nl/ws/portalfiles/portal/44026770/ConferencePaper.pdf.

A
Engine model parameters

Table A.1: Summary of the design parameters and characteristics of all engine models at TOC

	GTF-B	**GTF-2035BF**	**GTF-2050BF**	**DDTF-B**	**DD-2035BF**	**DD-2050BF**
	TOC	TOC	TOC	TOC	TOC	TOC
Intake Pressure Ratio	1	1	1	1	1	1
Inner Fan Pressure Ratio	1.310	1.347	1.332	1.355	1.417	1.380
Outer Fan Pressure Ratio	1.467	1.477	1.351	1.531	1.449	1.390
Core Inlet Duct Press. Ratio	0.985	0.985	0.987	0.985	0.985	0.987
IP Compressor Pressure Ratio	2.550	3.599	3.534	2.000	2.492	2.999
Compr. Interduct Press. Ratio	0.980	0.980	0.984	0.980	0.980	0.984
HP Compressor Pressure Ratio	12.900	11.164	12.351	15.700	12.556	10.694
Bypass Duct Pressure Ratio	0.980	0.980	0.989	0.980	0.980	0.989
Turb. Interd. Ref. Press. Ratio	0.985	0.985	0.985	0.985	0.985	0.985
Design Bypass Ratio	12.10	14.29	15.61	10.90	14.30	15.99
Burner Exit Temperature [K]	1580.00	1609.32	1523.25	1630.00	1643.77	1560.17
Burner Design Efficiency	0.995	0.997	0.9995	0.995	0.997	0.9995
Fuel Heating Value [MJ/kg]	43.031	43.031	43.031	43.031	43.124	43.031
Overboard Bleed [kg/s]	0.000	0.000	0.000	0.000	0.000	0.000
Power Offtake [kW]	0.000	0.000	0.000	0.000	0.000	0.000
HP Spool Mechanical Efficiency	0.990	0.990	0.990	0.990	0.990	0.990
Gear Ratio	3.063	2.128	2.006	1	1	1
LP Spool Mechanical Efficiency	0.990	0.995	0.995	0.990	0.995	0.995
Burner Pressure Ratio	0.960	0.960	0.970	0.960	0.960	0.970
Turbine Exit Duct Press Ratio	0.980	0.980	0.980	0.980	0.980	0.980
Number of HP Turbine Stages	2	2	2	2	2	2
HPT NGV 1 Cooling Air / W25	0.011	0.008	0.082	0.050	0.118	0.075
HPT Rotor 1 Cooling Air / W25	0.000	0.044	0.028	0.033	0.021	0.023
Number of LP Turbine Stages	3	3	3	7	7	7
Altitude [m]	10668	10668	10668	10668	10668	10668
Mach Number	0.780	0.780	0.780	0.780	0.780	0.780
Inlet Corr. Flow W2Rstd [kg/s]	593.825	662.796	832.878	551.000	676.488	745.703
Polytr.Inner LPC Efficiency	0.920	0.935	0.950	0.900	0.922	0.935
Polytr.Outer LPC Efficiency	0.920	0.932	0.946	0.900	0.920	0.932
Polytr.IPC Efficiency	0.900	0.915	0.923	0.880	0.900	0.908
IPC_Number of Stages	3	3	3	3	3	3
Polytr.HPC Efficiency	0.905	0.918	0.925	0.905	0.915	0.925
HPC_Number of Stages	8.000	8.000	8.000	10.000	10.000	10.000
Polytr.HPT Efficiency	0.900	0.908	0.910	0.900	0.903	0.910
Polytr.LPT Efficiency	0.915	0.924	0.930	0.900	0.912	0.930
* Output *						
Net Thrust [kN]	26.60	26.60	26.60	25.99	25.99	25.99
Sp. Fuel Consumption [g/kNs]	14.40	13.07	12.21	14.96	13.63	12.72
Fuel Flow [kg/s]	0.383	0.348	0.325	0.389	0.354	0.330
NOx Severity Index	0.81	1.09	1.18	0.81	0.81	0.78
Core Efficiency	0.58	0.60	0.60	0.56	0.58	0.59
Propulsive Efficiency	0.80	0.82	0.85	0.79	0.82	0.84
Overall Pressure Ratio P3/P2	41.60	52.25	56.45	41.07	42.81	42.97
Specific Thrust [m/s]	120.20	107.69	85.70	126.55	103.07	93.50
Ideal Jet Velocity Ratio V18/V8	0.60	0.85	0.85	0.72	0.85	0.85
LC01 Blade Tip Radius [m]	1.05	1.13	1.27	1.01	1.13	1.19
Engine Mass Flow W2 [kg/s]	221.31	247.01	310.40	205.35	252.11	277.91
HPC Exit Pressure P3 [kPa]	1482.69	1862.51	2012.03	1463.93	1525.81	1531.57
HPC Exit Temperature T3 [K]	815.49	855.94	864.96	817.32	815.22	806.39
LPT Inlet Temperature T45 [K]	1203.76	1205.05	1064.91	1167.85	1175.24	1148.69
Ovl_Total Mass [kg]	2594.16	2268.18	2951.38	2446.33	2306.08	2370.82
EINOx [g/kg]	16.50	22.58	22.36	17.32	17.65	15.76

B
Results summary of UF-models

Table B.1: Summary of results for lowest TSFC and lowest EINOx values for all models

			GTF-2035		DD-2035		GTF-2050		DD-2050	
			TSFC	EINOx	TSFC	EINOx	TSFC	EINOx	TSFC	EINOx
BF	DP		13.07	22.58	13.63	17.63	12.21	22.32	12.72	15.70
	OD		6.05	27.29	6.29	22.94	5.28	28.54	5.70	19.07
WI	DP	Min TSFC	12.50	17.29	13.11	13.92	11.59	16.97	12.17	12.21
		Min EINOx	14.90	11.27	15.04	8.49	13.94	11.45	14.41	8.48
	DP-MPLDI	Min TSFC	12.50	7.98	13.11	6.61	11.59	6.89	12.17	5.38
		Min EINOx	12.71	6.63	13.32	5.59	11.93	5.37	12.42	4.32
	OD	Min TSFC	4.59	10.89	5.30	10.67	3.70	8.31	4.54	7.75
		Min EINOx	4.59	10.89	5.30	10.67	3.70	8.31	4.54	7.75
	OD-MPLDI	Min TSFC	5.21	10.81	5.30	8.37	4.54	8.85	4.87	6.76
		Min EINOx	5.21	10.81	5.30	8.37	4.54	8.85	4.87	6.76
ITB	DP	Min TSFC	13.09	21.42	13.71	16.89	12.28	19.67	12.82	15.55
		Min EINOx	14.33	9.74	15.14	7.95	13.96	7.42	14.10	7.05
	DP-MPLDI	Min TSFC	13.09	8.26	13.71	7.41	12.28	7.88	12.82	6.22
		Min EINOx	14.33	1.48	15.14	1.32	13.87	1.44	14.10	1.04
	OD	Min TSFC	4.93	11.18	5.67	11.78	4.50	10.28	4.54	6.92
		Min EINOx	5.05	10.22	5.67	11.78	4.70	9.66	4.58	6.84
	OD-MPLDI	Min TSFC	4.93	1.87	5.67	1.87	4.50	1.41	4.54	0.98
		Min EINOx	5.05	1.54	5.67	1.87	4.70	1.23	4.58	0.96